National Library of Canada

Bibliothèque nationale du Canada

Acquisitions and Bibliographic Services Branch

Direction des acquisitions et des services bibliographiques

395 Wellington Street
Ottawa, Ontario
K1A 0N4

395, rue Wellington
Ottawa (Ontario)
K1A 0N4

Your file Votre référence

Our file Notre référence

NOTICE

The quality of this microform is heavily dependent upon the quality of the original thesis submitted for microfilming. Every effort has been made to ensure the highest quality of reproduction possible.

If pages are missing, contact the university which granted the degree.

Some pages may have indistinct print especially if the original pages were typed with a poor typewriter ribbon or if the university sent us an inferior photocopy.

Reproduction in full or in part of this microform is governed by the Canadian Copyright Act, R.S.C. 1970, c. C-30, and subsequent amendments.

AVIS

La qualité de cette microforme dépend grandement de la qualité de la thèse soumise au microfilmage. Nous avons tout fait pour assurer une qualité supérieure de reproduction.

S'il manque des pages, veuillez communiquer avec l'université qui a conféré le grade.

La qualité d'impression de certaines pages peut laisser à désirer, surtout si les pages originales ont été dactylographiées à l'aide d'un ruban usé ou si l'université nous a fait parvenir une photocopie de qualité inférieure.

La reproduction, même partielle, de cette microforme est soumise à la Loi canadienne sur le droit d'auteur, SRC 1970, c. C-30, et ses amendements subséquents.

Canadä

The Design and Fabrication of Micromachined Capacitive Micro Sensors for Pressure Measurement and Tactile Imaging

Gegi George

A Thesis
in
The Department
of
Mechanical Engineering

Presented in Partial Fulfillment of the Requirements
for
the Degree of Master of Applied Science
at
Concordia University
Montreal, Quebec, Canada.

December 1994

©Gegi George 1994

National Library of Canada

Bibliothèque nationale du Canada

Acquisitions and Bibliographic Services Branch

Direction des acquisitions et des services bibliographiques

395 Wellington Street
Ottawa, Ontario
K1A 0N4

395, rue Wellington
Ottawa (Ontario)
K1A 0N4

Your file Votre référence

Our file Notre référence

THE AUTHOR HAS GRANTED AN IRREVOCABLE NON-EXCLUSIVE LICENCE ALLOWING THE NATIONAL LIBRARY OF CANADA TO REPRODUCE, LOAN, DISTRIBUTE OR SELL COPIES OF HIS/HER THESIS BY ANY MEANS AND IN ANY FORM OR FORMAT, MAKING THIS THESIS AVAILABLE TO INTERESTED PERSONS.

L'AUTEUR A ACCORDE UNE LICENCE IRREVOCABLE ET NON EXCLUSIVE PERMETTANT A LA BIBLIOTHEQUE NATIONALE DU CANADA DE REPRODUIRE, PRETER, DISTRIBUER OU VENDRE DES COPIES DE SA THESE DE QUELQUE MANIERE ET SOUS QUELQUE FORME QUE CE SOIT POUR METTRE DES EXEMPLAIRES DE CETTE THESE A LA DISPOSITION DES PERSONNE INTERESSEES.

THE AUTHOR RETAINS OWNERSHIP OF THE COPYRIGHT IN HIS/HER THESIS. NEITHER THE THESIS NOR SUBSTANTIAL EXTRACTS FROM IT MAY BE PRINTED OR OTHERWISE REPRODUCED WITHOUT HIS/HER PERMISSION.

L'AUTEUR CONSERVE LA PROPRIETE DU DROIT D'AUTEUR QUI PROTEGE SA THESE. NI LA THESE NI DES EXTRAITS SUBSTANTIELS DE CELLE-CI NE DOIVENT ETRE IMPRIMES OU AUTREMENT REPRODUITS SANS SON AUTORISATION.

ISBN 0-612-01353-7

Canada

ABSTRACT

The Design and Fabrication of Micromachined Capacitive Micro Sensors for Pressure Measurement and Tactile Imaging

Gegi George

Micromachined pressure sensors have several advantages over conventional sensors due to their low cost, high sensitivity, small size, low power consumption, wide dynamic range, high stability and can be batch processed Design, fabrication and testing of two novel micromachined capacitive sensors, one for pressure measurement and the other for tactile imaging are described and the experimental results presented The sensors are fabricated using silicon micromachining technology and some well established VLSI (Very Large Scale Integration) techniques Micromachining techniques employed in fabricating these sensors such as anodic bonding, electrochemical glass drilling and KOH etching have been studied, both theoretically and experimentally A discussion on the experimental findings of these micromachining techniques are also presented

A parametric study is performed to establish the influence of rupture stress and sensitivity on the silicon membrane The results of the study showed that the sensitivity of the sensor can be increased, by reducing the thickness and increasing the diameter of the membrane The rupture pressure of the membrane, which determines the operating pressure of the sensor, can be increased by increasing the thickness and decreasing the diameter of the membrane.

The sensor chip is a silicon-glass sandwich structure having a pressure/touch sensitive silicon diaphragm The glass (Pyrex # 7740) and silicon wafers are sealed using anodic bonding The electrical contacts and pressure inlet hole for the pressure measurement sensor is realized using electrochemical glass drilling. The glass cover acts as

a mechanical stopping since it limits the diaphragm displacement. The fabricated 4 x 5 array of silicon capacitive pressure sensors (on a substrate of size 20 x 20 mm) for dynamic pressure measurements is well suited for measurement in non-corrosive gases (e.g., air) in a pressure range of 0 - 7.68 Bar/element Secondly, the fabricated 5 x 5 array of capacitive touch sensors (on a substrate of 20 x 20 mm) for tactile imaging has an estimated zero-pressure capacitance of 0.3755 pF, an average capacitance sensitivity of 7.22 fF/Bar and a maximum operating load capacity of 35 gm/element. The experimental results obtained for the fabricated sensors are compared with analytical models These sensors are especially attractive in automotive industry, space application, biomedical implant devices or in other telemetry devices where power consumption has to be minimized

Acknowledgments

The author is extremely thankful to his supervisors Dr. Ion Stiharu and Dr. Leslie Landsberger for their enthusiastic guidance and continuous encouragement during the course of this work. The author would also like to thank Dr. R B Bhat and Dr. M. Kahrizi for their intellectual guidance and moral support throughout this work.

In addition, the help and assistance provided at various stages of this work by John Elliott, Hans Hugener, Paul Scheiwiller, Ernest Haefeli, Joseph Sarruf, Joseph Hulet Catalin Miu, Thomas Cherian, Jagdish Patel and Geo George is highly appreciated Thanks are also due to Gianni Ferrari and Jacques Lajoie of Ecole Polytechnique for providing the facility to use the chromium evaporator during the course of the fabrication process.

Finally, the author owe thanks to his parents and brothers for their love and encouragement to achieve excellence, without them this would not have been possible. This thesis is dedicated to Dr. R B. Bhat, for his unrelenting guidance throughout the course of this research, and to the author's parents and brothers.

This research was financially supported by sources from both the Mechanical and Electrical Engineering & Computer Engineering Department of Concordia University. The Concordia Seagram Fund and the funding from the Canadian Space Agency are specifically acknowledged.

Dedication

This work is dedicated to

Dr. R.B. Bhat

and

author's parents and brothers.

TABLE OF CONTENTS

Page

i. List of Figures. xii

ii. List of Tables. xvii

iii. List of Acronyms and Symbols xix

Chapter - 1

Introduction, Literature Review and Thesis Objectives

1.1 General 1

1.2 Capacitive Micro-Pressure Micro Sensor . . 3

1.3 Mechanical Properties of Silicon . . 8

1.4 Advantages of Capacitive Sensors 10

1.5 Applications of Capacitive Pressure Sensor. 11

1 6 Tactile Imaging Sensor 12

1.6.1 Optical Sensors. 13

1.6.2 Piezo-resistive Sensors. 14

1 6.3 Piezoelectric Tactile Sensors. 15

1.6.4 Capacitive Tactile Sensors 16

1.7 Objectives and Scope of the Present Research work 16

1.8 Overview of the Thesis. 17

Chapter - 2

Design of Capacitive Micro Sensors for Pressure Measurement and Tactile Imaging

2 1 Introduction 19

2.2 Mechanical Design of Capacitive Pressure Sensor. 19

Page

2.3 Rupture Pressure Analysis 23

2.4 Sensitivity Analysis 25

2 5 Pressure Measurement Sensor . . 27

2.6 Tactile Imaging Sensor 29

2.6.1 Shape recognition 31

Chapter - 3

Characterization of Micromachining Techniques: Anodic Bonding and Electrochemical Discharge Drilling.

3.1 Anodic Bonding . . . 35

3.1.1 General 36

3 1.2 Principle 39

3.1.3 Residual Stress in Anodically Bonded Silicon-Glass Structure . 40

3 1 4 Characterization of Anodically Bonded Silicon-Pyrex Glass Structures 41

3.1.4.1 Vibration Analysis of Resonant Micro Micromechanical Structures 42

3 1.4.2 Experimental Setup. 43

3 1 5 Results and Discussion . . . 45

3.1.6 Conclusions 48

3 1.7 Application of Anodic Bonding 49

3.2 Electrochemical Glass Drilling 50

3.2.1 General 50

3.2 2 Principle 50

3.2.3 The Drilling Process 51

3.2.4 Procedure 53

3.2.5 Experimental Results of Electrochemical Drilling . . . 53

Page

3.2.6 Application of Electrochemical Discharge Drilling 55

Chapter - 4

Process Design and Fabrication

4.1 Capacitive Pressure Measurement Sensor 56

4.1.1 Materials Used for Fabrication of Capacitive Micro Sensor. . . 57

4 1.2 Process Design of Pressure Measurement Sensor . . . 57

4.1 3 Fabrication Process of Pressure Measurement Sensor . . . 58

4.1.3.1 Process A - The Glass Wafer Process 61

4 1.3.2 Process B - The Silicon Membrane Process . . 63

4 1 3.3 Process C - The Top Silicon Cover Process . . 71

4.1.3.4 Process AB-Anodic Bonding of Top Cover With Glass Assembly. . 71

4.1.3.5 Metal Deposition for Electrical Contact 72

4 2 Capacitive Tactile Imaging Sensor 73

4.2 1 Materials Used for Fabrication of Tactile Imaging Sensor 74

4.2.2 Fabrication Process of Tactile Imaging Sensor 74

4.2.2 1 Glass Wafer Process 76

4.2.2.2 Metal Deposition for Electrical Contacts 76

4.2.2.3 Silicon Membrane Process 77

4.2.2.4 Anodic Bonding of Membrane With Glass . . . 80

Chapter - 5

Characterization of Capacitive Pressure Micro Sensor

5.1. Experimental Setup for Sensor Characterization. 81

Page

5.2 Experimental Procedure for Characterization of Pressure Sensor 84

5.2.1 Effect of Frequency on the Capacitance Measurement . 85

5.2.2 Effect of Signal Amplitude and DC Bias on the Capacitance Measurement . 87

5.2.3 Effect of Parasitic Capacitance on the Capacitance Measurement . 87

5.2.4 Capacitance Measurement with Applied Pressure . 89

5.3 Experimental Results of Pressure Micro Sensor . 92

5 4 Summary of Characteristics of Pressure Micro Sensor . 95

Chapter - 6

Characterization of Capacitive Tactile Imaging Sensor

6 1 Experimental Setup for Tactile Imaging Sensor . 98

6.2 Experimental Procedure for Characterization of Tactile Imaging Sensor 100

6 2.1 Touch Understanding-Geometrical Shape Analysis 104

6.2.2 Pressure Response Test . 110

6.3 Statistical Analysis of Performance of Tactile Imaging Array Sensor 113

6.4 Experimental Results of Tactile Imaging Sensor . 118

6.5 Summary of Characterization of Tactile Imaging Sensor . 119

Chapter - 7

Conclusions and Suggestions for Future Work

7.1 Conclusions . 125

7.2 Suggestions for Future Work . 128

Page

Appendix - I

-Derivation of Relation Between Pressure and Capacitance. . . . 131

Appendix - II

-Cleaning Procedure for Silicon and Glass Wafer 138

Appendix - III

-Photolithography 139

Appendix - IV

-Mask Drawings for Micromachined Capacitive Pressure Micro Sensor. . . 142

Appendix - V

-Mask Drawings of Capacitive Tactile Sensor 148

Appendix - VI

-Anisotropic Silicon Etching Using KOH Etchant 152

Appendix - VII

-Mask Making Using Photographic Techniques 160

Appendix - VIII

-Thermal Oxidation Using Wet Oxidation Process . . . 162

Appendix - IX

-Chromium Deposition Evaporator 164

Bibliography 168

List of Figures

Figure		Page
1.1	The Stanford capacitive pressure sensor, measuring 3 mm x 3 mm and incorporating a bipolar circuit, as proposed in 1980	4
1.2	Different types of tactile sensor.	14
2.1	Parallel plate capacitor.	20
2.2	Deflection of Membrane in Regime - I and Regime - II	23
2.3	Analytical Rupture pressure Versus Radius of silicon membrane for an individual element (d = 10 μm).	24
2.4	Analytical Sensitivity Versus Radius of silicon membrane for an individual sensing element (d = 10 μm)	26
2.5a	Analytical results of capacitance as a function of pressure for each sensor element in 4x5 array pressure micro sensor.	28
2.5b	Analytical results of deflection of membrane with respect to applied pressure (in Regime-I) for each sensor element in 4x5 array pressure micro sensor	28
2.6a	Analytical results of capacitance as a function of applied force on each sensor element in 5x5 array tactile imaging sensor	30
2 6b	Analytical results of deflection of membrane with respect to applied pressure (in Regime-I) for each sensor element in 5x5 array tactile imaging sensor	30
2 7	Schematic representation of capacitance response of each sensor element corresponding to different objects placed on the tactile sensor.	32
3 1	Photograph showing the silicon membrane anodically bonded to glass substrate with bonding defects (x 60 magnification)	37
3.2	Photograph showing the ruptured silicon membrane (same membrane of Figure 3.1) after etching in KOH (x 60 magnification)	37
3.3	Initial and final equilibrium potential distribution across the glass during anodic bonding.	39
3.4	The hydrophilic Si surface	39
3.5	Thermal expansion properties of # 7740 Pyrex glass and single crystal silicon.	41
3.6	Schematic representation of anodic bonding apparatus	44
3.7	Schematic representation of anodic bonding characterization apparatus	45
3.8	Schematic representation of anodically bonded test structures	46

Figure		Page
3.9	Frequency response curve of anodically bonded silicon cantilever beam	. 47
3.10	Natural frequency curve for anodically bonded silicon cantilever beam for 22.2mm, 10.0mm, 3 4mm bond length.	. 42
3.11	Natural frequency curve for epoxy bonded silicon cantilever beam for 22.2mm and 10.0mm bond length	. 48
3.12	Principle of electrochemical glass drilling apparatus.	. 51
3.13	Schematic representation of electrochemical glass drilling apparatus .	. 52
3.14	A photograph of the electrochemical glass drilling apparatus . .	. 52
3.15	Drilling time vs glass thickness in the range from 300μm - 1500μm .	. 54
3.16	Two application of electrochemical drilling in micromachined devices.	. 55
4.1	Cross-sectional view of capacitive pressure measurement sensor .	57
4.2	Fabrication process for a capacitive pressure measurement sensor	. 59
4.3a	Photograph of the glass surface after etching for 30 sec. in conc. HF (49%) with positive photoresist as mask (x 60 magnification) . .	. 62
4.3b	Photograph of the glass surface after etching for 120 sec in conc HF (49%) with positive photoresist as mask (x 60 magnification) Therefore positive photoresist is not a good mask for glass . . .	62
4 4	Experimental results of glass etching as a function of time when etched in conc. HF (49%).	. 63
4.5	Photograph showing the formation of brown stains on silicon surface after boron diffusion (B type boron film borosilica film) (x 90 magnification)	. 66
4.6	Sequence of designed and executed fabrication steps for the silicon membrane of capacitive pressure measurement sensor	. 67
4.7a	Photograph showing the uneven surface of boron doped silicon membrane after etching for 20 minutes in KOH (x 60 magnification) . .	. 69
4.7b	Photograph showing the uneven surface of boron doped silicon membrane after etching for 120 minutes in KOH (x 60 magnification) . .	. 69
4.8a	Photograph showing the flat surface of the silicon membrane (70μm thickness) after etching in isotropic etchant ($HF \cdot HNO_3$) for 5 minutes (x 60 magnification)	. 70
4.8b	Photograph showing the flat surface of the silicon membrane (40μm thickness) after etching in isotropic etchant ($HF.HNO_3$) for 6 minutes (x 60 magnification)	. 70

Figure **Page**

4.9 Bottom view of 5 x 5 array tactile sensor . . . 73
4.10 Cross-sectional view of capacitive tactile sensor 73
4.11 Sequence of fabrication steps for the capacitive tactile sensor (view of a single element in the array) . . . 75
4.12 Photograph showing the glass wafer after metallization ready for anodic bonding (x 50 magnification) 78
4.13 Photograph showing the bottom electrode and contact pad of a sensor element (x 50 magnification) 78
4.14 Photograph showing the metal pad on the glass wafer for electrode on the silicon wafer (x 100 magnification) 79
4.15 A magnified view of the Photograph of Figure 4 14 showing the metal layer for the contact pad is continuous (x 500 magnification) . 79
5.1 Cross-sectional view of fabricated capacitive pressure measurement sensor with achieved dimensions in microns 81
5.2 Photograph of the fabricated capacitive pressure measurement sensor (x 60 magnification) 82
5.3 Block diagram of pressure measurement sensor testing system . 83
5.4 Experimental results of zero pressure capacitance as a function of signal frequency for each sensor element. (Level = 1V, Bias = No DC bias . 86
5.5 Dissipation factor (D) of the measuring instrument vs signal frequency . 86
5 6 Equivalent circuit of the pressure measurement sensor. . 87
5.7 Capacitance as a function of pressure for each individual sensor element (Frequency = 1 MHz, Level = 1V, Bias = No DC bias) . . 90
5.8 Experimental results of the capacitance vs pressure for a full cycle for an individual sensing element. (Frequency = 1 MHz, Level = 1V, Bias = No DC bias) 90
5.9 Experimental results of the high and low value of capacitance with respect to pressure for an individual sensing element measured at regular interval for two month. (Frequency = 1 MHz, Level = 1V, Bias = No DC bias) . 91
5.10 Comparison of simulated sensor performance for a range of geometrical dimensions with the experimental results. (Frequency = 1 MHz, Level = 1V, Bias = No DC bias) 94
6.1 Tactile sensor with sensor number illustrated for characterization purpose . 96

Figure **Page**

6.2a Photograph showing a single element of the fabricated tactile imaging sensor (x 60 magnification) 97

6 2b Photograph showing the bottom electrode pad of a single element of the fabricated tactile imaging sensor (x 100 magnification) . . . 97

6.3 Block diagram of sensor testing system. 98

6 4 Experimental results of zero pressure capacitance as a function of signal frequency for each sensor element (level = 1V, bias=no DC bias). . . 102

6 5 Distribution of zero pressure capacitance for each sensor element in the array (frequency=1MHz, level=1V, bias=no DC bias). . . . 103

6 6 Dissipation factor (D) of the measuring instrument as a function of signal frequency (semi-log scale). 104

6 7 Sensors below the hatched area are affected when the rectangular block (12x12x40 mm) is placed on the sensor. 106

6.8 Sensors lying below the hatched area are affected when the cylinder (12 mm radius and 12 mm long) is placed on the sensor. . . . 108

6.9 Sensor lying below the hatched area is affected when the sphere is placed on the chip 109

6.10 Capacitance as a function of pressure for selected sensor element (frequency=1MHz, level=1V, bias=no DC bias) . . . 112

6.11 Zero pressure capacitance measured at regular interval for selected sensor elements to verify long term stability of device (frequency=1MHz, level=1V, bias=no dc bias) 116

6.12 Equivalent circuit of the tactile imaging sensor . 121

6.13 Experimental results of capacitance Vs pressure for a full cycle for an individual sensing element (frequency=1MHz, level=1V, bias=no dc bias) 121

6.14 Experimental results of the high and low value of capacitance for an individual sensing element measured at regular interval for 45 days (frequency=1MHz, level=1V, bias=no dc bias). 123

A3.1 Photolithography 139

A4.1 Mask-1 (Scale 1:5) 143

A4.2 Mask-2 (Scale 1:5) 144

A4.3 Mask-3 (Scale 1:5) 145

A4.4 Mask-4 (Scale 1:5) 146

A4.5 Mask-6 (Scale 1:5) 147

Figure		Page

A5.1 Mask-1 (Scale 1:5) 149

A5.2 Mask-2 (Scale 1:5) 150

A5.3 Mask-2 (Alternate) (Scale 1:5). 151

A6.1 Silicon crystallographic planes.. 152

A6.2 Schematic representation of a constant temperature KOH etching apparatus . 156

A6.3 Silicon wafer holder used for KOH etching apparatus. . . . 157

A6.4 Silicon etch rate as a function of KOH concentration at 86°C . . 158

A6.5 Silicon etch rate as a function of temperature at 35% KOH concentration. . 159

A9.1 Chromium Evaporator 164

A9.2 Photograph showing defective chromium deposition due to high evaporation pressure inside the evaporator (x 200 magnification) 167

A9 3 Photograph showing a well deposited metal pad (chromium) on glass wafer (x 200 magnification) 167

List of Tables

Table		Page
1.1	Literature survey of capacitive-type pressure sensor fabricated using silicon technology (based on progress made since 1980)	5
1.2.	A comparison of mechanical properties of silicon with stainless steel	9
2.1	calculated performance characteristics of 4x5 array capacitive pressure measurement sensor	27
2.2	Analytical results of capacitive pressure micro sensor	29
2.3	Calculated performance characteristics of tactile imaging sensor	33
2 4	Analytical results of tactile imaging sensor	34
3.1	Natural frequency of anodically bonded structures	46
3 2	Natural frequency of epoxy bonded structures	46
5.1	Designed and achieved dimensions of capacitive pressure sensor	83
5.2	Comparison of the analytical and experimental performance characteristics of the 4 x 5 array pressure measurement sensor	92
5 3	Comparison of simulated results for different sensor dimensions with experimental results	93
6 1	Experimental results of zero pressure capacitance of each element in the tactile array sensor with respect to different signal frequency.	101
6.2	Analytical capacitance of each element in the tactile sensor chip for different loads placed on it.	105
6.3	Experimental data of capacitance when rectangular block is placed on tactile imaging sensor for geometrical shape analysis.	106
6.4	Experimental value of capacitance when cylindrical block is placed on tactile imaging sensor for geometrical shape analysis	108
6.5	Experimental results each sensor element in the tactile imaging sensor when spherical objects of different weights are placed on the sensor for geometrical shape analysis	110
6.6	Experimental and analytical response of capacitive tactile imaging sensor with respect to applied pressure	111
6.7	Experimental results of zero pressure capacitance of tactile imaging sensor measured at regular interval for 45 days.	114
6.8	Summary of statistical analysis of zero pressure capacitance of each sensor element taken at regular interval for 45 days.	115

Table		Page
6.9	Correlation between each sensor element and the measured data for zero pressure capacitance taken at regular interval for 45 days	115
6.10a	Summary of regression analysis of sensor element with respect to applied pressure.	117
6.10b	Summary of regression analysis of sensor element with respect to applied pressure.	117
6.11	Correlation between capacitance of sensor elements and applied pressure	118
6.12	Comparison of analytical and experimental performance characteristics of an element (Sensor-3) in the 5 x 5 array tactile imaging sensor.	118
6.13	Comparison of simulated results for different geometrical dimensions with the experimental results	119
A6 1	<100> silicon etch rates in (μm/h) for various KOH concentrations and etch temperatures as calculated from Eq. A6.2 by setting E_a=0.595 eV and K_o=2480 μm/h. (mole/liter)$^{-4\ 25}$.	154
A6.2	<110> silicon etch rates in (μm/h) for various KOH concentrations and etch temperatures as calculated from Eq. A6 2 by setting E_a=0.60 eV and K_o=4500 μm/h. (mole/liter)$^{-4.25}$.	155
A6.3	Calculated silicon etch rates of thermally grown silicon dioxide in (nm/h) for various KOH concentrations and etch temperatures. E_a=0.85 eV.	155

List of Acronyms and Symbols

Symbol	Description
a	Radius of membrane
b_0	Mean of zero pressure capacitance
b_1	Slope of the function curve for regression equation - Capacitance Vs Pressure
B	Parabolic reaction rate
B/A	Linear reaction rate constant
BW	Band Width
C_1	Constant for calculating wet oxidation time (=2.14 x 10^2 $\mu m^2/hr$)
C_2	Constant for calculating wet oxidation time (= 8.95 x 10^7 $\mu m/hr$)
C_c	Capacitance when parallel plates of the capacitor are in contact
C_e	Effective capacitance of the area between two parallel plates
C_{in}	Capacitance of insulating medium between parallel plates
C_{air}	Capacitance of air medium between parallel plates
C_B	Boron concentration in silicon substrate
C_r	Regression equation
C_0	Zero pressure capacitance.
C_{tot}	Total capacitance of the sensor
C_p	Total parasitic capacitance of the sensor.
C_1, C_2, C_3 and C_4	Coefficients given by the boundary conditions
C(P)	Sensor capacitance at a given pressure (P)
CMOS	Complimentary Metal Oxide Semiconductor
d	Distance between the parallel plate capacitor
D	Flexural rigidity of the membrane
DI	Di-ionized
E_2	Activation energy (2 eV/K for wet oxidation)

E	Young's modulus of membrane
E_a	Activation energy for KOH etching
E_1	Activation energy for calculating wet oxidation time (0.71 eV)
E_p	Electric field (V/cm)
f_o	Natural frequency of a clamped cantilever silicon wafer
f_r	Resonant frequencies
H	Diaphragm thickness (silicon)
H_{in}	Thickness of insulation (SiO_2)
k	Boltzmann's constant (= 8.62×10^{-5} eV/K)
k_0	Constant for silicon etch rate in KO H etchant (Equation A6.2)
l	Length of the wafer
L	Length of the resulting crack.
LCR	Inductive, Capacitive, Resistance
LSI	Large Scale Integration
MEMS	Micro Electro Mechanical Systems
P	Pressure range
P_{cr}	Critical pressure
P_{ext}	External pressure applied to the membrane
P_{in}	Pressure inside hermetically sealed membrane cavity
P_{error}	Pressure error caused due to electrostatic force
P_n	Mean pressure
PVC	Poly Vinyl Chloride
Q_1	First quartile
Q_3	Third quartile
r	Radial distance from the center of the membrane
R	Radius of the area in contact for parallel plate capacitor in Regime-II

R^2	Coefficient of determination
R^2(adj)	Adjusted coefficient of determination
R_e	Etch rate
s	Surface area of the diaphragm.
S	Pressure sensitivity
T	Temperature of the oxidation furnace
t_d	Electrochemical glass drilling time (minutes)
t	Oxidation time
V	Voltage
VLSI	Very Large Scale Integration
w	Deflection at any point of the membrane
w(P)	Diaphragm deflection due to applied pressure at any point (x,y) in the membrane
w_{max}	Maximum deflection
X_o	Thickness of Silicon dioxide
y	Thickness of the knife edge
ν	Poisson's ratio
ε_0	Permittivity of vacuum (8.85×10^{-14} F/cm)
ε_r	Dielectric constant of the medium.
σ_r	Rupture stress
σ_s	Surface energy (= 0.8-1.8 $j.m^{-2}$ for silicon-glass anodically bonded structure)
σ	Thermal stress
ρ	Density
ΔC	Change in capacitance
ΔP	Change in pressure
ΔL	Change in length

Chapter - 1

Introduction, Literature Review and Thesis Objectives

1.1 General

Measurement of pressure and tactile imaging are quite essential in several industrial situations such as manufacturing and process industries and in robotic automation. Miniaturization of such sensors, by enchancing their sensitivity and reliability using silicon technology and integrated microelectronics, is possible today as a result of advancements achieved in the fields of microelectronics, VLSI technology and microfabrication techniques

The miniaturization of electronics has produced a technological revolution in micro mechanical systems. A mechanical micro world had emerged from the technology developed for Integrated Circuits (IC). Silicon is an ideal material for electromechanical devices. The electrical properties of silicon are well known due to its wide use in the semiconductor industry and being a single crystal its mechanical properties are known to be stable The first attempts were made in late 1960's for the fabrication of Micro-Electro-Mechanical-Systems (MEMS), such as Pressure and Temperature Sensors using micromachining technology. The field of silicon micromachining as rightly conveyed by Kurt. E. Petersen [1] "silicon micromechanics is not a diverging, unrelated or independent extension of silicon microelectronics, but rather a natural, inevitable continuation of the trend toward more complex, varied and useful integration of devices on silicon" Micromachining refers to processes that enable precise three dimensional shapes to be formed on silicon. Presently, the technology allows control of dimensions from less than a

micron to a few millimeters with tolerances of less than one micron. It has helped in realizing structures such as diaphragms, bridges, cantilever beams, precision grooves, holes and miniature probes The process of micromachining involves various steps, such as photolithography, three-dimensional silicon etching, thin film deposition, epitaxy, anodic bonding and electrochemical glass drilling. Some of the key features of micromachining are as follows:

(a) Ability to create precise three dimensional structures.

(b) Repeatable dimensional stability for each device

(c) Uniform surface thickness for the processed silicon wafer

(d) Ability to vary the device dimensions without major changes in the fabrication process.

Several innovative fabrication techniques have recently been developed specifically for micromachining structures, and they fall into two categories: bulk micromachining and surface micromachining The first involves sculpting the silicon substrate by means of chemical etchant and the second for building structural layers and etching sacrificial layers of thin films deposited upon the substrate Silicon micromachining is also used to selectively thin silicon wafers to form diaphragms having a typical thickness of 5μm or less with a precise lateral and vertical thickness control Presently, researchers are working towards creating microdynamical systems out of silicon that typically measure less than 1 mm^2[1]. The advantage of silicon as a material for these devices is the possibility of integrating the signal processing electronic circuitry on the same chip. Such Micro-Electro-Mechanical-Systems (MEMS) or micromechatronic systems fall broadly into two categories: microsensors and microactuators. Much research has gone into both the microsensor and microactuator areas, however in view of their applications microsensors have received significant attention. The important advantages of these devices are:

(a) The mass of the device is very small and therefore the inertial forces are negligible

when compared to the electrostatic forces. These miniature mechanical structures can be operated with less force and be more efficient.

(b) Batch technology for micro-fabrication and integrated circuitry for signal processing offers the promise of high reliability and repeatability of the devices

(c) The energy requirements of the device are very small.

(d) Space requirements are very small making them ideal as instruments for spacecraft and other applications where size and weight are considered to be severe constraints

1.2 Capacitive Pressure Micro Sensor

The initial major efforts were undertaken nearly two decades ago to fabricate miniaturized sensors based on the processing sequences used in electronic circuit fabrication, and expanding these to suit specific requirements for the realization of novel devices. The new techniques or processing sequences are often referred to as micromachining This involves all kinds of three dimensional structuring of silicon to fabricate mechanical sensors One of the most-needed sensors for the next generation are **Silicon Pressure Sensors**. Though silicon pressure sensors have existed for many years, they were expensive and prone to temperature drift as well as other instabilities The pervasiveness of the microcomputer is creating high-volume markets for sensors which in near future will provide sufficient motivation to develop the low-cost high-performance devices. Silicon based pressure sensors have made substantial progress in recent years, partly because of advances in integrated circuit technology. The enormous progress of integrated circuit (IC) technology in recent years have changed many things in our daily lives because digital systems can be manufactured with much lower costs, lower power consumption, higher speed and in smaller sizes As more components, systems and

software go into single chips of LSI or VLSI, the manufacturing processes of electronic products have been changing drastically.

An overview of capacitive devices currently under development or devices that have been demonstrated so far is summarized in Table-1.1 [2]. From this table it is apparent that pressure measurement sensors for biomedical applications were the very first technology drivers to stimulate research in this direction, where low power consumption is a major design criteria. Numerous devices that followed, the first one developed was for use in cardiology, was with an object to decrease the sensor size. Later advancement led to integration with an oscillator circuit using bipolar technology to yield an overall current drain of 20μA for a supply voltage ranging from 2 5V to 10V. Figure 1.1 illustrates a cross-section of the pioneering structure in this field

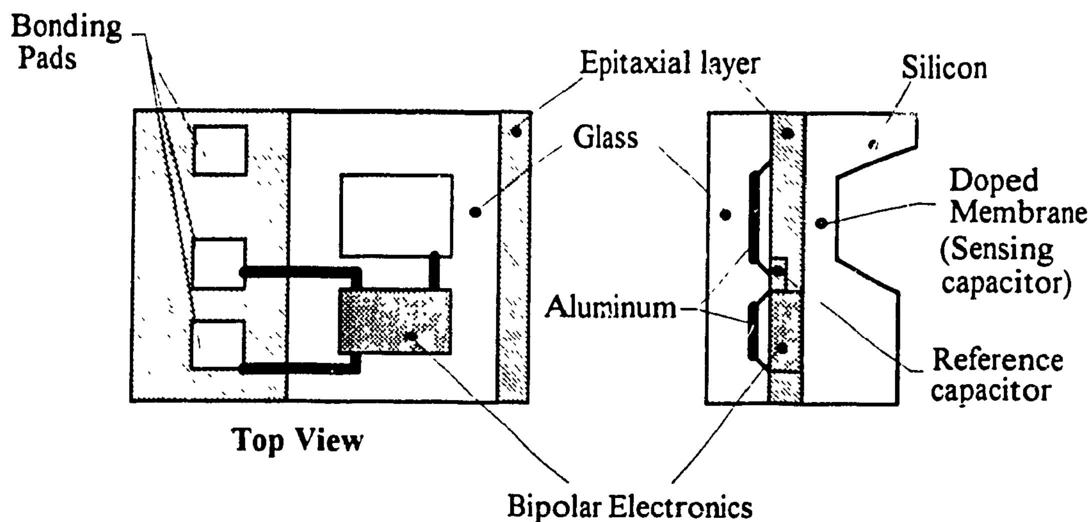

Figure 1.1 The Stanford capacitive pressure sensor, measuring 3 mm x 3 mm and incorporating a bipolar circuit, as proposed in 1980.[2]

Table-1.1 Literature survey of capacitive-type pressure sensor fabricated using silicon technology (based on progress made since 1980) [2].

Authors	Year	Size (mm)^2	C_o (pF)	Etch	Seal	Circuit	Application	Discussion	Ref
Sanders, Knutti and Meindl	1980	3 x 3	22	bulk	anodic	Schmitt Oscillator, bipolar	Cardio	Early device	15
Ko, Bao and Hong	1982	2 x 4	—	bulk, hydrazine	anodic	integrated, bipolar	general	ring versus square membrane, drift aspects	3
Lee and Wise	1982	4 x 4	12	bulk, KOH	anodic	separate	general	effect sealing on TCO and TCS	16
Ko, Shao, Fung, Shen and Yeh	1983	2 x 4	6	bulk, hydrazine	anodic	integrated CMOS	biomedical	ref capacitor integrated with sensing capacitor	17
Smith, Prisbe, Shott and Meindl	1984	2 x 6	22	bulk	anodic	integrated Oscillator, bipolar 10 μm	cardio	temperature compension	18
Hanneborg and Ohlkers	1985 1990	4 x 4	—	bulk	sputtered glass	separate chip	general	low TCO and drift	19 20
Smith, Bowman, and Meindl	1986	2 x 6	22	bulk	anodic	integrated Oscillator, bipolar 10 μm	cardio	comparision with piezoresistive devices	21
Chau and Wise	1987	1 x 5	0 5	EDP,bulk	anodic	separate	cardio	minaturized	22
Miyoshi Akiyama, Shintaku, Inami and Hijkigawa	1987	—	8	surface etch	n a	no	general	Ni diaphragm, sacrifical layer, cheap large batch prod	23
Sumnto, Yeh, Spear and KO	1987	2 x 3	8	bulk, EDP	anodic	seperate, CMOS	general	membrane with central mass for linearity	39
Shoji, Nisase, Esashi and Matsuo	1987	2 x 3	10	bulk, EDP	Si Si fusion	CMOS	biomedical	direct fusion bonding	24
Furuta, Esashi, Shoji and Matsumoto	1989	3 5x0 7	3 5	bulk, KOH	anodic	seperate, CMOS	cardio	small assembly, complete backside etch	25
Puers, Peeters and Sansen	1989	2 x 3 5	10	bulk, KOH	anodic	no	general	FEM analysis & linearization	26
Backlund,Rosengren, Hok and Svedbergh	1990	3 x 3	25	KOH, bulk	fusion bonding	LC circuit only	eye pressure	LC tuned by pressure transponder system	27

Authors	Year	Size (mm)^2	C_o (pF)	Etch	Seal	Circuit	Application	Discussion	Ref
Kandler, Eichholz, Manoli and Mokwa	1990	array 81x100 μm φ	2	sacrifical layer, polysilicon	n a	SC /CMOS	general	preliminary results	28
Matsumoto, Shoji and Esashi	1990	2 x 1 7	---	bulk, KOH	anodic	integrated, CMOS	cardio	throughhole connection, backside etch	29
Puers, Peeters, Varden Bossche and Sansen	1990	2 x 3 5	10	bulk, KOH	anodic	separate CMOS	biomedical	parasitic capacitance rejection	30
Puers, Vanden Bossche, Peeters and Sansen	1990	1 8x2 2	10	bulk, KOH	anodic	seperate	cardio	miniaturized biocompatiable package	31
Artyomov, Kudryashov, Shelenshkevich and Shulga	1991	4 5x4 5	7	bulk	---	no	general	three electrode, linearization by reducing electrode	32
Ji, Cho, Zhang, Najafi and Wise	1991	1 4x0 4	0 3	bulk	anodic	seperate	cardio	subminiature assembly	33
Kudoh, Shoji and Esashi	1991	2 3x3 7	---	bulk, KOH	anodic	integrated CMOS oscillator	general	advanced assembly, electrical feedthroughs	34
Kung and Lee	1991	0 4x0 5	---	Surface etch, KOH through	n a	integrated CMOS	general	polydiaphragm miniature size	35
Nagata, Terabe, Fukaya Sakurai, Tabata, Sugiyama and Esashi	1991	5 x 5	---	bulk, TMAH	anodic	integrated CMOS oscillator	general	frequency output, linearized response	36
Rosengren, Soderkvist and Smith	1992	2 x 2	3	bulk, KOH	fusion bond	no	test	linearization techniques by constructions	37

Authors	Year	Size (mm)^2	C_m (pF)	Etch	Seal	Circuit	Application	Discussion	Ref
Schnatz, Schoneberg, Brockherde, Kopystynski, Mehlhorn, Obermeier and Benzel	1992	8 4x6 2	6	bulk	anodic	integrated, CMOS SC	general	includes band-gap reference for temp correction	38
P Pons, G Blasquez, and R Behocaray	1993	2 9x2 9	24	—	—	without compensation circuits	general	association of dual capacitive cell	53

With the advancement of VLSI technology, steady improvement was made to incorporate more electronic circuitry to avoid parasitic effects in the device. Ko and his co-workers [3] introduced the idea of incorporating a dummy (reference) capacitor in the same cavity to reduce the effects of parasitic capacitance and temperature sensitivity. They also compared different shapes of electrodes, like square and circular, and illustrated that circular electrodes having 36% central area of the pressure sensitive diaphragm yield the highest sensitivity. The group at University of Michigan led by Wise [4] made considerable progress in this field and during their various research stages they have reported miniature sensors having capacitance in the range of 0 3pF to 0.5pF. Evidently, such low intrinsic capacitive values cannot be handled without the matching circuitry integrated to the sensor. Later on, Wise et al [5] proposed an interesting approach to further miniaturize the size of the sensor unit using anodic bonding and anisotropic etching of silicon to realize the membrane.

Esashi et al [6], proposed a series of sensors combined with compatible electronic circuitry in one package. All of these devices are fabricated based on the approach of first bonding the wafers and then etching the silicon to yield the membrane Furthermore, the

electrical contact through the glass was made using a novel micromachining technique called electrochemical glass drilling.

A Norwegian group of researchers lead by Hanneborg [5] studied the stress effects in the membrane affecting the sensitivity of the sensor. They proposed the technique of bonding the silicon to another silicon substrate using thin sputtered glass. Many efforts have been made in understanding the phenomenon of capacitive transducers and to reduce the parasitic effects either by special circuitry or by specific electrode configuration.

As the field advanced, more and more efforts are made to merge with the latest VLSI technology of integrating CMOS processes with capacitive pressure sensor. Guckel and Burns [7] introduced the use of sacrificial layer technology to realize polysilicon membranes. Other approaches to this field include an alternative etchant such as TMAH to perform the bulk etch of the silicon, thus avoiding possible contamination of the CMOS process by KOH.

1.3 Mechanical Properties of Silicon

Silicon as a processing material has already revolutionized the field of electronics Silicon can be used as an excellent mechanical material with the ultimate goal of obtaining numerous miniature mechanical devices. Therefore, in conjunction with silicon's conventional role in microelectronics, and taking advantage of the already advanced micro fabrication technology, it can be used as a high-precision, high-strength and highly reliable mechanical material It can also be utilized wherever miniaturized mechanical devices and components are to be integrated or interfaced with electronics. It is an exceptionally strong material and be chemically machined into unique and extremely precise reproducible shapes. The following four factors have played crucial roles in the

phenomenal success of silicon in micro mechanical applications[1]:

a. Silicon is abundant, inexpensive, and can now be produced and processed controllably to unparalleled standard of purity and perfection.

b. Silicon processing is performed by depositing thin films that are amenable to miniaturization.

c. The fabrication of device shapes and patterns is performed by using photolithography techniques that are capable of high precision.

d. Silicon micro mechanical devices can be batch fabricated so that a few hundreds of devices can be made on a single wafer.

Single-Crystal-Silicon (SCS) has mechanical properties approaching that of stainless steel as presented in Table 1.2 [1]. The main difference is that silicon fails by fracturing (at room temperature) while metals usually yield by deforming inelastically. Polysilicon, silicon dioxide, silicon nitride, phosphosilicate glass are the main materials used in surface micromachining Silicon dioxide and silicon nitride can be used as separation layers Mechanical structures such as membranes, beams, cantilevers are generally machined using polysilicon but sometimes they are also machined using SiO_2 and Si_3N_4 Sacrificial layer techniques can be employed to get suspended or free standing structures in silicon Sealed cavities in silicon are obtained by anodically bonding silicon with glass wafers.

Table 1.2 A comparison of mechanical properties of silicon with stainless steel [1].

Material	Yield strength ($x10^9$ N/m^2)	Young's Modulus ($x10^{11}$ N/m^2)	Density (gm/cm^3)	Thermal Conductivity (W/cm ^oC)	Thermal Expansion ($x10^{-6}$ / ^oC)
Silicon	7.0	1.9	2.3	1.57	2.33
Stainless Steel	2.1	2.1	7.9	0.329	17.3

1.4 Advantages of Capacitive Sensors

Semiconductor-based sensors use both piezo-resistive and capacitive principles to develop high-performance pressure sensors Basically, silicon capacitive sensors differ from piezo-resistive sensors in that they measure the overall displacement of the membrane instead of its stress When the distance between the membrane and the fixed electrode changes in proportion to applied force or pressure, it alters the electrical characteristics of the circuit Piezo-resistive devices offer higher linearity and simpler packaging than capacitive devices However, capacitive pressure sensors are about an order of magnitude more pressure sensitive for a given device size and more than an order of magnitude less sensitive to temperature[8] The capacitive type has the potential for lower power consumption and high sensitivity in comparison with the piezoresistive method In addition, down scaling of the size of the sensor gives rise to certain problems in the piezoresistive method [61], whereas the limiting factor in the capacitive readout method is the smallest detectable change in capacitance, which can be in the sub-fF range [52].

The main advantages of this type of sensor are as follows:

1. conveniently interfaced with electronic circuitry.
2. high reliability.
3. high resolution and stability over a wide range of temperature.
4. batch processed inexpensively.
5. small mass and low power consumption.
6. low hysteresis and non-linearity.
7. can be easily scaled over a wide operating force range.

1.5 Applications of Capacitive Pressure Sensor

Silicon pressure sensors have found numerous applications in the field of medical engineering and space technology, primarily because of their extremely small size, which do not affect the behavior of the system being monitored. These sensors further possess some highly desirable intrinsic properties, such as high reliability, negligible mass and low power consumption Silicon capacitive pressure sensors have been well known for the past 10 years. However, different design and processes are usually employed based on some convenient technology.

Silicon integrated circuit technology has been responsible for creating new industries in electronics and in information processing Now, this same material and processing technology are becoming a dominating force in miniature mechanical devices and components

The potential applications for capacitive pressure sensors are in the following fields

(a) Space/military applications

(b) Medical and surgical equipment (e.g disposable catheter tubes with sensing features)

(c) Scientific instruments

(d) Manufacturing miniature equipment and consumer products

(e) Automobile Industry (e.g. manifold vacuum sensor and barometric pressure sensor)

(f) Industrial control devices

Some of the most exciting possibilities are tools for medical therapies, microsurgery, improved prosthetic devices, cell sorters, instruments for use in spacecraft, HVAC, system for fiber optics communications, computer input and output devices. The pressure, temperature and vibration sensors manufactured using this technology will have numerous applications in industry.

The principle of capacitive sensors can be extended to the field of tactile imaging. The tactile imaging sensors can be used in a wide variety of applications. Tactile sensors can be used in telerobotics which extends human ability to perform complex manipulative tasks in remote locations. It is especially useful in identifying objects which are obscured by the manipulator's finger. These systems are especially useful in environments too hazardous or inaccessible to humans. Examples include nuclear power plants, mines, space, rescue missions, handling electric transmission lines and underwater works. Another important application for a tactile sensor is to provide proper force feedback to control the object being grasped by the manipulator. For this purpose the sensor should be sensitive to the tangential and the normal component of the force to detect slippage. High resolution tactile sensors can be used in three dimensional pattern recognition

1.6 Tactile Imaging Sensor

Touch, vision and proximity are the sensory needs that in combination or alone are the desirable features of robots [9]. In the past, research was mainly oriented on visual pattern recognition and hence tactile sensing did not attract much attention. Tactile sensing has several problems which are also common to vision sensing and thus it can benefit from some of the solutions already devised in the field of vision [10]. Touch-sensing technology enables dexterous robot manipulators to determine the surface curvature, hardness and texture of different objects. Tactile sensors have the capability of controlling the grasping pressure applied on the objects and provide an image of the applied pressure. To understand the behavior of tactile sensors, in both physical and robotics systems, the responses of individual sensing elements within and beneath such elastic continua must be quantified In the present analysis an object in contact with a

tactile sensor is modeled as a dense array of concentrated load distributed over the area of contact. The magnitude of each concentrated load is determined from the total force exerted between the object and the sensor and a description of the pressure distribution This tactile sensor offers high resolution and high stability. It can be interfaced with electronic circuitry and can be easily scaled over a wide operating force range

In many areas sensors are the most critically needed elements in the realization of next-generation smart systems In robotics, sensors enhance the capabilities of performing various tasks in a non-structured environment One of the most important sensors required for robots is the tactile sensor, which gives the robot gripper an analog sense of touch Although many different approaches have been explored, silicon based devices remain very attractive due to their potential for high-density, high accuracy, low temperature drift and low price.

Tactile sensors using different designs have been fabricated based on the wide variety of physical properties of the material The different principles utilized for fabrication of these sensors include. resistivity, capacitance, magnetic fields and optical properties of the transducer material.

In general, most tactile sensors that have been developed can be grouped into four categories, namely, optical sensors, piezo-resistive sensors, piezoelectric sensors and capacitive sensors [8,11]. A brief description of these sensors is presented below.

1.6.1 Optical Sensors

In an optical sensor a light source is modulated in direct correlation with the force, deflecting a flexible sensor element as shown in Figure 1.2 a. This type of sensor gives only binary (contact or non-contact) type of output. The principle involves having pairs of fibre optic strands arranged in an array. One fibre transmits light which is reflected off the

device's elastic cover while the second is connected to a photo detector. Normally, when no pressure is applied, the light is reflected entirely into the second fibre. When pressure is applied, the light is deflected away from the second fibre. The main disadvantage of this scheme is that there are a large number of I/O connections. In addition, scanning the optical array requires large number of A/D converters. The main advantages of optical sensors are high resolution and high immunity to electromagnetic noise sources[63].

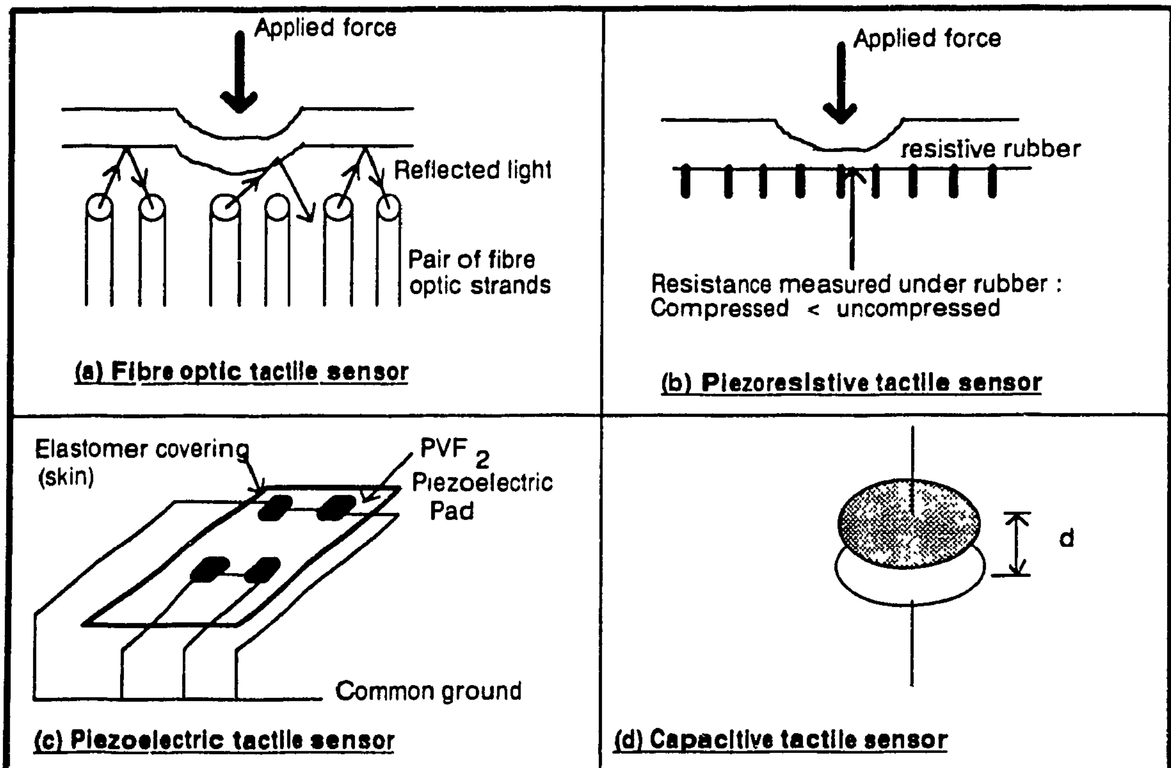

Figure 1.2 Different types of tactile sensor [63].

1.6.2 Piezo-resistive Sensors

All sensors in this family, work based on two phenomena: decrease in resistance due to an increase in the contact area caused by the deformation of the piezo-resistive material under pressure; and a decrease in resistance due to a compression of the piezo-

resistive material also caused by pressure, as shown in Figure 1.2.b. Piezoresistive sensors, utilizing the piezoresistive properties of the sensing material, are primarily of two types· silicon strain gauges and conductive elastomers. Both rely on the change in electrical conductivity of the active material as it is stressed by force or pressure. Conductive rubber, generally used as piezoresistive materials, consist of resistive rubber sheet as their top layer and an array of metal probes as the subsequent layer. Application of pressure to the rubber layer yields a decrease in resistance between two adjacent electrodes The major setback in these types of sensors is to accurately model the inherent non-ohmic behavior of resistive rubber. It is also observed that these rubbers suffer from hysteresis and low sensitivity.

1.6.3 Piezoelectric Tactile Sensors

Piezoelectric sensors are based on the generation of an electric charge in response to an applied force. The classic examples of materials that exhibit the piezoelectric effect are quartz, ceramic and polymer materials like PVF_2 as tactile sensing element [63]. A piezoelectric material generates an electric charge when subjected to a mechanical stress or deformation. The sensor consists of an array of piezoelectric plastic-like compound sandwiched between a plastic skin and a common ground. In addition each PVF_2 element has a wire lead at the top as shown in Figure 1.2.c. The crystalline structure of piezoelectric materials have no electrical center of symmetry and the dipoles are arranged along a single axis When pressure is applied to the skin, the piezoelectric material compresses, the dipoles shift from the axis, resulting in a change in voltage. This voltage is measured to give the change in pressure. The major disadvantage of piezoelectric sensors is the fact that they will operate only while the active material is being deformed; a steady state tactile reading is not possible [64].

1.6.4 Capacitive Tactile Sensor

Capacitive tactile sensors are designed on the principle of two parallel plates acting as capacitor electrodes, as illustrated in Figure 1.2d. When the distance between the plates changes with respect to applied pressure it alters the electrical characteristics of the sensor [64]. Most capacitive type silicon tactile sensors consists of a silicon wafer with a diaphragm etched on it. These force sensitive membranes are either bonded on to a silicon wafer or on a glass plate. Wolffenbuttel et al [54] proposed a tactile sensor using sacrificial layer technology. In this technique, a sacrificial layer is deposited and then patterned on the silicon wafer A cross-over layer is deposited, followed by removal of the sacrificial layer, which undercuts the cross-over layer A freestanding structure is left released from the substrate.

Silicon technology offers the possibility to create high-density tactile imagers This technology helps in integrating with electronic circuitry resulting in a very compact sensing device. The close distance between the sensor elements and the signal processing unit increases the sensitivity of the sensor. The sensor surface should be protected against mechanical damage when they come in physical contact with rigid objects The aforementioned problem can be solved by overlaying an elastic protective layer on the force sensitive silicon membrane

1.7 Objectives and Scope of the Present Research Work

The primary objective of this thesis research is to present novel capacitive sensors for pressure and tactile measurements Further, the detailed study and analysis of micromachining techniques is carried out so that it can be implemented for the fabrication

of mechanical devices with integrated electronics.

The scope and specific objectives of the thesis research are as follows:

1. Design, fabrication and testing of a micromachined capacitive pressure micro sensor.
2. Design, fabrication and testing of a micromachined capacitive tactile imaging sensor.

Further, secondary objectives contributing to the main objectives given in (1) and (2) are also dealt with as given below:

3. Characterization of the boundary conditions of silicon structures anodically bonded to Pyrex glass.
4. Design and realization of an apparatus for precision electrochemical drilling and determining the drilling time, for glass with different thickness
5. Design and setting of a constant temperature KOH etching apparatus and performing experiments to determine the etch rate at different temperatures and with different KOH concentration.

1.8 Overview of the Thesis

The design of a capacitive pressure sensor is described in Chapter-2 The pressure sensitive silicon membrane is modeled as a circular plate with clamped boundary conditions. The deflection of the membrane is analyzed in two regimes i.e. for dynamic pressure measurement and static pressure measurement.

Chapter-3 presents the characterization of micromachining techniques like anodic bonding and electrochemical discharge drilling. The boundary conditions of silicon structures anodically bonded to Pyrex glass is analyzed and its results presented Secondly, the design and fabrication of an apparatus for precision electrochemical drilling of glass is presented. The experimental results and application of drilling in micromachined devices is

also presented

Chapter-4 is devoted to the fabrication process of a novel capacitive pressure micro sensor The sensor is fabricated using micromachining techniques. The success in fabrication of the above sensor has motivated to extend the same design principles to realize a tactile imaging sensor The fabrication process of the tactile sensor is also presented.

Chapter-5 presents the characterization of the fabricated pressure measurement sensor and the experimental results compared with analytical results

Chapter-6 presents the characterization of the fabricated force measurement tactile imager and the experimental results compared with analytical results.

Chapter-7 summarizes the various theoretical and experimental investigations presented in the thesis This chapter also presents the conclusions and suggestions for the future work

Appendix-I presents the derivation of relation between pressure and capacitance, Appendix-II presents the cleaning procedure for silicon and glass wafer, Appendix -III presents the photolithography process, Appendix-IV and V illustrates the mask used for pressure measurement sensor and tactile imaging sensor respectively. Appendix-VI is devoted to the design and fabrication of a KOH etching device. The experimental results of the KOH etch rate is also presented in this appendix. Appendix-VII presents a photographic technique for making masks used for micromachining process fabrication. Appendix-VIII provides a sample calculation for determining the oxidation time using wet oxidation process Finally, Appendix-IX presents the procedure used for depositing chromium on glass using chromium deposition evaporator.

Chapter - 2

Design of Capacitive Micro Sensor for Pressure Measurement and Tactile Imaging.

2.1 Introduction

A capacitive type pressure sensor is used to measure pressure from the change in sensor capacitance caused by it. The capacitive type silicon sensors are potentially good for pressure or force feedback mainly because of its outstanding sensitivity, wide dynamic range, good linearity, low hysteresis and low temperature error. The principle can be extended to realize tactile imaging sensors by measuring the normal and in some circumstances the tangential force acting on the sensor. This chapter introduces a systematic approach to the design of capacitive type micro sensors, utilizing the very basic principles of mechanical deflection of thin membranes due to pressure loading and the resulting change in capacitance The response of a capacitive sensor having circular membrane is modeled as a thin circular plate with clamped boundary conditions Sensitivity and rupture stress analysis of these type of devices for a particular application is also presented.

2.2 Mechanical Design of Capacitive Pressure Sensor

The mechanical design of a capacitive type pressure sensor essentially consists of determining the thickness and diameter of the pressure sensitive membrane and the gap between this membrane and a back plate, forming a parallel plate capacitor These geometrical parameters are designed for detecting a measurable change in capacitance for

the range of applied pressures in particular applications. The pressure sensitive silicon membrane is modeled as a circular plate which acts as a movable electrode clamped onto the glass substrate. The transverse deflection of the membrane changes the capacitance which helps in measuring the normal pressure acting on the sensor.

Consider a parallel-circular-plate capacitor, as shown in Figure 2.1, whose capacitance can be expressed as [12]

$$C(P) = \varepsilon_0 \varepsilon_r \int_0^a \int_0^{2\pi} \frac{r dr . d\theta}{d - w(r,\theta)} \tag{2.1}$$

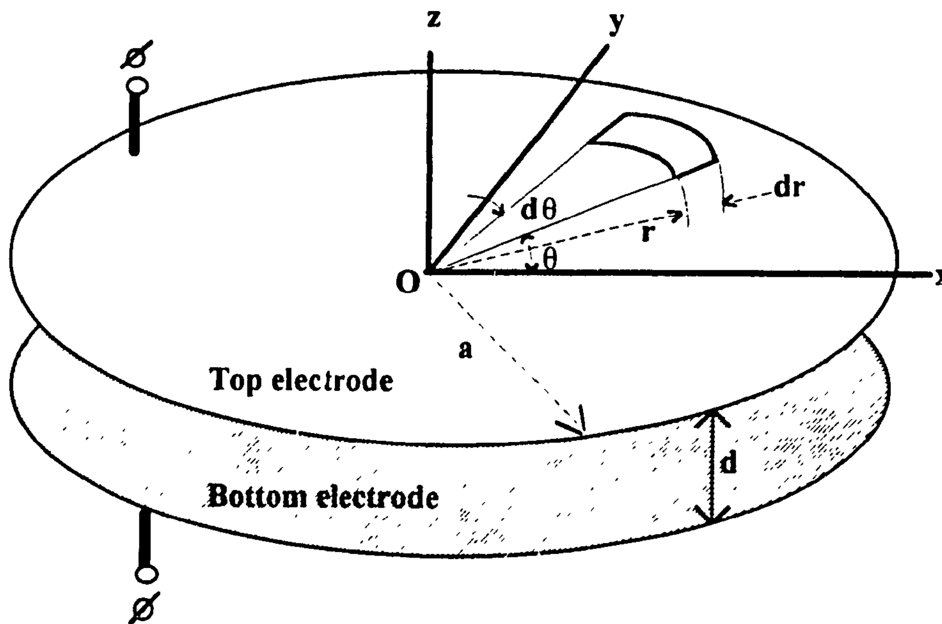

Figure 2.1 Parallel plate capacitor.

Where, O is taken to be at the center of the undeflected top electrode, r, is the radial distance of points in the middle plane of the top electrode, C(P), is the sensor capacitance for a given pressure P, w(r,θ) is the diaphragm deflection at any point (r,θ) assumed to be small compared to the membrane thickness, ε_0 is the permitivity of vacuum (8.85 x 10^{-12} F/m); ε_r is the dielectric constant of the medium. The capacitance between the two parallel

plates changes with change in d, the distance between the plates.

The parallel plate electrodes are separated by a small gap, d, allowing for the membrane deflection This forms a variable capacitor and the gap forms a reference pressure cavity. The difference between the pressure inside the chamber, P_{in}, and outside, P_{ext}, creates a distributed load that deforms the diaphragm. The pressure range, P, is given by the expression:

$$P = (P_{ext} - P_{in})_{max} \tag{2.2}$$

where, P_{ext}, is external pressure applied to the membrane, and

$P_{in} = \frac{P_1 V_1}{V_1 - \Delta V}$, is pressure inside the membrane

with, $P_1 =$ 0.4 atm. [3],which is the initial pressure inside hermetically sealed membrane cavity, and $P_1 = 1$ atm. is the membrane is not hermetically sealed

The pressure range of the sensor is determined by choosing the membrane thickness and diameter The change in sensor capacitance is determined by a signal detection circuit which can be either an integrated or an off-chip circuitry If an off-chip measurement circuit is used, higher variation from the analytical value is expected The change in capacitance which is to be detected for these type of micro-sensor is in the order of 20-50 fF. Therefore, to achieve high precision and a wide range at low cost the following points must be considered:

(a.) minimizing internal stresses in the different materials used (e.g. glass, silicon etc.)

(b.) low stray capacitance and high electrical insulation.

(c.) low and stable reference pressure.

The deflection of the silicon membrane not only depends on the mechanical properties of silicon material but also on the geometric configurations and dimensions Here, circular membranes are considered due to their higher sensitivity compared to square membranes [3]. In a practical situation, the presence of parasitic capacitance cannot be eliminated but it can be minimized for a capacitive array sensor. To reduce the

stray capacitance, one must shorten the leads and place the measuring circuit as close as possible to the sensor. The total capacitance (C_{tot}) is expressed as

$$C_{tot} = C(P) + C_p \tag{2.3}$$

where, C_p is the total parasitic capacitance of the sensor.

For fixed boundary conditions, the deflection at the edges of the membrane is zero (w=0) and maximum at the center of the membrane. The deflection of the membrane can be classified into two regimes. Regime - I starts with the undeflected membrane until it deflects enough to touch the bottom electrode, as shown in Figure 2.2 (a), and is used to measure the dynamic pressure. Regime - II starts when the membrane touches the bottom plate, as shown in Figure 2.2 (b), and continues as the membrane stretches on it and is used for static pressure measurement. Assuming that the pressure acts uniformly on the membrane, deflections $w(r,\theta)$ in Regime - I and Regime - II are independent of θ and are given by equation-(2 4) and equation-(2.5) respectively[14].

$$w = \frac{C_1 r^2}{4} + C_2 \log\frac{r}{a} + C_3 + \frac{Pr^4}{64D} \tag{2 4}$$

$$w = C_1 + C_2 \log r + C_3 r^2 + C_4 r^2 \log r + \frac{Pr^4}{64D} \tag{2.5}$$

where, r is the radial distance from the center of the membrane, and the coefficients C_1, C_2, C_3 and C_4 are determined using the boundary conditions as derived in Appendix - I The flexural rigidity, D, of the membrane is expressed as

$$D = \frac{EH^3}{12(1-\nu^2)} \tag{2.6}$$

where, ν is the Poisson's ratio of silicon taken as 0.3. [3], H, is the membrane thickness (silicon), and, E, is the Young's modulus of silicon. The modulus of elasticity of silicon is dependent on the crystallographic orientation. Here, for design propose, we have considered 1.9×10^{11} Pa [1] for undoped silicon and 2.27×10^{11} Pa [40] for heavily

doped P+ silicon.

The maximum deflection is expressed as:

$$w_{max} = \frac{Pa^4}{64D} \tag{2.7}$$

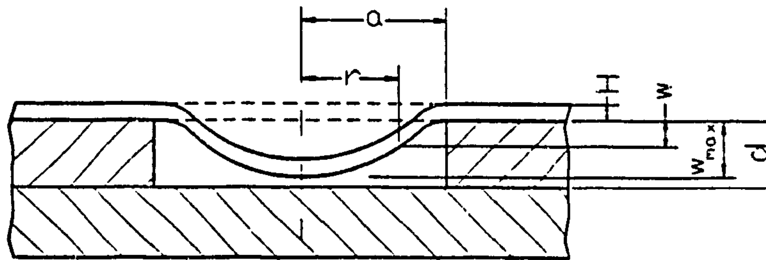

(a) Deflection of membrane before touching the bottom plate - dynamic measurement (Regime - I).

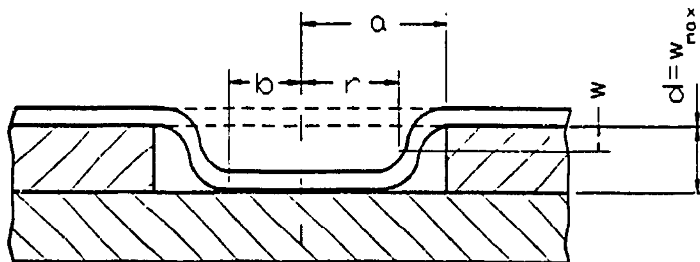

(b) Deflection of membrane after touching the bottom plate - static measurement (Regime - II).

Figure 2.2 Deflection of Membrane in Regime - I and Regime - II.

2.3 Rupture Pressure Analysis

When the stress at any point on the diaphragm exceeds the elastic stress limit of silicon, the material ruptures. The rupture stress can damage or destroy the silicon diaphragm. Silicon has a tendency to cleave along crystallographic planes, especially if

edge, surface or bulk imperfections cause stresses to concentrate and orient along cleavage planes. Slip lines and other flaws at the edges are usually responsible for wafer breakage. However, thin film wafers can be mechanically supported by micromachining techniques such as anodic bonding to suppress the shocks encountered in normal handling and transportation. For monocrystalline silicon, the rupture stress σ_r is of the order of 3.6×10^8 Pa [4]. The critical pressure P_{cr} at which the circular diaphragm ruptures is mathematically written as [12]:

$$P_{cr} = \left(\frac{4}{3}\right)\sigma_r \frac{H^2}{a^2} \tag{2.8}$$

Figure 2.3 represents a graph showing the rupture pressure versus the radius of the membrane for different diaphragm thickness, *H*, of individual sensing element.

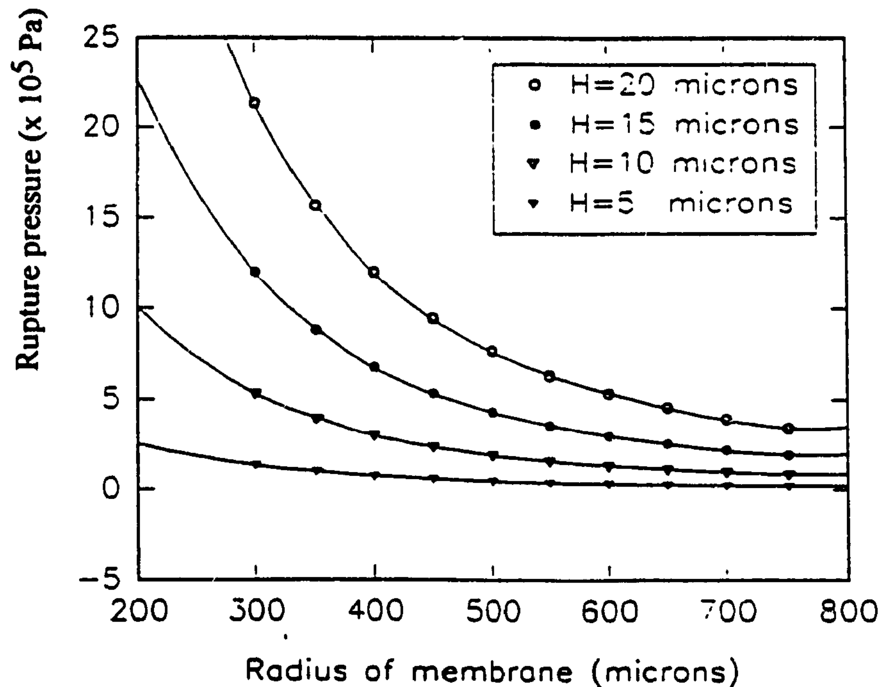

Figure 2.3 Analytical rupture pressure Versus Radius of silicon membrane for an individual sensing element (d = 10 μm).

2.4 Sensitivity Analysis

The sensitivity of a sensor is defined as the ratio of change in sensor capacitance to the corresponding change in applied pressure. It is influenced most strongly by the diaphragm thickness and the size of the sensor. A sensitivity analysis is performed to establish the influence of geometric parameters of the pressure sensitive membrane in capacitive type sensors. This analysis will further provide the lower and upper limits on the design variables and their relative significance on different design criteria. The pressure sensitivity, S, of the sensor in Regime-I is calculated as follows [72]·

$$S = \left(\frac{\Delta C}{\Delta P}\right) \tag{2 9}$$

where, ΔC, is the change in capacitance and ΔP, is the change in applied pressure

The relative sensitivity of the sensor in Regime-I is calculated as [73]

$$S = \left(\frac{\Delta C / C_0}{\Delta P}\right) \tag{2 10}$$

where, C_0 is the zero pressure capacitance of the sensor.

A parametric study is performed by varying a single parameter at a time and measuring the influence of each parameter on the rupture pressure and sensitivity of the sensor as a function of the radius of the membrane. The process induced variations in diaphragm thickness, size and alignment change the pressure sensitivity of the sensor. An ideal capacitive pressure sensor is not temperature dependent Nevertheless, actual devices display a small temperature drift, under 100 ppm/°C [41] . This device is fabricated to be almost free of hysteresis which remains stable for a long period of time The geometry of the capacitive type sensors have a profound effect on their performance The most significant parameter is the plate thickness, H, whose impact on sensitivity and deflection is plotted in Figure 2.4.

The results of the parametric study are summarized as follows:

- The influence of membrane thickness on the sensitivity in general is significant i.e., sensitivity increases with decrease in thickness of membrane.
- The sensitivity of the sensor can be increased by increasing the diameter and decreasing the gap between the parallel plates.
- The rupture pressure is mostly affected by the diameter and thickness of the sensor membrane i.e., rupture pressure increases with thickness and decreases with diameter of the membrane.
- By properly selecting *H*, *a* and *d* it is possible to construct a wide variety of capacitive type sensors for different pressure ranges and sensitivities.

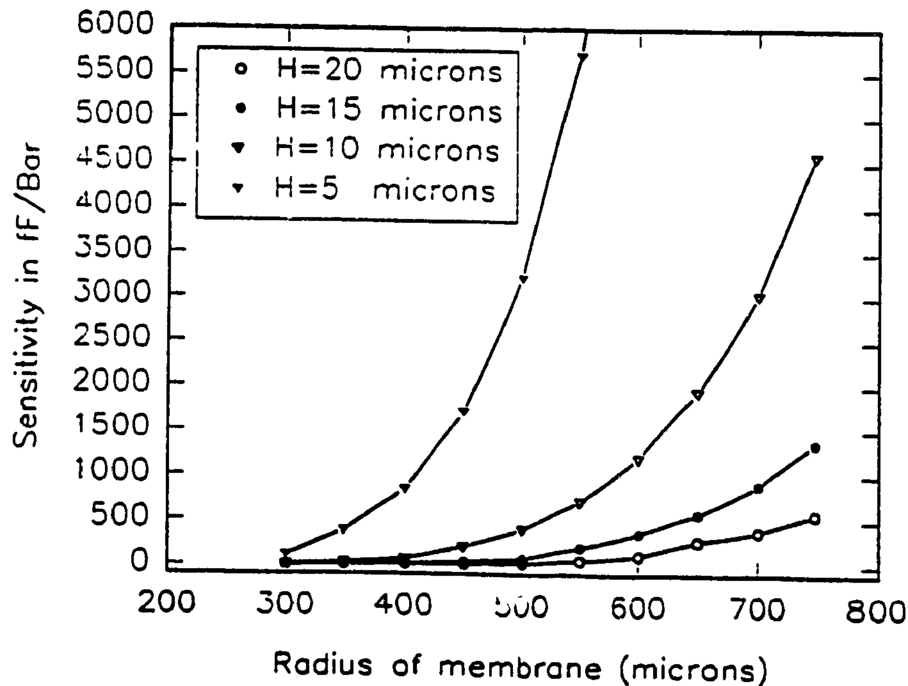

Figure 2.4 Analytical sensitivity Versus Radius of silicon membrane for an individual sensing element (d = 10 μm).

2.5 Pressure Measurement Sensor

A 4x5 array capacitive type pressure measurement microsensor is selected to be fabricated using micromachining techniques The geometrical size of each sensor is determined depending on the existing fabrication facilities and the required sensitivity of the device. Two sizes, 1000 μm and 800 μm diameter, are considered for the pressure sensitive element (membrane). The thickness of the diaphragm is assumed to be 20 μm and the enclosed air gap space is considered to be 10 μm. The computed performance characteristics of the selected pressure sensors are tabulated in Table 2.1. The analytical results of capacitance and deflection of membrane with respect to applied pressure are shown in Table 2.2. Figure 2 5a illustrates the analytical results of the capacitance as a function of pressure for each sensor element The analytical values of deflection of the pressure sensitive membrane considered is in the linear region (regime-I) is plotted in Figure 2.5b. The analytical results in the regime-I, show that the sensor has a linear response in the range of pressure measurement

Table 2.1 Calculated performance characteristics of 4x5 array capacitive pressure micro sensor.

Diameter of silicon membrane (2a)	800 μm	1000 μm
Thickness of silicon membrane (H)	20 μm	20 μm
Thickness of air gap (d)	10 μm	10 μm
Zero Pressure Capacitance (C_0)	0.4451 pF	0 6954 pF
Max. Pressure Capacitance (C_{max})	0.5119 pF	0.9024 pF
Max. operating Pressure	12 x10^5 Pa/element	7.5 x10^5 Pa/element
Type of Silicon Wafer	375μm thick, P-type, <100> orientation	375 μm thick, P-type, <100> orientation
Type of Glass wafer	1500 μm thick, Pyrex # 7740	1500 μm thick, Pyrex # 7740
Rupture Pressure (P_r)	12 0x10^5 Pa/element	7.68x10^5 Pa/element
Sensitivity (S)	5.5667 fF/Bar	26.953 fF/Bar

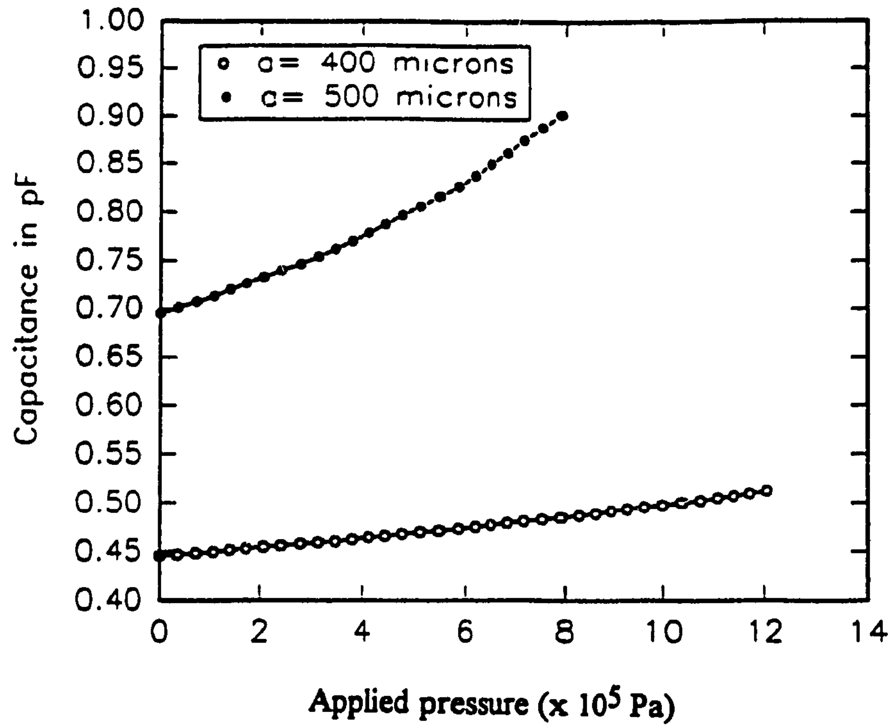

Figure 2.5a Analytical results of capacitance as a function of pressure for each sensor element in 4x5 array pressure micro sensor.

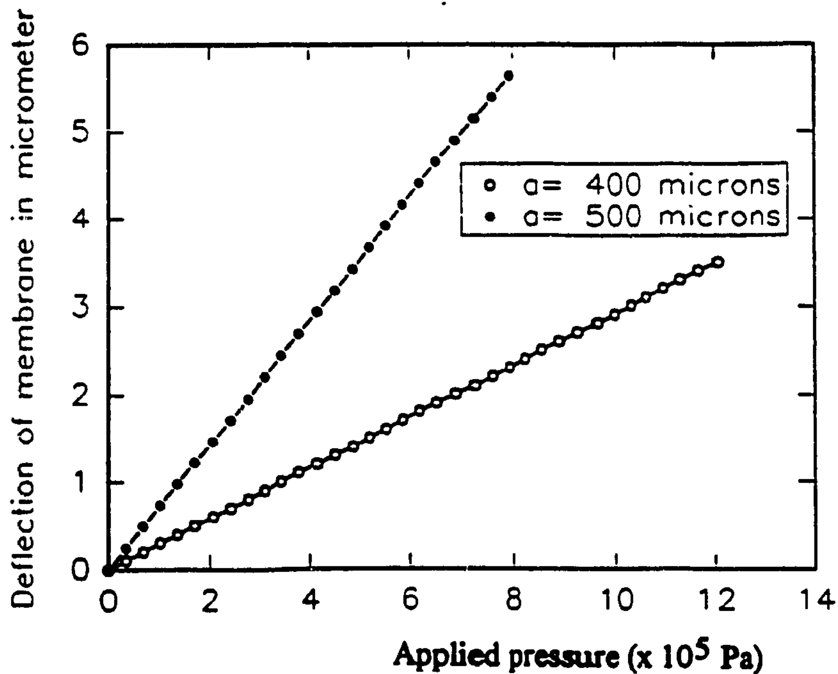

Figure 2.5b Analytical results of deflection of membrane with respect to applied pressure in (Regime - I) for each sensor element in 4x5 array pressure micro sensor.

Table-2.2 Analytical results of capacitive pressure micro sensor (H=20 μm and d = 10 μm)

Applied Pressure	800 μm diameter membrane		1000 μm diameter membrane	
x 10^5 Pa (lb./in ^{2})	Capacitance (pF)	Maximum deflection (μm)	Capacitance (pF)	Maximum deflection (μm)
0.0000 (0)	0.4451	0.0	0.6954	0.0
0.3445 (5)	0.4465	0.1003	0.7012	0.2448
0.6890 (10)	0.4481	0.2005	0 7071	0.4895
1.0335 (15)	0.4496	0.3008	0.7132	0.7343
1.3780 (20)	0.4511	0 401	0.7195	0 9791
1 7225 (25)	0.4527	0.5013	0 726	1.224
2.0670 (30)	0 4543	0 6016	0.7328	1.469
2.4120 (35)	0.4559	0 7018	0 7398	1 713
2.7560 (40)	0 4576	0 8021	0.747	1 958
3.1010 (45)	0.4592	0 9023	0 7545	2 203
3.4450 (50)	0.4609	1.003	0 7623	2 448
3.7900 (55)	0 4626	1.103	0.7703	2 693
4.1340 (60)	0.4643	1 203	0.7788	2 937

2.6 Tactile Imaging Sensor

The principle of capacitive type pressure sensor is used to realize tactile sensors by measuring the normal force acting on the sensor The construction of tactile sensor depends on the array structure, the sensing element and covering material [13]. The design should take into consideration the following criteria. (a) keep the active surface of the tactile imager freely accessible to objects to be sensed, (b) the sensitive side of the device must be fully flat and wiring on the top layer should be avoided; (c) the sensor should be confined to a minimum number of electrical connections due to practical reasons, in particular for robot applications, where the sensor is mounted on a rather small and movable gripper; and (d) the sensor must withstand physical contact with rigid objects and therefore the sensitive surface should be protected against mechanical damage.

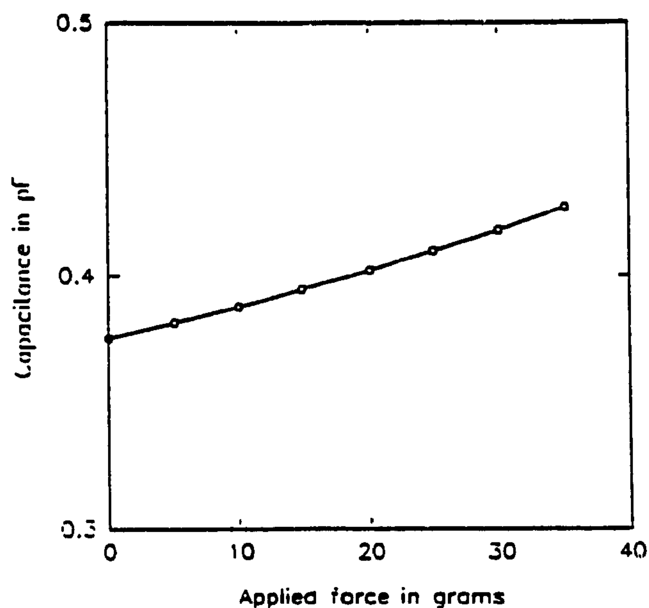

Figure 2.6a Analytical results of capacitance as a function of applied force on each sensor element in 5x5 array tactile imaging sensor.

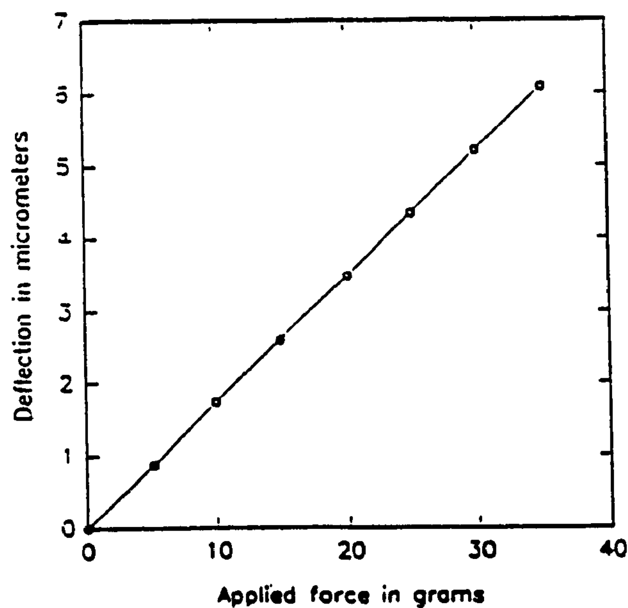

Figure 2.6b Analytical results of deflection of membrane with respect to applied force in (Regime - I) for each sensor element in 5x5 array tactile imaging sensor.

The aforementioned design problems can be solved by using a combination of silicon thin film sensing material, micromachining technology, integration of sensor elements in an array and selecting appropriate read-out electrical circuitry. The overall goal is to explore the practical performance of capacitive type tactile imager principle for robotic applications. The graph in Figure 2.6a illustrates the simulated analytical results of capacitance as a function of pressure for each sensor element. The calculated value of deflection as a function of pressure of the touch sensitive membrane is shown in Figure 2.6b.

2.6.1 Shape recognition

Tactile sensors are devices that provide local surface geometry information of objects, by coming in physical contact with them. These sensors detect the pressure distribution caused by the object surface Here, we have presented a tactile sensor with a pressure sensitive membrane which deforms corresponding to the object shape The distribution of membrane displacement is read as change in capacitance (C_X - C_O) of each sensor element. Thus by measuring the capacitance of each sensor in the array the shape of the object can be analyzed. The capacitance response of each sensor element corresponding to different geometric objects placed on the tactile sensor is schematically illustrated in Figure 2.7.

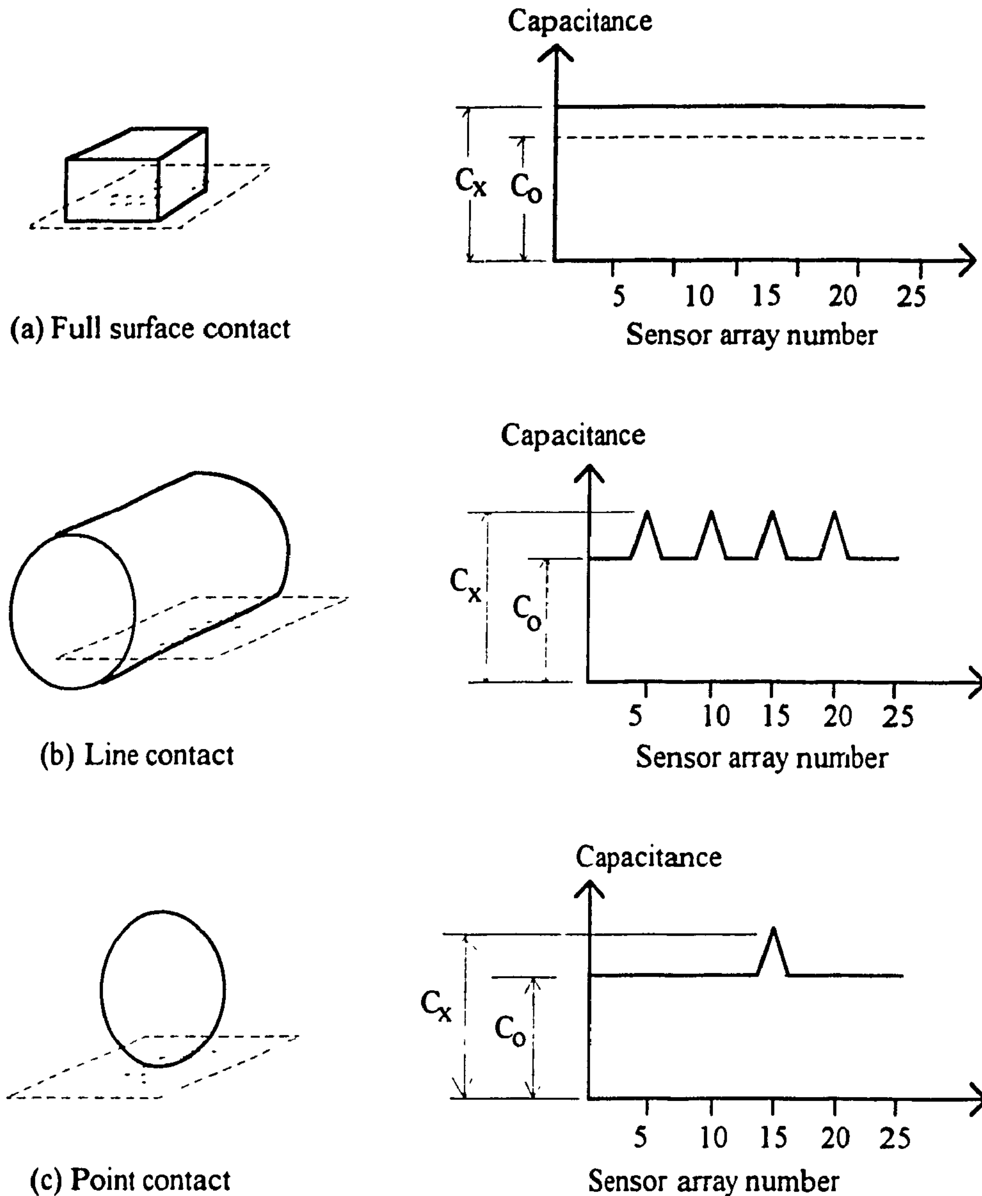

Figure 2.7 Schematic representation of capacitance response of each sensor element corresponding to different geometric objects placed on the tactile sensor.

The optimal thickness for the touch-sensitive membrane selected for the 5x5 array tactile imaging sensor from the fabrication and design considerations point is 15μm. Each sensor has a diameter of 1000μm and the gap between the two parallel plates is 15μm. Although the radius and gap between the two parallel plate capacitor influence the performance, the pressure range is set primarily by the thickness of the sensing element.

This type of capacitive sensor is potentially good for force feedback and tactile imaging mainly because of its outstanding sensitivity, wide dynamic range, good linearity, low hysteresis and low temperature error. The optimized dimensions for the tactile sensor, depending on the existing fabrication technology and design constraints of rupture pressure and sensitivity, are found to be as tabulated in Table 2.3. Table 2.4 presents the analytical results for each element in the tactile sensor array:

Table 2.3 Calculated performance characteristics of tactile imaging sensor

Array size	5 x 5
Diameter of bottom electrode	900 μm
Diameter of the silicon membrane (2*a*)	1000 μm
Thickness of silicon membrane (*H*)	15 μm
Thickness of dielectric (air gap) (*d*)	15 μm
Zero Pressure Capacitance (C_0)	0.3755 pF
Maximum Pressure Capacitance (C_{max})	0.4274 pF
Maximum operating Pressure (P_{max})	4.32×10^5 Pa/element
Maximum operating force range	35 gm/element
Type of Silicon Wafer	15 μm thick, P-type, <100> orientation
Type of Glass wafer	760 μm thick, Pyrex # 7740
Rupture Pressure (P_r)	4.32×10^5 Pa/element
Sensitivity (S)	9.724 fF/Bar

Table - 2.4 Analytical results of tactile imaging sensor
(a=500 μm, d=15μm, H=15μm)

Applied load	Maximum deflection of membrane	capacitance
x 10^5 Pa (gmf)	μm	pF
0.0000 (0)	0.0	0.3755
0.6245 (5)	0.8693	0.3816
1.2490 (10)	1.739	0.388
1.8740 (15)	2.608	0.3948
2 4980 (20)	3.477	0.4021
3.1230 (25)	4.347	0.4099
3.7470 (30)	5.216	0.4183
4 3720 (35)	6.085	0.4273

Chapter - 3

Characterization of Micromachining Techniques: Anodic Bonding and Electrochemical Discharge Drilling

This chapter presents a detailed analysis of micromachining techniques like anodic bonding and electrochemical discharge drilling which were used for the fabrication of the capacitive sensors Micromachining is a term generally applied to denote fabrication techniques that were originally developed for the microelectronics industry in order to make wide range of three dimensional structures [46] The results obtained from the experimental study conducted for these techniques are also presented in this chapter

3.1 Anodic Bonding

Anodic bonding is a simple and rapid method of making reliable, strong hermetic bonds between glass and metal at relatively low temperatures. The advantages of this type of bonding are that the surfaces remain solid during the sealing process, no adhesives or fluxes are used and no macroscopic distortion of glass takes place The technique of anodic bonding is applicable only when the following conditions are met [42]

1. At least one of the two parts to be bonded should act essentially as a solid electrolyte at the bonding temperature.
2. The surface of glass to be bonded should be depleted of mobile ions when a dc voltage is applied
3. The two materials to be bonded should have reasonably matched thermal expansion to avoid cracking when it is cooled in atmosphere after bonding

3.1.1 General

Certain micromechanical systems such as microsensors and microactuators employ anodic bonding to bond the flexible silicon part on to other parts which may be considered to be relatively rigid The aim of this process is to build multi-layer micromachined devices. Here we have performed an experimental study to prove that the quality of anodic bonding is superior when compared to other types of bonding like epoxy bonding. For this purpose, the dynamical characteristics of anodically bonded silicon-glass structures with different bond lengths were tested and compared with epoxy bonded structures. The dynamic characteristics of the flexible part are dependent on the prevailing boundary conditions. The natural frequencies of a silicon cantilever beam anodically bonded to a Pyrex glass base are measured for different lengths of the bonded portion in the beam, keeping the beam length constant Measurements are also taken on a similar silicon cantilever beam bonded to the glass using epoxy bonding. The experimental setup and the results are presented in this section.

Many micromechatronic devices such as sensors and actuators employ flexible silicon components which deflect in proportion to the external stimulation. The dynamic characteristics of such components are significantly influenced by the boundary conditions. Anodic bonding used in a micromachined device like capacitive pressure sensor is shown in Figure 3.1 and 3.2. Figure 3.1 (magnification x60) shows a silicon membrane with bonding defects. When subsequent processes (like etching) are performed on such bonded structures the bonding becomes weaker changing the dynamic characteristics of the membrane. The photograph in Figure 3.2 shows the ruptured membrane after etching in KOH.

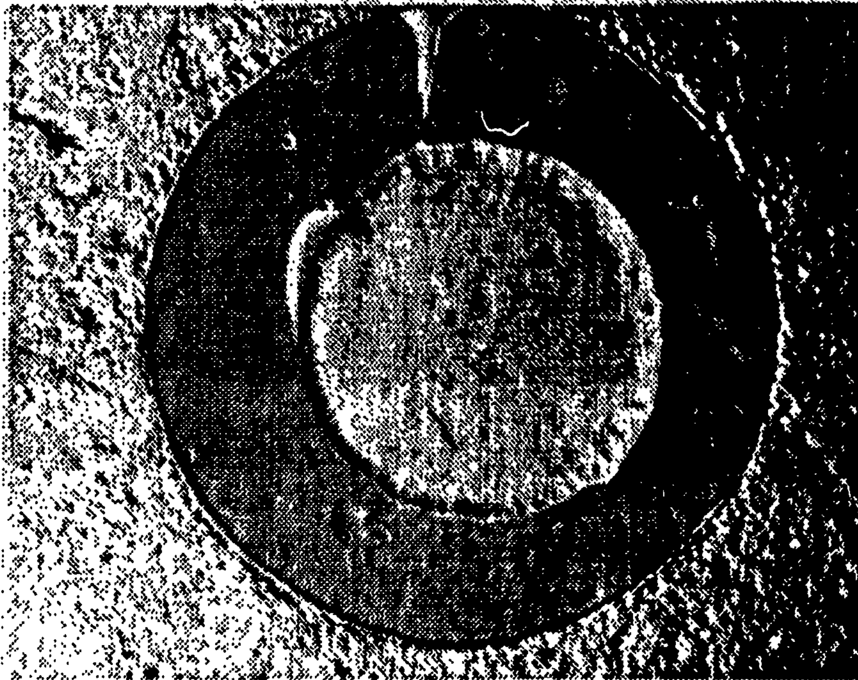

Figure 3.1 Photograph showing the silicon membrane anodically bonded to glass substrate with bonding defects (x 60 magnification).

Figure 3.2 Photograph showing the ruptured silicon membrane (same membrane of Figure 3.1) after etching in KOH (x 60 magnification).

It has been well established [48] that the electric field in glass causes a drift of positively charged alkali (Na+) ions at elevated temperatures around 300-350°C. At this temperature, the mobility of impurities present in glass are enhanced which in turn reduces the time required for the formation of space charge region. The time-varying potential distribution as a function of position in the glass wafer is shown in Figure 3 3. After the Na+ ions have drifted towards the cathode, most of the potential drop in the glass occurs at the surface next to the silicon. In the case of silicon, it is observed that every silicon surface exposed to an oxidizing ambient has at least 1 5 nm of native oxide. Thus, by proper cleaning (as mentioned in Appendix - II), the surface of silicon can be terminated in silanol (Si-OH) bonds which exhibit hydrophilic behavior necessary for anodic bonding (as shown in Figure 3.4).

Anodic bonding can be successfully performed with metals and alloys whose thermal properties match with those of commercial glass Seals have been successfully made to tantalum, titanium, kovar, niromet44 and to semiconductors like silicon, germanium and gallium arsenide [43] In 1968, Pomerantz discovered that an electrostatic field between a metal foil and a sheet of glass produced strong bonds between them at a much lower temperature than required for simple thermal bonding of metal and glass [44] The primary requirement for a good glass-metal seal is that the glass and metal parts must be brought into intimate contact. For ideal surfaces which are perfectly planar and clean, intimate surface contact is easily achieved. If the surface is not clean then surface contact will occur only at a few isolated points because of non-planarity and contamination with solid particles [45] Therefore, a perfectly planar and clean surface is required to achieve a good bonding.

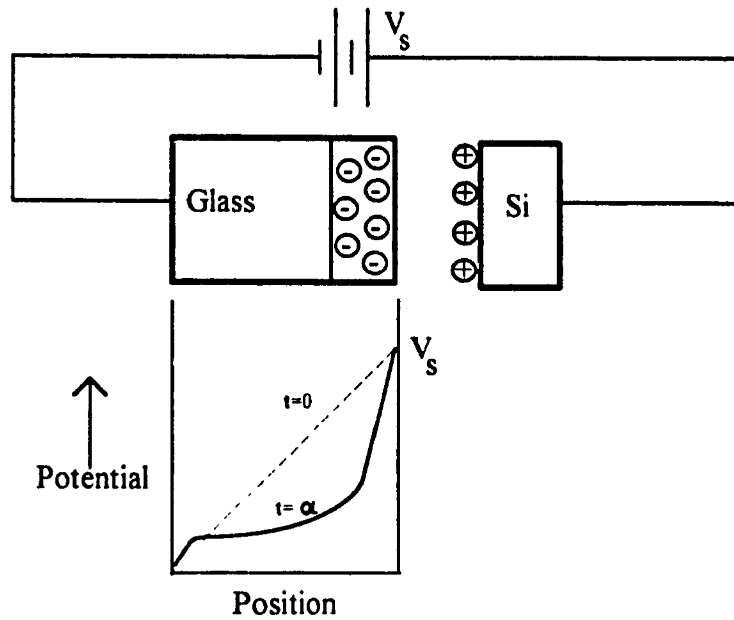

Figure 3.3 Initial and final equilibrium potential distributions across the glass during anodic bonding [47].

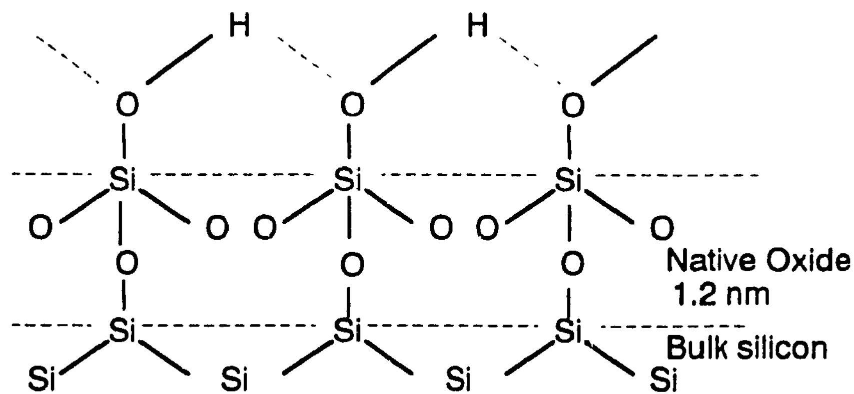

Figure 3.4 The hydrophilic Si surface [46].

3.1.2 Principle

Anodic bonding occurs due to the electrostatic attraction between the glass and silicon wafers. At elevated temperatures (below the softening point of glass), the positive sodium ions in the glass becomes quite mobile and they are attracted to the negative electrode on the glass surface where they are neutralized. The more permanently bound

negative ions in the glass are left, forming a space charge layer in the glass adjacent to the silicon surface After the Na+ ions have drifted towards the cathode, most of the potential drop in the glass occurs at the surface next to the silicon. The two wafers then act as a parallel plate capacitor with most of the potential being dropped across the several micron wide gap between them. The resulting electric field between the surfaces serves to pull them into contact with a force of approximately 2.41 x 10^6 N/m^2 (350 psi) for E_p=3 x 10^{-6}V/cm [47] Once the wafers are in contact, almost all of the applied potential is dropped across the space charge layer in the glass The extremely high fields which develop in that region transport oxygen out of the glass to bond with the silicon surface The anodic bonding appears to be chemical in nature and possibly a very thin layer of SiO_2 layer is formed at the interface[47].

3.1.3 Residual Stress in Anodically Bonded Silicon-Glass Structure

The residual stress in anodically bonded structures results due to mismatch in thermal expansion coefficient of the materials Residual stress is a major cause of long-term drift in the performance of the device Therefore, it is very important to choose the best material and bonding parameters in order to minimize residual stress. Corning #7740 Pyrex glass and silicon have closely matched thermal expansion properties at lower temperatures (<350 ^oC), as shown in Figure 3.5, and can be bonded anodically. A study conducted by Ko et al [47], revealed that the residual stress due to bonding between the two materials can be minimized when bonded at temperatures in the range 300 - 350°C. They observed that above 450°C there is a drastic increase of thermal expansion coefficient for glass compared to silicon.

Experiments conducted on anodic bonding at different temperatures concluded that at low temperature (< 250°C) the substrates does not bond together and at high temperatures (>450°C) the thin silicon wafer was spoiled while cooling in atmosphere

Therefore, for this experimental study, anodic bonding was performed at 350°C with applied voltage of 1000 V.

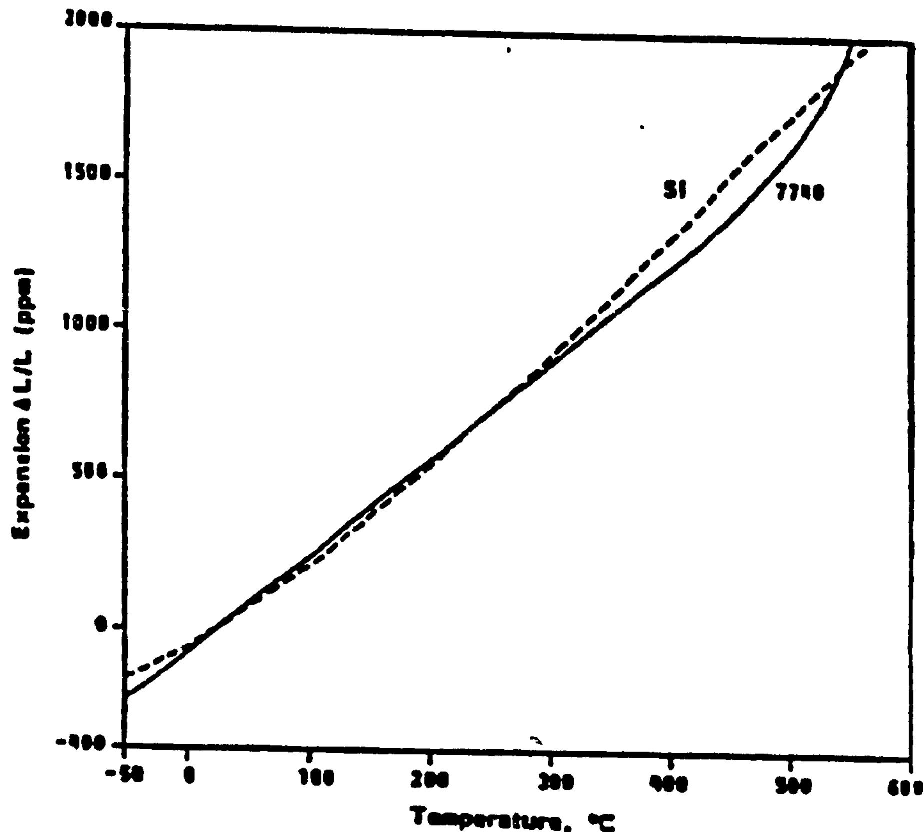

Figure 3.5 Thermal expansion properties of # 7740 Pyrex glass and single crystal silicon [47].

3.1.4 Characterization of Anodically Bonded Silicon - Pyrex Glass Structures.

The bond strength of anodically bonded structures was evaluated using the Crack propagation method by Kendall et al [46]. This technique involves forcing a knife edge between the bonded wafers. The surface strength (bond strength) is proportional to y^2/L^4, where y is the thickness of the knife edge and L is the length of the resulting crack. Esashi et al [48] used a tensile test to evaluate the bond strength in anodically bonded structures. In this method the bond strength is measured by applying a tensile load on the silicon wafer keeping the glass wafer fixed to a rigid support. They also performed a similar test

determining the bond strength of a Si-Si bonding using sputtered glass film and the bond strength was found to be greater than 1.5 MPa The experiments conclude that the bond strength depends on the surface roughness and impurities present on the surface Stefan Johansson et al [65], performed a three-point test for small beams and reported a fracture limit of 220±70 MPa for field assisted bond seals between silicon and Pyrex glass. The above tests evaluated the bond strengths of bonded structures.

The purpose of the present work is to determine the nature of boundary conditions in silicon structures anodically bonded to glass. The characterization of the boundary conditions of anodically bonded silicon-glass structures helps in understanding the boundary conditions pertaining to this technique. For this purpose, silicon cantilever beams with different lengths, bonded to Pyrex (# 7740) glass base were used as test structures The natural frequency of these cantilever beams were measured and the results are presented and discussed.

3.1.4.1. Vibration Analysis of Resonant Micro mechanical Structures

The vibration analysis of beams has been a subject of great interest in the industrialized world. The solutions for lateral, torsional and longitudinal vibration of high speed equipment are essential for proper design. The lateral free vibration of beams can occur in an infinite number of mode shapes, referred to as mode, and that each modal shape has a discrete frequency associated with it. The first or fundamental mode is the mode associated with the lowest frequency.

The vibration analysis of micromechanical devices follows the classical theory of vibration used for macro structures. In this paper we have considered cantilever beams of different bond lengths anodically bonded to glass substrates Even though bonding only on one face does not imply a fully clamped condition, it is meaningful to compare the results for the fully clamped structure. The natural frequency of a clamped cantilever silicon wafer

is given as [49]:

$$f_o = 3.494\frac{H}{l^2}\left(\frac{E}{12(1-\nu^2)\rho}\right)^{\frac{1}{2}} \tag{3.1}$$

where H is the thickness, l is the length of the wafer, E is Young's modulus of elasticity, ν is the Poisson's ratio, and ρ is the mass density.

It has been observed by Lagowski et al [49] and Gustafsson [50] that semiconductor cantilever beams encounter a non-classical behavior when the thickness is reduced to tens of micron The model of Lagowski et al predicts that the surface energy has a strong impact on the resonant properties The influence of surface energy is based on the fact that small variations in surface area occur upon bending, thereby modifying the potential energy of the system. The resulting expression for the resonant frequency f_r is

$$f_r = f_0\left(1-\frac{12\sigma_s\nu}{EH}\right)^{\frac{1}{2}} \tag{3.2}$$

where σ_s is the surface energy which is of the order of 0.8-1.8 $j.m^{-2}$ [50] It is clear that the surface energy is important only when the thickness approaches atomic dimensions.

3.1.4.2 Experimental Setup

P-type (boron doped) <100> silicon wafer of 0.32 mm thickness is cut into long strips of varying lengths from 74 mm to 55.2 mm. A strip of silicon is selected and bonded onto the glass. The glass is Pyrex type (# 7740) and its chemical composition is:

SiO_2 - 81 %, Li_2O_3 - 2 % B_2O_3 - 13 % and Na_2O - 4 %

The coefficient of thermal expansion for Pyrex glass is given as 32 5 x 10^{-7} /°C and that of silicon is 35 x 10^{-7} /°C. The bonding surfaces of the glass and silicon are mirror grade polished (surface roughness less than 400 Å). The fabrication is carried out in a clean room (class 5000). The silicon and glass wafers are cleaned using the standard cleaning procedure used for the fabrication of micromachined structures. The wafers are

then dried using a nitrogen gun. The fabrication setup is as shown in Figure 3.6. The silicon strip is placed on a flat metal base which acts as the anode. The metal base is placed on a hot plate. The glass wafer is placed on top of the silicon wafer and the temperature of the hot plate is set at 350°C. A point electrode is placed on the glass which forms the cathode. The weight of the point electrode is around 0.20 N. The silicon and glass wafers are aligned to the required bond length and then allowed to reach steady state with respect to the hot plate. The time required for reaching steady state is around 7-8 min. Once steady state is reached, a dc voltage in the range of 1000 V -1100V is applied between the wafers The time for bonding is around 5 -10 minutes After bonding the assembly is allowed to cool in atmosphere.

The experimental setup for the determination of the natural frequency is as shown in Figure 3.7. The test structure is mounted on a electro-dynamic shaker (B & K type 4810). A sweep sinusoidal signal, with a frequency range of 0 Hz - 200 Hz , was provided by an external oscillator. The frequency of excitation is selected in such a way that it includes the natural frequency of the silicon cantilever beam. The response was measured using a microphone (B & K type 4181). The microphone was held close to the test structures and the output is analyzed using a frequency analyzer.

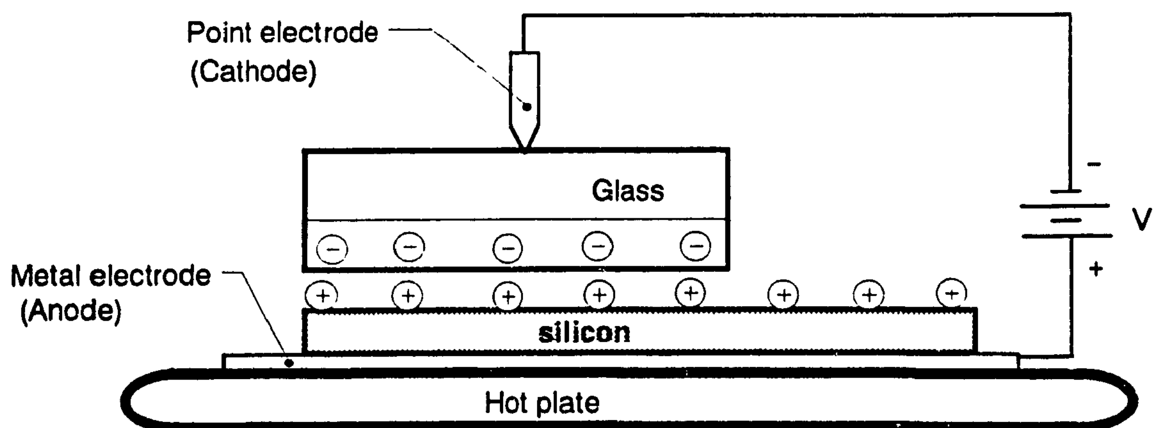

Figure 3.6 Schematic representation of anodic bonding apparatus [48].

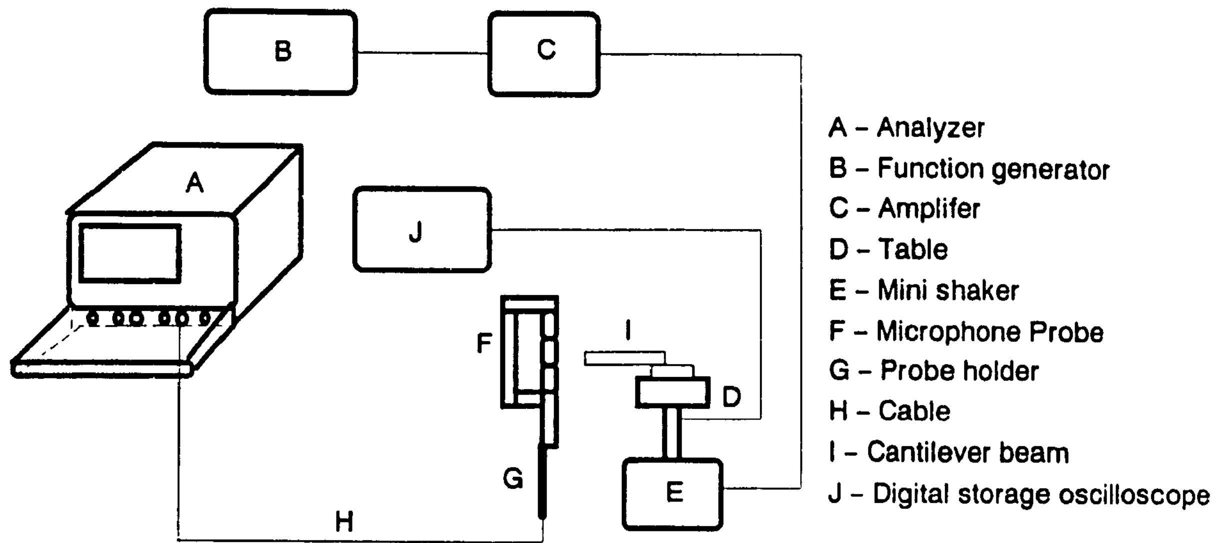

Figure 3.7 Schematic representation of anodic bonding characterization apparatus.

3.1.5 Results and Discussion

The tests were conducted to obtain the frequency response and hence the natural frequency of the cantilever beams under different bond length conditions Determination of natural frequency of such test structures forms a non-destructive method to compare the boundary conditions and quality of bonding for different bond length A schematic representation of silicon-glass bonded test structure is illustrated in Figure 3 8 Initially, the background noise level in the laboratory was measured The frequency response of the cantilever beam with a bond length of 22.2 mm along with the background noise is shown in Figure 3.9 in the frequency range from 0 to 200 Hz The sound response from the beam is clearly seen to be much higher compared to the background levels The natural frequency of the beam is seen to be at 152 Hz The results for the natural frequency with different bonded lengths for the same cantilever beam are shown in Table-3.1. It can be seen that the natural frequency is not affected by the bond lengths considered. The frequency response curve in the frequency range of 100 - 150 Hz for an anodically bonded test structures having bond lengths of 22.2, 10.0 and 3.4 mm length is shown in Figure 3.10.

Tests were also carried out on silicon cantilever strips bonded to glass bases with epoxy bonding for comparison with anodically bonded assembly. The epoxy used for the experimental study was scotch VHB (Very High Bonding) acrylic adhesive suitable for bonding variety of substrates including metals and glass[71]. The results for two bond lengths of epoxy bonded structure are tabulated in Table-3.2 and the frequency curve is shown in Figure 3.11 It was observed that the natural frequencies are affected significantly by varying the epoxy bond lengths.

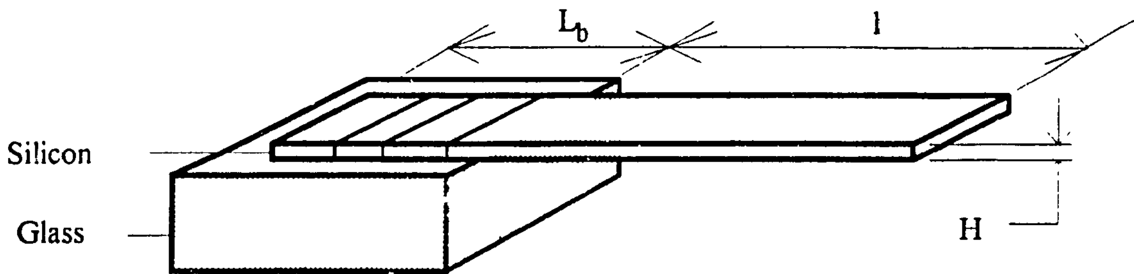

Figure 3.8 Schematic representation of anodically bonded test structure.
(L_b - bond length, l - free length of cantilever and H- thickness of silicon wafer)

Table - 3.1. Natural frequency of anodically bonded structures

Bond length in millimeters	Natural frequency in Hz. (Measured)	Natural frequency in Hz (Calculated for clamped condition)
22 2	152	176 394
18 3	152	176.394
10 0	152	176 394
7.3	152	176.394
5 8	152	176.394
3 4	152	176.394

Table - 3.2. Natural frequency of epoxy bonded structures

Bond length in millimeters	Natural frequency in Hz (measured)	Natural frequency in Hz. (Calculated for clamped condition)
22 2	125.5	176.394
10.0	120 0	176.394

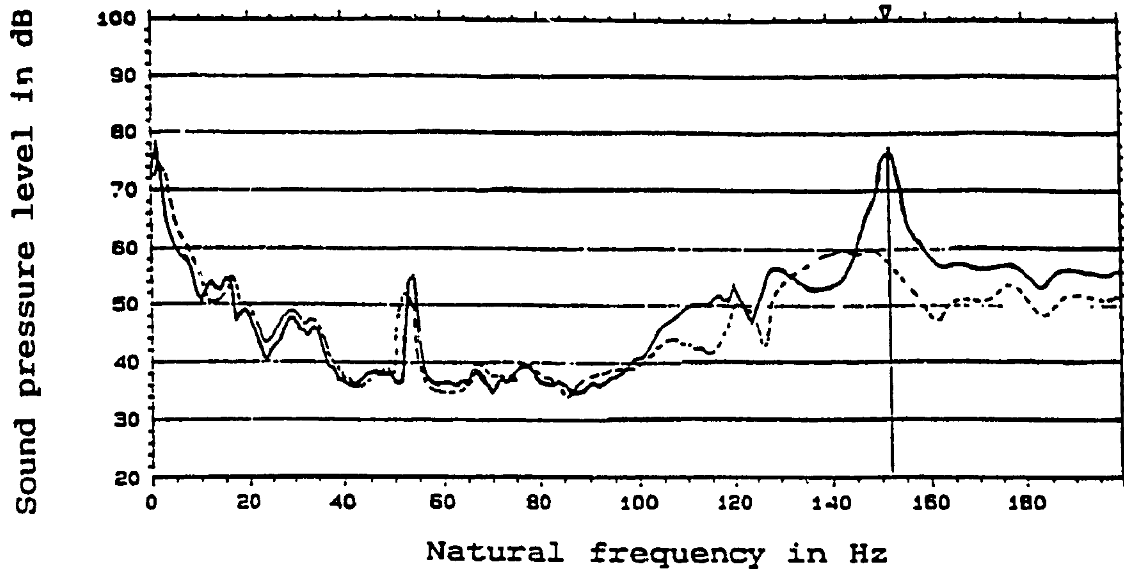

Figure 3.9. Frequency response of anodically bonded silicon cantilver beam.

------- Frequency response of sound signal in the laboratory.

_____ Frequency response curve for 22.2 mm bond length.

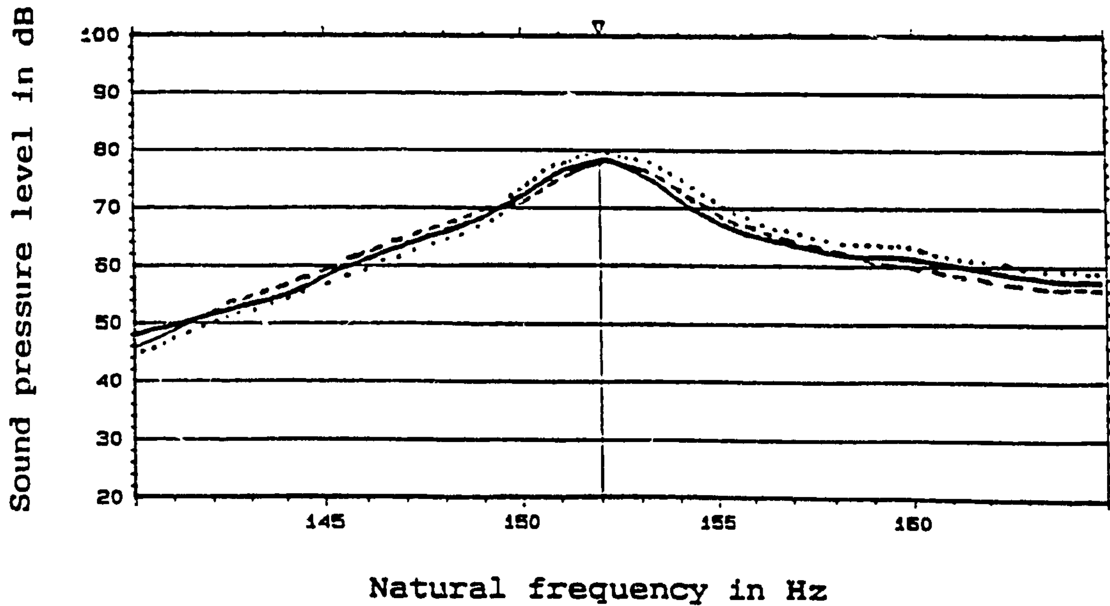

Figure 3.10 Natural frequency curve for anodically bonded silicon cantilever beam for 22.2 mm, 10.0 mm and 3.4 mm bond length.

_____ Frequency response curve for 22.2 mm bond length.

------- Frequency response curve for 10.0 mm bond length.

.... Frequency response curve for 3.4 mm bond length.

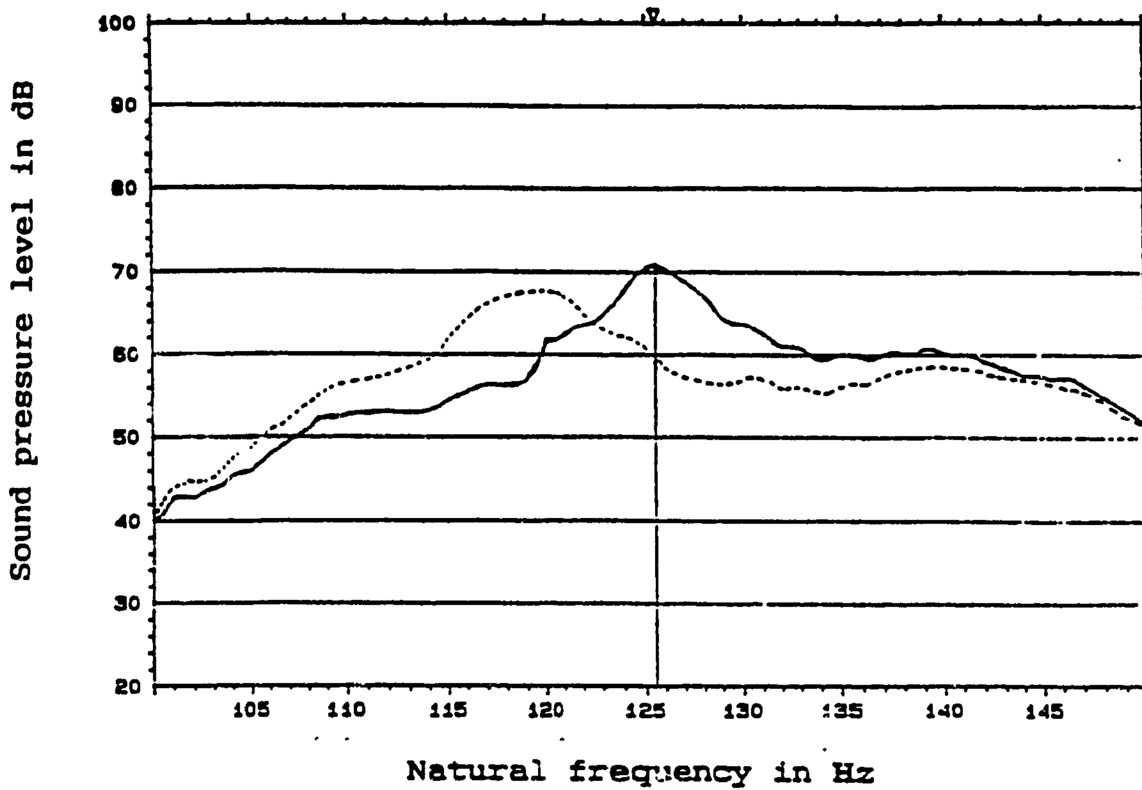

Figure 3.11 Natural frequency curve for epoxy bonded silicon cantilever beam for 22.2 mm and 10.0 mm bond length.

_____ Frequency response curve for 22.2 mm bond length.

-------- Frequency response curve for 10.0 mm bond length.

3.1.6 Conclusions

The natural frequency of silicon cantilever strips anodically bonded to a glass base are measured. For comparison purpose, cantilever strips bonded to glass base using epoxy bonding were also tested. The results show that for the range of bonded lengths considered in the test, the natural frequencies are not be affected by the bond length. The measured frequency was lower than that corresponding to theoretically computed results

with clamped conditions. However the cantilever strips bonded to glass base using epoxy bonding showed significant change in the natural frequency with changing bond lengths Therefore, the results of the experimental study can be summarized as the glued bonding, which is normally used to bond silicon with glass in packaging microelectronic devices, is inferior in strength and performance compared to anodic bonding This type of non-destructive testing can be carried out further to determine the optimal anodic bond length for micro mechatronic devices

Anodic bonding solves major problems like packaging and long term stability of miniature pressure transducers Earlier studies have shown that the major cause of long-term drift in the device is not related to the sensor design or processing, but rather to the assembly and packaging of the device The thermal stresses developed by thermal expansion during the sealing process appears to be the major cause of baseline drift. Therefore, choosing the right technique and the right material to seal the device is an important consideration in micromachining technology

3.1.7. Application of Anodic Bonding

Bonding of one surface to another is one of the important steps in the fabrication of microsensors Since the silicon chip will be used in exposed, hostile and potentially abrasive environments, it is often necessary to use mounting techniques substantially different from the usual packaging methods like eutectic solder, epoxies, polyamides and ceramics. Electrostatic bonding of glass or other ceramic materials to metal and semi-conductors fulfill many of the requirements for bonding and mounting micromechanical structures. In IC circuit packaging, this technology can be used to bond the IC die to the lead frame and as a final seal for hermetic packages The attachment of the die to a package substrate serves the purpose of providing a mechanical support, a thermal path and sometimes an electrical contact. Hermetic packages are used to protect or isolate the

IC chip from hostile environment. Anodic bonding can be used in the fabrication of silicon sensors, e.g. pressure sensors, solar cells etc. to bond silicon to glass.

3.2. Electrochemical Glass Drilling

3.2.1 General

Electrochemical discharge drilling is a electro-discharge process of etching narrow through holes or an indentation in glass. The important parameters to be controlled are the concentration of electrolyte, applied voltage and the force applied on the needle. The application of this process in micromachining is to make leak free electrical feed through and as a vent to apply pressure on the silicon membrane. The dimensions of the hole are limited by the dimensions of the needle electrode which is generally around 200μm. The electrolyte used is either NaOH or KOH (35 wt. % to 50% wt) and the voltage around 36V (dc). The applied force to the needle is about 0.2 N (20 gmf) [6]

3.2.2 Principle

A schematic diagram of electrochemical drilling apparatus is shown in Figure 3 12. The glass is placed in an alkaline hydroxide (NAOH or KOH) solution. A metal needle is placed on the glass and a force of 0.2 N (20 gmf) is applied on it A negative voltage is applied on the needle while the solution is kept at the ground potential by a reference electrode. When the peak voltage is over 36V, electric discharge takes place at the tip portion of the needle The temperature of the solution around the needle is elevated locally by the electrodischarge energy, and the glass at that point is removed by thermally accelerated chemical reaction. A stainless steel needle of about 30μm tip diameter is used to drill glass.

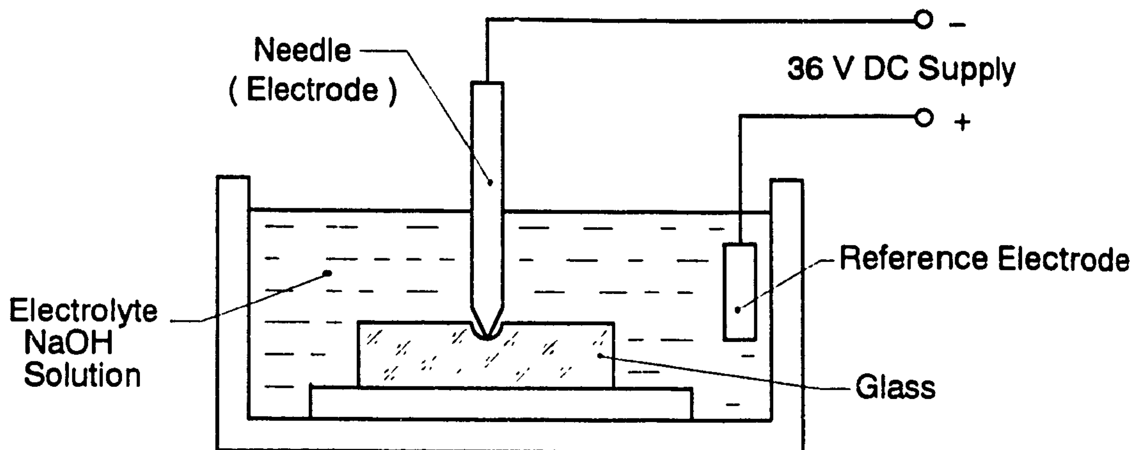

Figure 3.12 Principle of electrochemical glass drilling apparatus.

3.2.3 The Drilling Process

A drilling apparatus was designed and fabricated for precision drilling of holes in glass. The schematic representation of an electrochemical glass drilling apparatus is illustrated in Figure 3.13 and a photograph of the device is shown in Figure 3.14 The glass is placed inside a beaker with electrolytic solution which is placed on the x-y table of the machine. The x-y table can be maneuvered precisely (within 10μm radius) thereby drilling holes at the desired location on the glass A needle, which is used as the positive electrode is inserted into the vertical holder held on top of the beaker The needle can be moved up and down and it is held by two springs so that the required force can be precisely applied on the glass. A calibrated dial gauge is fitted on to the vertical holder which measures the applied force on the glass.

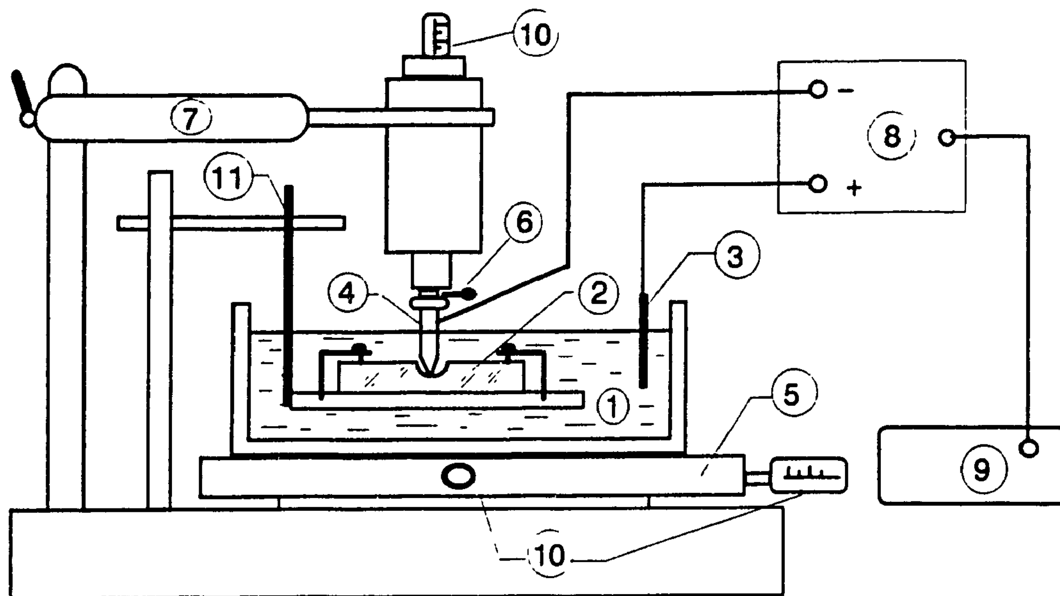

1. Electrolyte (NaOH)
2. Glass Wafer
3. Positive Electrode
4. Negative Electrode
5. X-Y Table
6. Dial Gauge
7. Needle Holder
8. Control Switch with Stop Clock
9. D.C. Power Supply
10. Vernier
11. Glass Holder

Figure 3.13. Schematic representation of electrochemical glass drilling apparatus.

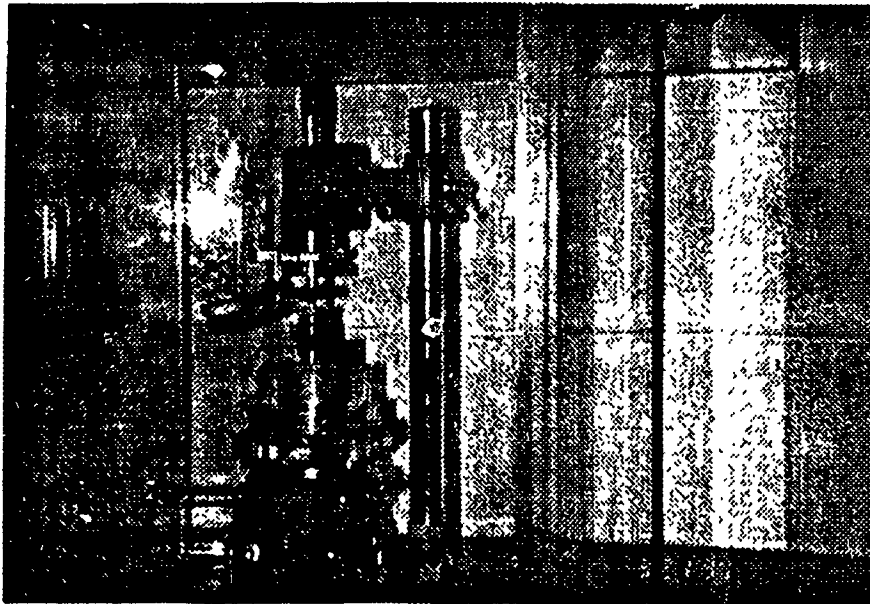

Figure 3.14 A photograph of the electrochemical glass drilling apparatus.

3.2.4 Procedure

The glass wafer to be drilled is placed and held tightly on to a wafer holder which is placed inside the beaker containing the electrolyte The vernier on the x-y table is used to move the beaker below the drilling needle The needle is now gently brought down using the knob which has a vertical sliding motion. Once the needle just touches the glass, the dial gauge starts indicating. Now the vernier on top of the needle holder is moved downwards to apply the desired load on the glass Once the load is applied the electric supply is switched on A control switch with a timer placed in the circuit provides the electric supply for the required time for drilling

3.2.5 Experimental Results of Electrochemical Drilling

Electrochemical drilling is used to drill through holes of about 200μm diameter in glass wafers of varying thickness in the range from 300 - 1500μm The experimental results of drilling time for different glass thickness (in the range 300 - 1500μm) is illustrated in Figure 3.15. It can be observed from the figure that, the drilling time saturates with increase in glass thickness (i e , thickness between 1400 μm and 1500 μm) in the measured regime. It is assumed at this stage of the research that the drilling time might increase with further increase in glass thickness above this regime

An empirical formula for the calculation of drilling time (t_d, in minutes) for different glass thickness (H_g, in millimeters), in the range 300μm - 1500μm, found to be in close agreement with the experimental data is mathematically written as:

$$t_d = \left(c_1 + c_2 \frac{\ln H_g}{H_g} \right)^{-1} \qquad (3.4)$$

The constants for the above equation were found to be $c_1 = 0.075$ and $c_2 = -0.03$.

To get very high reproducibility the parameters to be controlled are the

concentration of electrolyte, applied voltage and the force applied on the needle. From the experimental study conducted for electrochemical discharge drilling, the optimal conditions are summarized as follows:

(a) Concentration of electrolyte = 35%

(b) Applied voltage = 36 V (DC)

(c) Force applied on the needle electrode = 0.20 N

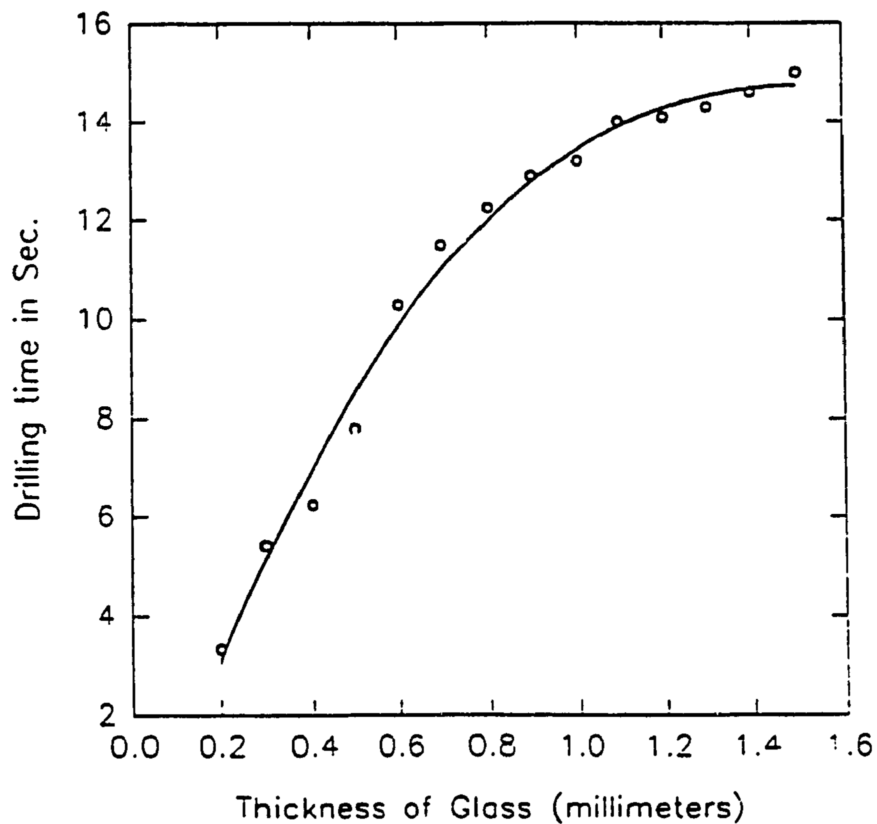

Figure 3.15 Drilling time vs glass thickness in the range 300μm - 1500μm.

3.2.6 Application of Electrochemical Discharge Drilling

The application of this process in micromachining is to make leak free electrical feed through and as a vent hole for applying pressure on pressure sensitive membranes as illustrated in Figure 3.16. The conical shape of the hole is suitable for metallization

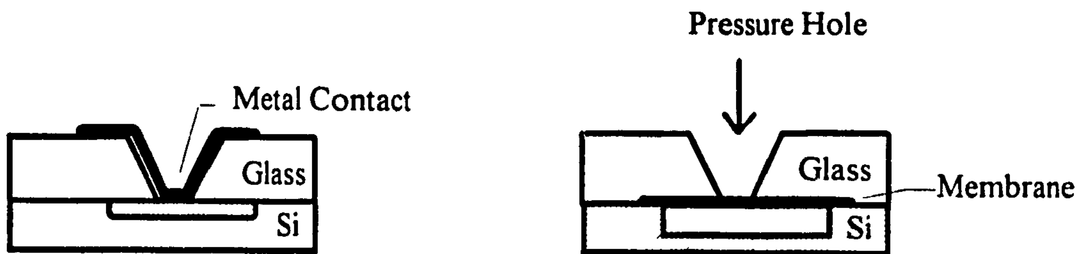

Figure 3.16 Two applications of electrochemical drilling in micromachined devices.

Chapter - 4

Process Design and Fabrication

Silicon microfabrication technology has been a key factor for the rapid development of microsensors and microactuators. A variety of precise three dimensional microstructures can be fabricated such as diaphragms, bridges, cantilever beams, needles, gears, springs, grooves, orifices, pyramids, complex mechanical suspensions, linkages and micromotors [52]. This chapter covers the process design and fabrication details of a capacitive type pressure measurement sensor fabricated using standard integrated circuit (IC) photolithography techniques and micromachining techniques The experience achieved during the successful fabrication of the pressure measurement sensor has motivated the design and fabrication of a tactile imaging sensor using the same design principles. The process design and fabrication details of the tactile imaging sensor is also presented in this chapter.

4.1 Capacitive Pressure Measurement Sensor

The capacitive pressure measurement sensor chip is a 4 x 5 array glass-silicon-silicon sandwich structure on a 3x3 mm substrate. Batch processing is performed in order to prove the possibility to achieve these type of sensors on large scale. Several etching techniques were experimented with to realize the membrane and the cavity in the top-silicon cover The geometrical size of the sensor is selected from the design calculations performed in Chapter-2. Two sizes (1000μm and 800μm diameter) are considered for the fabrication of the pressure sensitive silicon element The designed diaphragm thickness is 20 μm and the enclosed air gap thickness is 10 μm The cross-sectional view of a single cell capacitive pressure measurement sensor is shown in Figure-4 1.

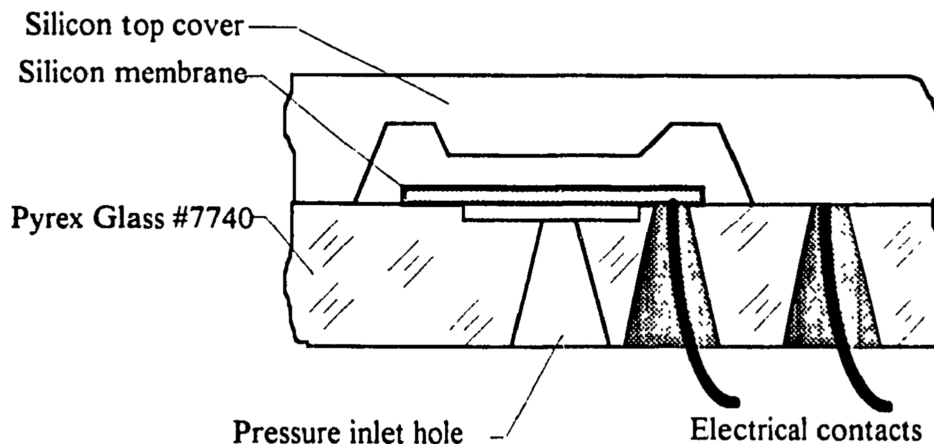

Figure 4.1 Cross-sectional view of capacitive pressure measurement sensor.

4.1.1 Materials Used for Fabrication of Capacitive Micro Sensor

Glass and silicon wafers are the materials used for the fabrication of the capacitive type micro sensor for pressure-measurement The coefficient of thermal expansion of the selected glass should be very close to that of silicon so that they can be anodically bonded to each other. The bonding surface of the glass and the silicon should also be mirror grade polished (surface roughness less than 400Å) Pyrex glass (#7740) which satisfies the above mentioned properties is selected as the sensor substrate material The Pyrex glass (#7740) has a chemical composition of SiO_2 - 81%, H_2O_3 - 2%, B_2O_3 - 13% and Na_2O - 4% Glass having a thickness of 1500 μm and dimension of 30 x 30 mm is selected for the fabrication of the pressure measurement sensor. Single side polished low p-doped (boron) silicon wafers having thickness of 375 μm and <100> orientation is selected for the fabrication of the membrane and top-cover of pressure measurement sensor .

4.1.2 Process Design of Pressure Measurement Sensor

The pressure measurement sensor designed is a three layer structure two silicon layers bonded on a glass wafer. The significant aspect of the transducer process design is that, the fabrication procedure was carefully planned to satisfy the primary objectives of

the geometrical size and pressure range of the sensor The pressure measurement sensor requires six masking steps regardless of its geometric parameters The mask design takes into consideration the size and tolerance required for each masking step The mask drawings (x 5 magnification) required for processing the glass and the silicon wafers are presented in Figures A4 1 to A4 5 of Appendix-IV. The glass and the membrane require only one mask each (Mask-1 and Mask-2 respectively). Three masks (Mask-3, Mask-4 and Mask-5) are required for the top cover. The Mask-5 is the negative of the Mask-3 Mask-6 is used for making metallic contact on the sensor. The masks were prepared using photographic techniques which is presented in Appendix-VII The masking steps involved in the fabrication process is explained in section 4 1 4 of this chapter

The pressure-sensitive diaphragm of the sensor is a flat plate of monocrystalline silicon Initially, electrochemical drilling of glass is performed and then it is anodically bonded to the silicon wafer Later the bonded silicon wafer is etched to realize the membrane The top silicon wafer is etched to have a reference cavity that determines the capacitor plate separation Then the top cover is bonded on to the glass wafer that has the membrane on it The depth of the pattern shaped into the top wafer creates the gap required for pressure measurement The deep etch obtained by etching the ring structure surrounding the insulated top layer creates a larger closed reference volume This ring shaped structure improves the linearity response range of the capacitive sensor

4.1.3 Fabrication Process of Pressure Measurement Sensor

The fabrication process of the capacitive pressure sensor chip is divided into three main streams of the process, each corresponding to a layer of the sensor The device is constructed as a sandwich structure with two silicon wafers anodically bonded to a glass wafer. The sequence of the fabrication process of a single sensor chip is presented in Figure 4.2. The details of each stream of fabrication steps are described below.

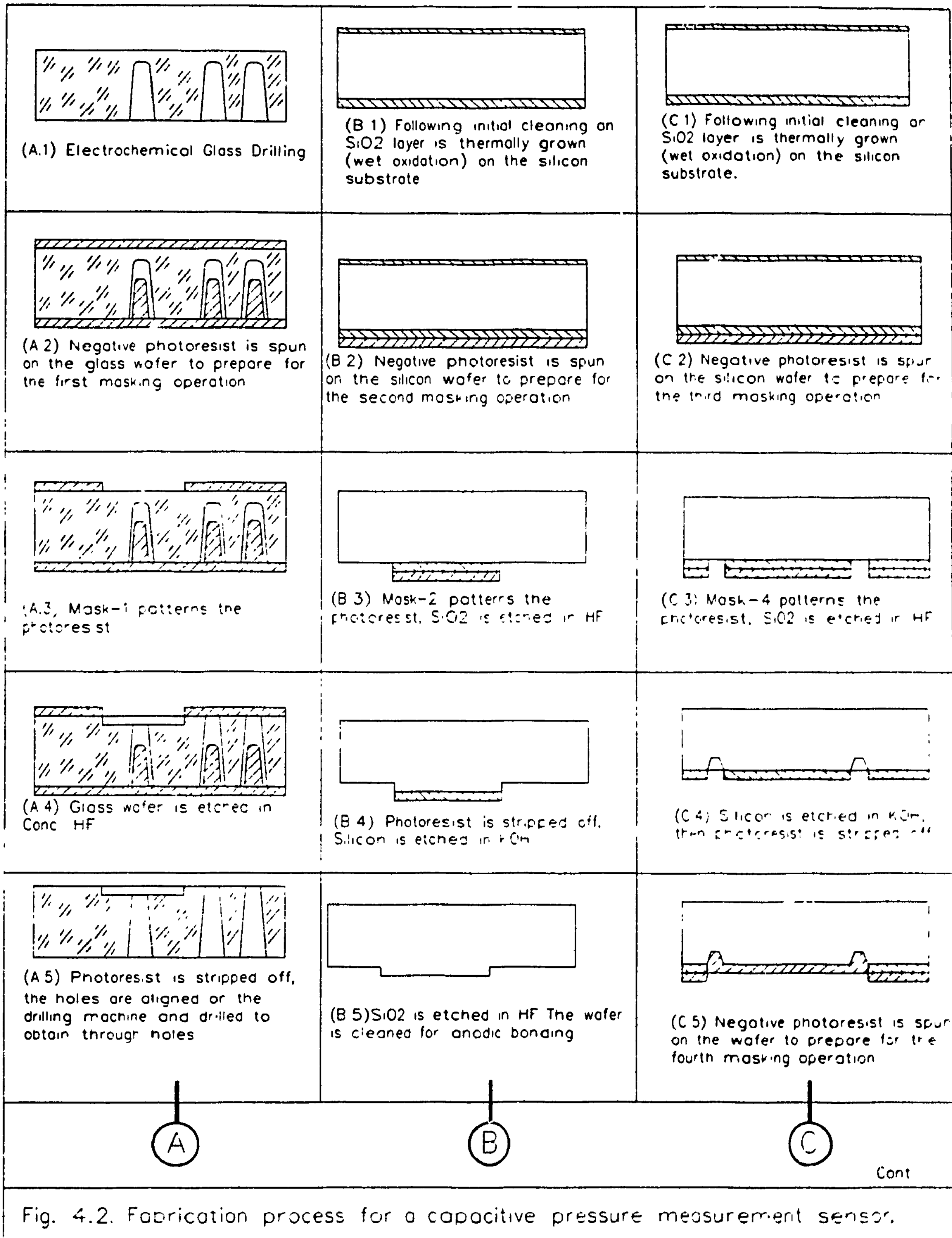

Fig. 4.2. Fabrication process for a capacitive pressure measurement sensor.

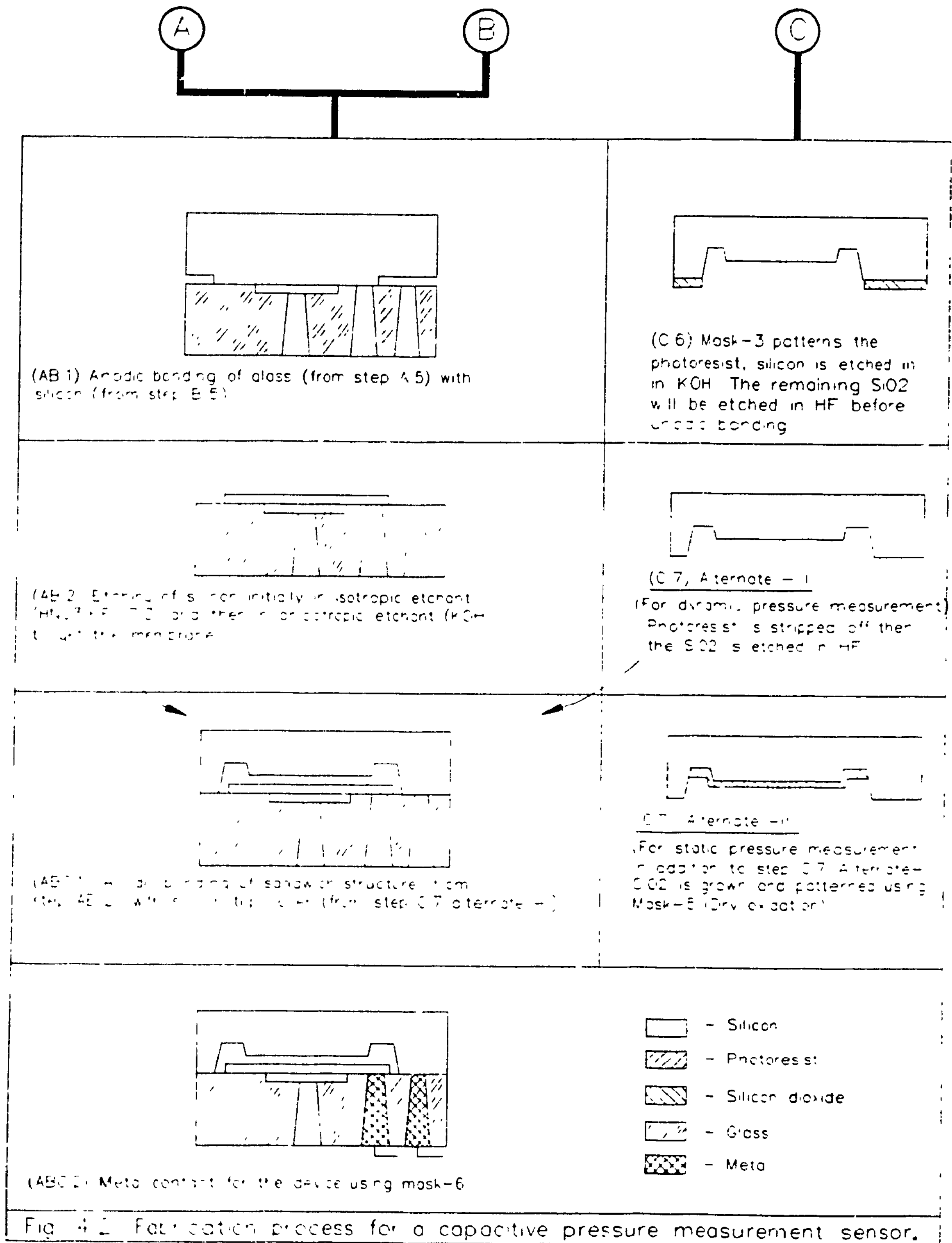

Fig 4.2 Fabrication process for a capacitive pressure measurement sensor.

4.1.3.1 Process A - The Glass Wafer Process

A 30 x 30 x 1.5 mm Pyrex glass wafer is selected as the substrate material which forms a cover for the pressure sensitive silicon diaphragm. Each sensor has three holes drilled using electrochemical glass drilling Two holes are used for electrical metal contact and the central hole is used for pressure inlet The glass wafer is cleaned as mentioned in Appendix-II. After cleaning, a standard photolithography process as mentioned in Appendix-III is performed using mask-1 Positive or negative photoresist were used as masks against HF etchant The photolithography step involves spin coating a layer of photoresist on the wafer, soft baking, exposing to ultra violet (UV) light, developing in developer and finally hard baking After the photolithography steps, the glass wafer is etched in concentrated hydrofluoric acid (HF with 49 % concentration) for 40 sec It was observed that the photoresist was peeled off after 40 sec and for this period the glass was etched to depth of 7 µm Once the photoresist was removed from the masked region of the glass, the etchant attacks the whole surface Once the polished surface of the glass is spoiled by the etchant, it cannot be used for bonding operation The photograph in Figure 4.3a illustrates the smooth glass surface after etching in conc HF, for 30 seconds, to a depth of 5µm. The photograph of the glass when etched more than 40 sec is as shown in Figure 4.3b During this part of the fabrication several tests were conducted to determine the etch rate of HF on glass wafer at room temperature The experimental results are illustrated in Figure 4.4 It was observed that the etch rate of HF on glass for the first minute was 9 µm/min and gradually stabilizes to 4 µm/min. after 6 minutes of etching The glass wafer was then cleaned and the holes were drilled by electrochemical discharge drilling technique. After drilling, the wafer is cleaned as mentioned in Appendix-II and kept ready for the bonding process

Figure 4.3a Photograph of the smooth glass surface after etching for 30 sec. in conc. HF(49%) with positive photoresist as mask (x60 magnification).

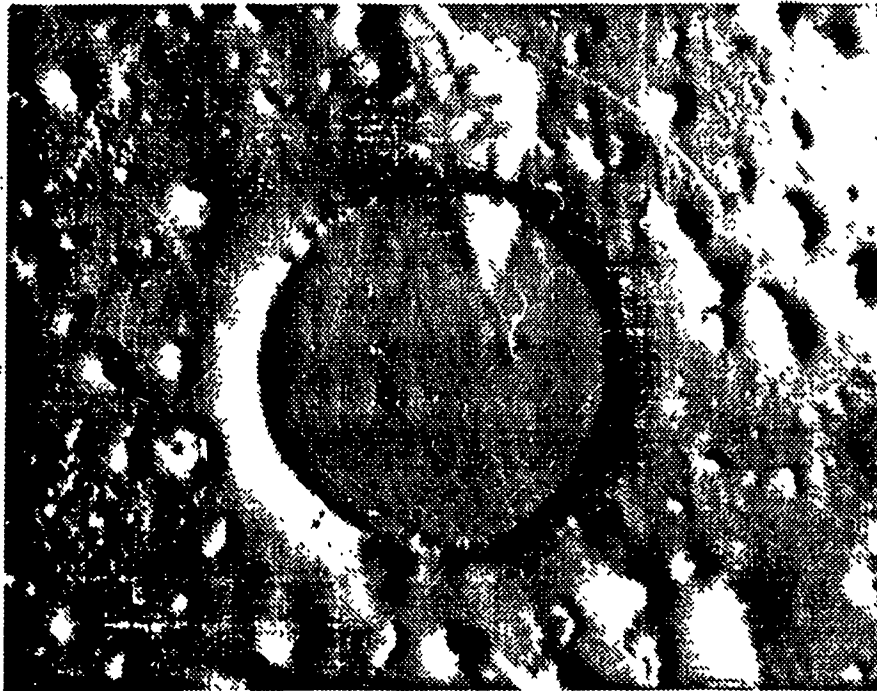

Figure 4.3b Photograph of the spoiled glass surface after etching for 120 sec. in conc. HF(49%) with positive photoresist as mask (x60 magnification). Therefore positive photoresist is not a good mask for glass.

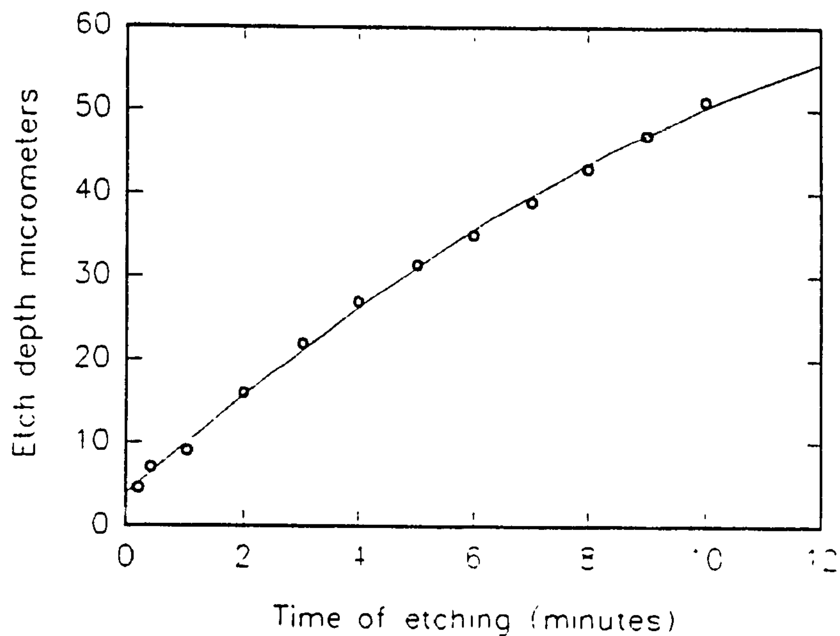

Figure 4.4 Experimental results of glass etching as a function of time when etched in conc. HF (49%).

4.1.3.2 Process B - The Silicon Membrane Process

The micromachining technique of producing thin semi-conductor membrane is to start with a thick wafer and then etch with suitable etchant to realize the thin membrane The starting material used here, for the fabrication of the membrane, is a 3 x 3 x 0.375 mm <100> orientation single side polished low doped p-type silicon wafer. The aim of the process is to achieve a thin flat silicon membrane (20μm) which forms the pressure sensitive membrane of the sensor. For this purpose the silicon wafer is initially cleaned as mentioned in Appendix-II. After cleaning, the wafer is oxidized in an oxidizing furnace using wet oxidation as explained in Appendix-VIII. A standard photolithography process (as mentioned in Appendix-III) is performed using mask-2 The silicon wafer is then

etched in buffered HF, to remove the SiO_2 from the unprotected region, until it becomes hydrophobic. Photoresist is now stripped off using photoresist remover.

The initial design was to diffuse Boron in the membrane region so that it acts as an etch stop against KOH etchant. The principle of etch stop is that, in highly doped silicon surface the width of the space charge layer shrinks drastically. Therefore, electrons injected into the conduction band by an oxidation reaction cannot be confined to the surface and rapidly recombine with holes from the valence band. The lack of these electrons impedes the reduction of water and thereby the formation of new hydroxide ions at the silicon surface.

The anisotropic etching of highly boron doped silicon in aqueous solutions of EDP, KOH, NaOH and LiOH was studied by Seidel et. al. [56, 57] They found a strong reduction of the etch rate for boron doped silicon exceeding approximately 2×10^{19} cm^{-3} The reduction in etch rate was found to be inversely proportional to the fourth power of the boron concentration When the substrate is etched away, the membrane gets stretched and appears smooth and flat with no wrinkles, cracks or bowing [1] The procedure consists of heavily doping the surface of the silicon with boron (p-type) and then etching away most of the silicon substrate from the back side of the wafer with dopant sensitive etchant like KOH The silicon slice is cleaned as mentioned in Appendix-II and dried using purified nitrogen After drying, the slice is loaded on the spinner chuck and held tight using a vacuum pump Using a syringe equipped with a "minisart" 0.45 microfilter, apply 2-3 drops of borosilica gel on the wafer and spin at 3000 rpm immediately for 30 sec. The slice is then dried in a forced-air convection at $95^{o}C$ for 15 minutes. Now the wafer is loaded on the diffusion boat and placed at the mouth of the diffusion furnace tube for 5 minutes Then the slice is moved slowly to the center of the furnace and the time for

the diffusion process is started. At the end of the diffusion process, oxidize the slices (in the same reactor) using wet oxidation process.

A constant temperature KOH etching apparatus was assembled and several tests were conducted to determine the characteristics of the etchant. A detailed study was conducted to establish the silicon etch rate using KOH etchant and the experimental results are presented in Appendix-VI. Since heavily boron doped silicon is not rapidly attacked by KOH a self supporting membrane is obtained whose thickness is controlled by the boron diffusion depth.

During this part of fabrication, it was observed that boron diffusion (B type Boron film or borosilica film) produced brown stains which could not be removed using the standard cleaning procedure. The experiments revealed that brown stains formed using the borosilica gel had unusually high series resistance[55]. Thus, the boron diffusion technique used for this project did not ensure a uniform concentration. A photograph of a silicon wafer with brown stains formed after boron diffusion is shown in Figure 4 5. The square holes showed up on the boron doped silicon surface after a short etching time (3 minutes) The surface of the silicon was not smooth after one minute of etching i.e it is not suitable for the subsequent bonding process. Due to the above reason, an alternate design was used to realize the membranes without boron diffusion. The fabrication process for this design is schematically shown in Figure 4.6.

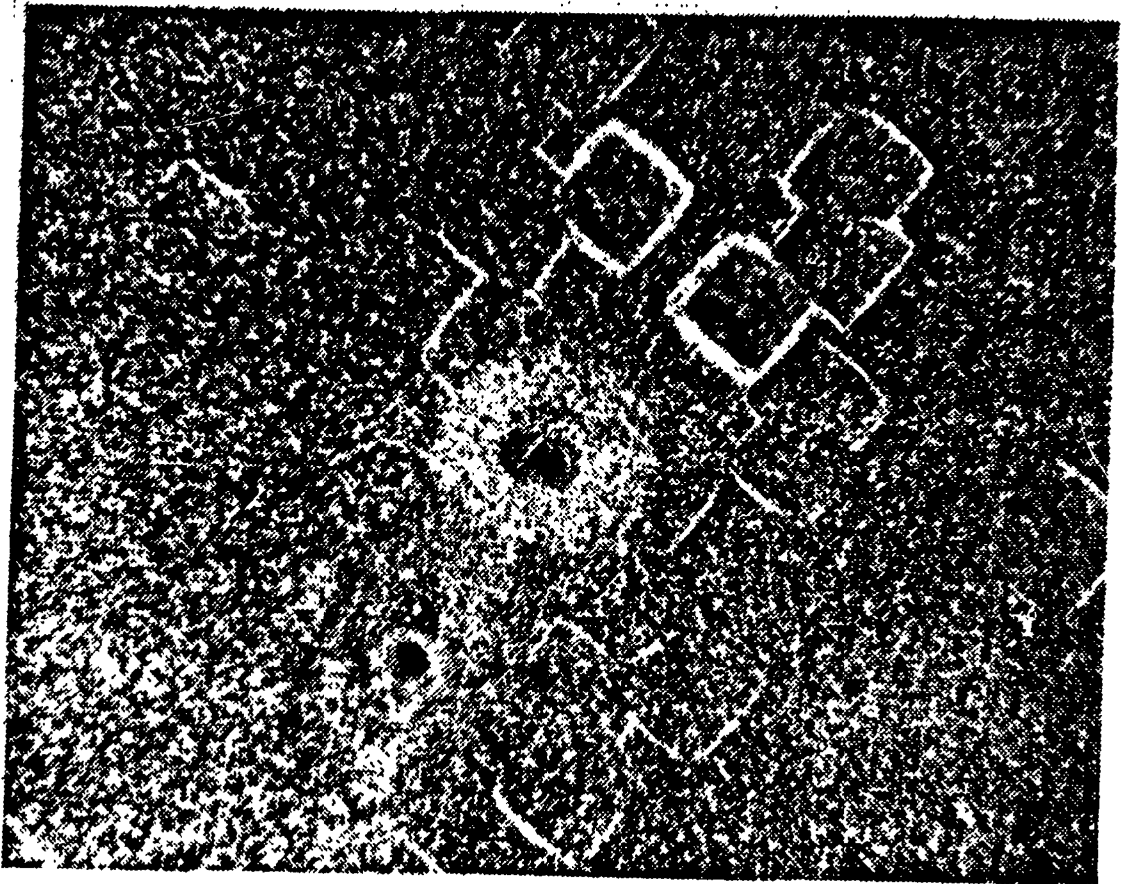

Figure 4.5 Photograph showing the formation of brown stains on silicon surface after boron diffusion (B type borosilica film) (x90 magnification).

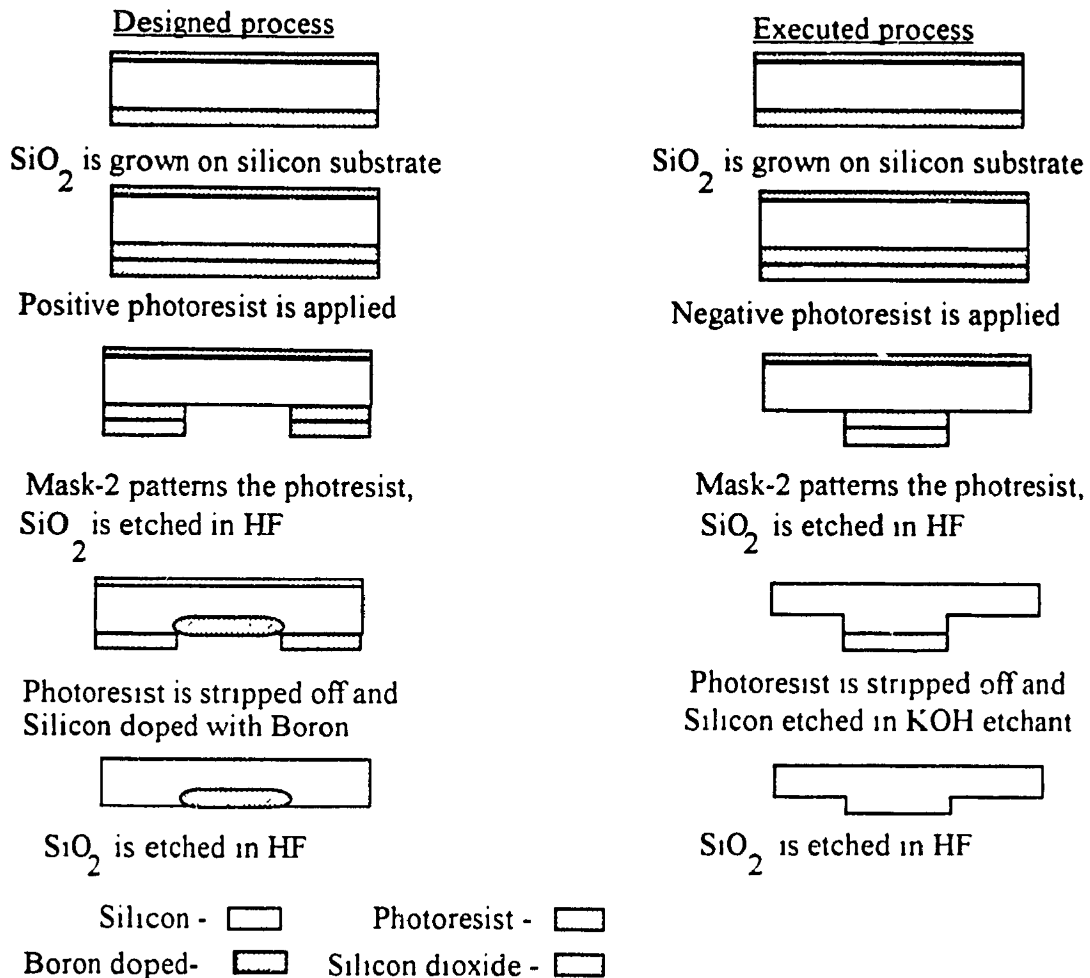

Figure 4.6 Sequence of designed and executed fabrication steps for the silicon membrane of capacitive pressure measurement sensor.

The alternate process involves etching the silicon surface outside the membranes, using SiO_2 as a mask. This ensures a flat membrane surface suitable for bonding The wafer is first etched to a depth of 12 μm in KOH for 5 minutes (which also reduces the thickness of SiO_2 mask by 70Å) The SiO_2 is now removed in concentrated HF solution until the surface is hydrophobic. Thus a wafer with smooth circular portion projecting out was obtained. The silicon wafer is now bonded to the glass wafer (obtained from process A) using the silicon-glass anodic bonding technique It was observed that if above sandwich structure was etched in KOH the surface of the membrane obtained was not flat

as photographed in Figures 4.7a. The etchant, KOH , etches along the <110> surface twice as fast as that the <100> surface at 86°C [57] (see Appendix-VI). Thus, as the membrane gets thinner the etchant etches the bonded region of the membrane and as a consequence the bonded membrane gets spoiled as illustrated in Figure 4.7b.

To solve the aforementioned problem, an alternate etchant was adopted, to etch the bonded structure first in isotropic etchant ($HF:HNO_3$: 3:7) for five to six minutes and then etch in anisotropic etchant (KOH). The etch rate for $HF:HNO_3$ was observed to be 40 μm/min [1] at room temperature and for KOH, an etch rate of 1.4 μm/min. at 86° C (see Appendix-VI) The isotropic etchant was used only to etch the unbonded silicon surface at a faster rate Later it is etched in KOH to reduce the thickness of the silicon membrane in a controlled condition. While etching in anisotropic etchant (KOH), the test structure should be held in a fixed position (see Appendix-VI) and dipped completely in the etchant. The etchant should be maintained at a steady temperature (86° C) to get a uniformly etched surface The photographs in Figure 4 8a and 4 8b show the smooth surface of the membrane of thickness 70μm and 40μm respectively after etching in isotropic etchant Next, the sandwich structure is etched in KOH to get the membrane of desired thickness

It was also observed that prolonged etching attacks the bonding. To overcome the above problem, the etching was stopped when the membrane attained a thickness of 22μm instead of etching it down to 20μm. The structure is now cleaned as mentioned in Appendix-II and kept ready for the second bonding with the top cover silicon.

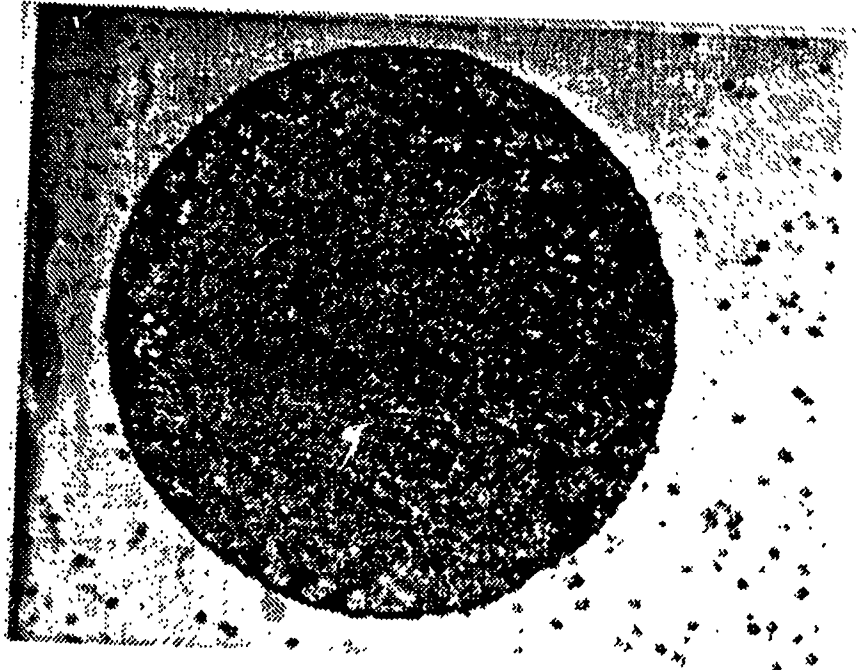

Figure 4.7a Photograph showing the uneven surface of boron doped silicon membrane after etching for 20 minutes in KOH (x60 magnification).

Figure 4.7b Photograph showing the spoiled surface of boron doped silicon membrane after etching for 120 minutes in KOH (x60 magnification).

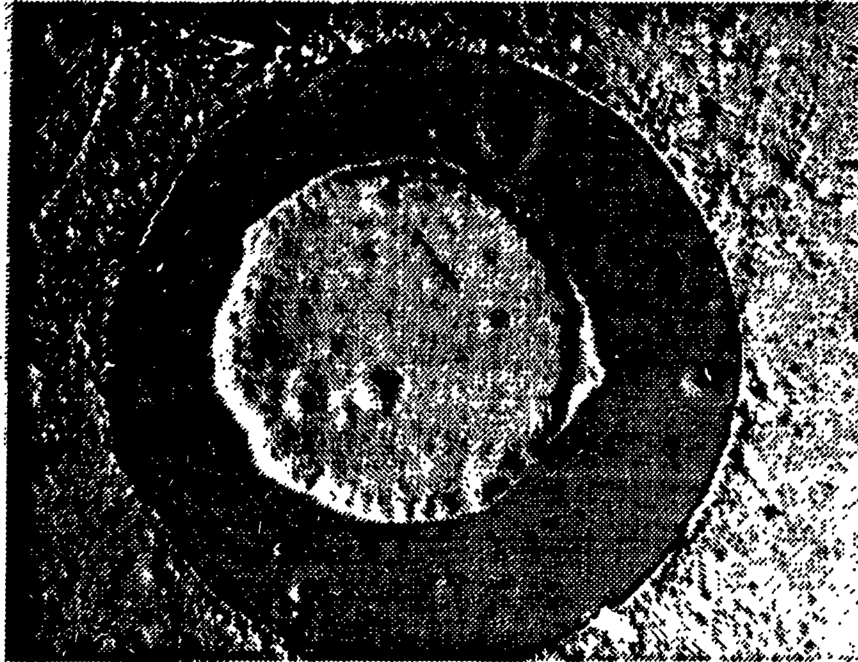

Figure 4.8a Photograph showing the flat surface of the silicon membrane (70 μm thick) after etching in isotropic etchant (HF:HNO_3) for 5 minutes (x60 magnification).

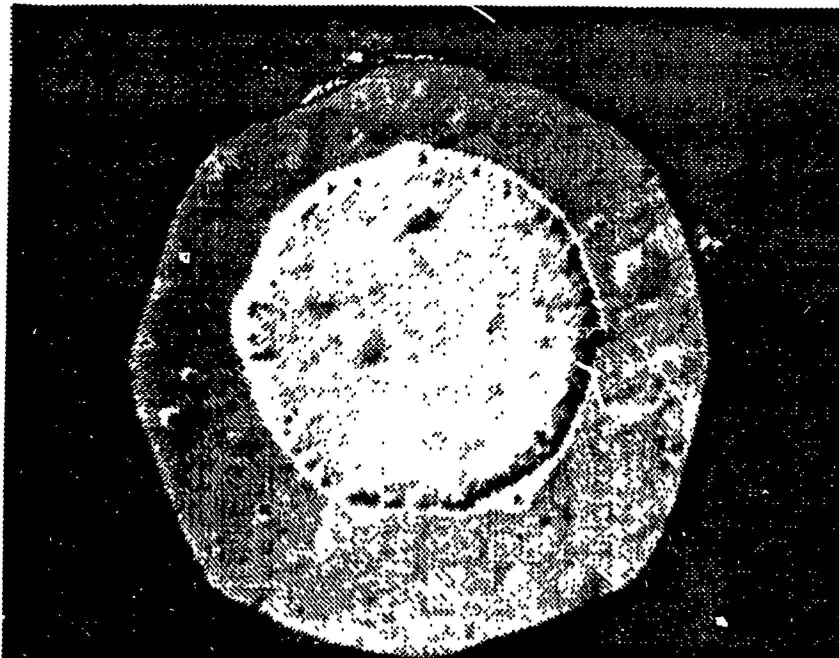

Figure 4.8b Photograph showing the flat surface of the silicon membrane (40 μm thick) after etching in isotropic etchant (HF:HNO_3) for 6 minutes (x60 magnification).

4.1.3.3 Process C - The Top Silicon Cover Process

A n-type <100> silicon is selected as the starting material for the top cover The top cover is processed to enclose the pressure sensitive membrane The etched depth of the top cover wafer defines the air gap around the pressure sensitive membrane To fabricate the top cover a silicon 3x3x0.375 mm single side polished silicon wafer is taken and cleaned as described in Appendix-II. The wafer is oxidized using wet oxidation process as mentioned in Appendix-VIII After oxidation the standard photolithography technique, as explained in Appendix-III, is performed on the wafer using Mask-4. Then the wafer is etched in buffered HF for a minute to remove the SiO_2 from the unmasked region The photoresist is now stripped off and etched in KOH for five minutes to get the ring shaped structure. After KOH etching, the wafer is exposed through Mask-3 (see Appendix-IV) and patterned The wafer is again etched in KOH for fifteen minutes to get the top cavity After this process the wafer is etched in HF to remove all the remaining SiO_2 from the wafer If the sensor is used as a static pressure measurement device a thin layer of SiO_2 has to be grown on the bottom of the cavity using Mask-5 or else it can be used as a dynamic pressure measurement device The native oxides present on the silicon surface does not form a uniform insulating layer, so that it can be used as a static measurement devices Here, we have fabricated a dynamic pressure measurement device The wafer is now cleaned using the standard cleaning procedure (refer to Appendix-II) and kept ready for bonding with the sandwich structure obtained from process A and B

4.1.3.4. Process AB - Anodic Bonding of Top Cover with Glass Assembly

The sandwich structure from process A and the top cover from process B are cleaned as mentioned in Appendix-II. Then they are dried using purified compressed nitrogen If the membrane is thin (< 10 μm) it becomes fragile and therefore drying using nitrogen must be performed carefully Next, the glass with silicon membrane (from

process B) on it is aligned and anodically bonded with the top cover. After bonding, the device is allowed to cool in atmosphere

4.1.3.5. Metal Deposition for Electrical Contacts

Capacitive sensors are basically semi-conductor devices having the same electrical connections techniques as that of semi-conductor devices Generally, thin gold wire is used to connect the sensor to the aluminum pad of the package connector. Gold has a low melting temperature and is compatible with aluminum This technique makes a good electrical contact and give a low-impedance connection over wide temperature range.

In this project, the metal contacts for the capacitive pressure sensor device was made using silver paste commercially known as Electrodag 415. Electrodag 415 is a dispersion of finely divided silver in a thermoplastic resin that rapidly air dries to form a conductive shield on non conductive substrates[67]. It exhibits excellent adhesion and provides controlled electrical properties (sheet resistance of 0 04-0 07 Ω/□) in coating as thin as 7.5 μm (0 3 mil) The surface to be coated must be dry and free of dust Mix the silver paste thoroughly until it is of uniform consistency and then using standard paint-spray technique make a thin coating on the glass substrate The paste is allowed to dry, which takes approximately 10 minutes, before carrying out subsequent process. Once the silver paste is dried the photoresist is peeled off from the glass surface

Metallization is performed on the sandwich structure obtained from process-AB The glass surface of the sandwich structure is patterned using Mask-6. After the photolithography process, a layer of silver paste is sprayed on the glass wafer. The procedure used for metallization is as mentioned in the previous paragraph. The fabrication process is completed and the device is ready to be tested and characterized for different pressure applied within the design limit.

4.2 Capacitive Tactile Imaging Sensor

The fabrication process of tactile imaging sensor is designed to be simple and compatible with achieving high yield The process technology offers precise dimensional control and straight forward scaling of array dimensions to meet variety of application needs. The process requires two masks (the mask drawings are illustrated in Appendix-V) none of them are critical masking steps. The basic structure of the proposed tactile array sensor (5 x 5) is shown in Figure 4 9 and a cross-sectional view of a single sensor element and the details of the top metal electrode is illustrated in Figure 4.10

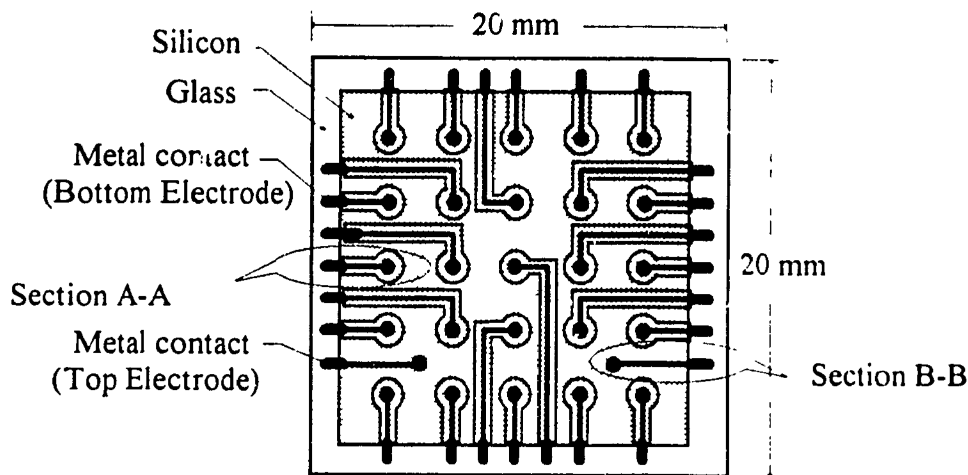

Figure 4.9 Bottom view of 5 x 5 array tactile sensor.

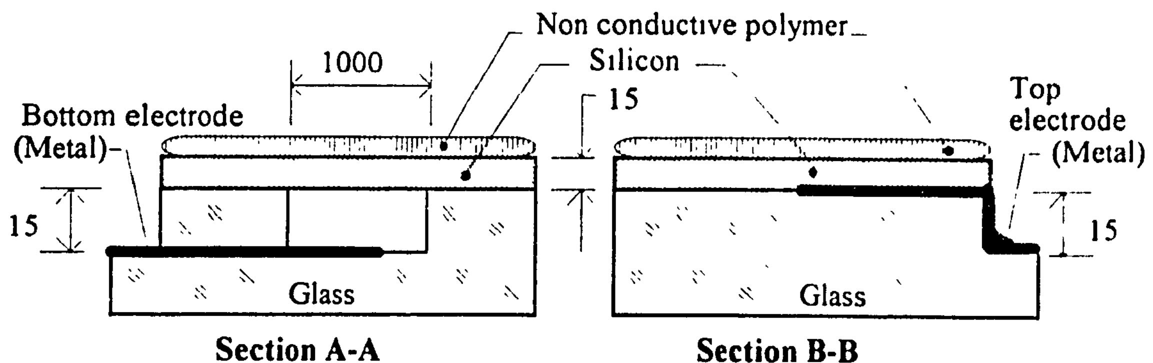

Note: (a) Metal thickness = 0.05 μm (b) All Dimensions in μm

Figure 4.10 Cross-sectional view of capacitive tactile sensor.

4.2.1 Materials Used for Fabrication of Tactile Imaging Sensor

Glass and silicon wafers are the materials used for the fabrication of the capacitive tactile imaging sensor The coefficient of thermal expansion of the selected glass should be very close to that of silicon so that they can be anodically bonded to each other. The bonding surface of the glass and the silicon should be mirror grade polished (surface roughness less than 400Å) Pyrex glass (# 7740) which satisfies the above mentioned properties is selected as the sensor substrate material Ultra thin silicon wafer which are commercially available are used as the sensing element for the tactile sensor The specifications of the glass and silicon wafers are as described below.

The Pyrex glass (# 7740) has a chemical composition of SiO_2 - 81%, H_2O_3 - 2%, B_2O_3 - 13% and Na_2O - 4%. Glass having a thickness of 760 μm and diameter of 50 mm is used for the fabrication of the tactile imaging sensor. A thin silicon wafer (15 μm thickness) with p-type doping (boron concentration $3x10^{19}$ cm^{-3}) is used for tactile sensor fabrication The high doping concentration in silicon wafer reduces the resistivity (0 002 Ω-cm) so that it can be used as an electrode. These ultra thin wafers provide precise thickness control and assured uniformity of the final etched geometry They also provide dimensional stability in flatness (tolerance of ±0 5μm) and good surface planarity The wafers used are double side polished and are extremely flexible due to the dominance of the elastic nature of single crystal silicon. Thus by controlling the three important parameters of the micromachined sensing element (i.e total thickness variation, flatness and planarity) enables the micromachining engineer to ensure precision in designed product.

4.2.2 Fabrication Process of Tactile Imaging Sensor

An outline of the sequence of steps in the fabrication process of the proposed tactile sensor is as shown in Figure 4.11.

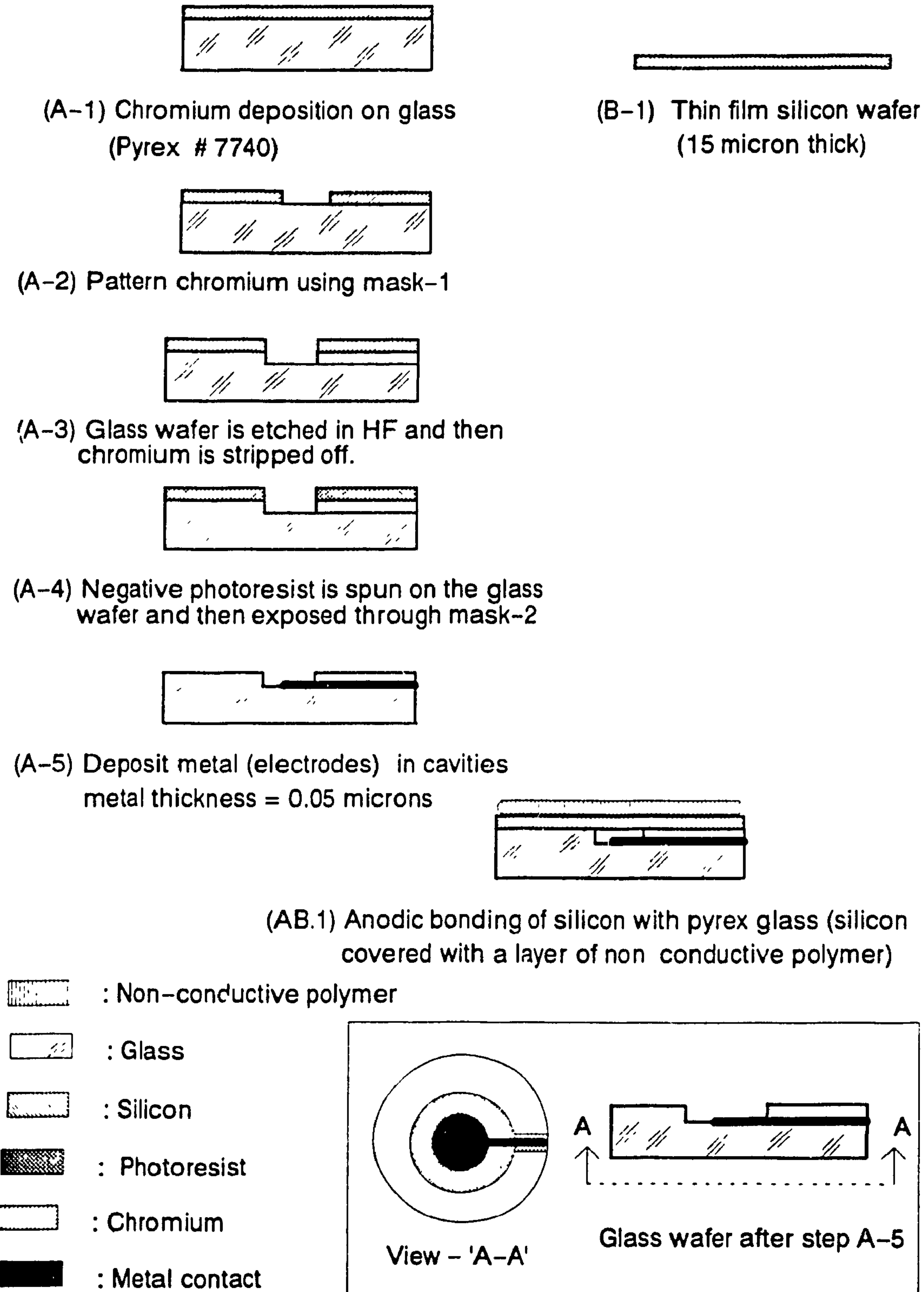

Figure 4.11 Sequence of fabrication steps for the capacitive tactile sensor (view of a single element in the array).

The starting materials used for processing the sensor chip involves two wafers a Pyrex glass (# 7740) wafer and a thin film silicon wafer. The initial preparation for cleaning these wafers are as mentioned in Appendix-II. The fabrication process for both the silicon and glass are as described below

4.2.2.1 Glass Wafer Process

The glass substrate for the tactile sensor is prepared from a 50 mm diameter and 0.76 mm thick optically polished Pyrex glass (# 7740). The Pyrex glass (# 7740) is chosen because it is suitable for anodic bonding with silicon The glass wafer is cleaned as mentioned in Appendix-II. The first step is to deposit a layer of chromium on the glass wafer using a chromium deposition evaporator as explained in Appendix-IX. The chromium film protects the underlying glass against the etchant HF. After chromium deposition, the glass wafer is cleaned in de-ionized (DI) water and then a standard photolithography process (see Appendix-III) is performed using Mask-1 (see Appendix-V) Negative photoresist is used because it adheres to the chromium deposited on glass better than positive photoresist. Now the exposed chromium is etched in a mixture of ceric ammonium nitrate (150 gm) + acetic acid (35 ml) + 1 litre water[68] The etch rate for chromium in this etchant is 1500 Å/min. After removing the chromium from the selected region the glass wafer is dipped in concentrated HF (49%) to form a circular recessed area of about 15μm deep. The etch rate for glass in HF is approximately 9μ m/min. at 25°C. Now the negative photoresist is stripped off in negative photoresist remover and the remaining chromium is etched in ceric ammonium nitrate mixture.

4.2.2.2 Metal Deposition for Electrical Contacts

The glass wafer from the above process is cleaned in DI water and then the second photolithography process (see Appendix-III) is performed using Mask-2. Here the mask

has to aligned so that metallization can be done at the bottom of the circular recessed area as shown in Figure 4.12. After the photolithography process, 500Å thick layer of chromium is deposited on the glass which forms the metal contact for the sensor. The photoresist is then stripped off and the glass wafer kept ready for anodic bonding. Figure 4.13 shows the photograph of the bottom electrode and the contact pad of a sensor element on the glass substrate

The metal contact for the top electrode is also provided on the glass wafer eliminating lead wire contact on the pressure sensitive silicon membrane. The thickness of the top electrode (500Å) is within the surface roughness limit required for anodic bonding (< 1μm [47]) Therefore, the area surrounding the top electrode will be perfectly bonded leading to a stable surface contact between silicon and metal Figure 4.14 shows the photograph of the metal pad on the glass wafer which forms an electrical contact for the silicon membrane. Figure 4 15 illustrates a magnified (x 500) view of the metal pad indicating that the metal layer is continuous

4.2.2.3 Silicon Membrane Process

There are two general classes of techniques for producing semiconductor membranes that are a few microns or less in thickness. One can either start with a thick single-crystal semi-conductor wafer and etch it to give a thin membrane (using surface micromachining techniques) or one can grow a sacrificial layer and thin film (epitaxial) on a silicon substrate from which the sacrificial layer can be removed to realize the membrane. Here, we have used a prefabricated thin silicon membrane which gives high dimensional tolerance (± 0.1μm) This method of using thin silicon wafers helps in skipping many intermediate micromachining steps. The silicon wafer is cleaned using N_2 gas and kept ready for anodic bonding.

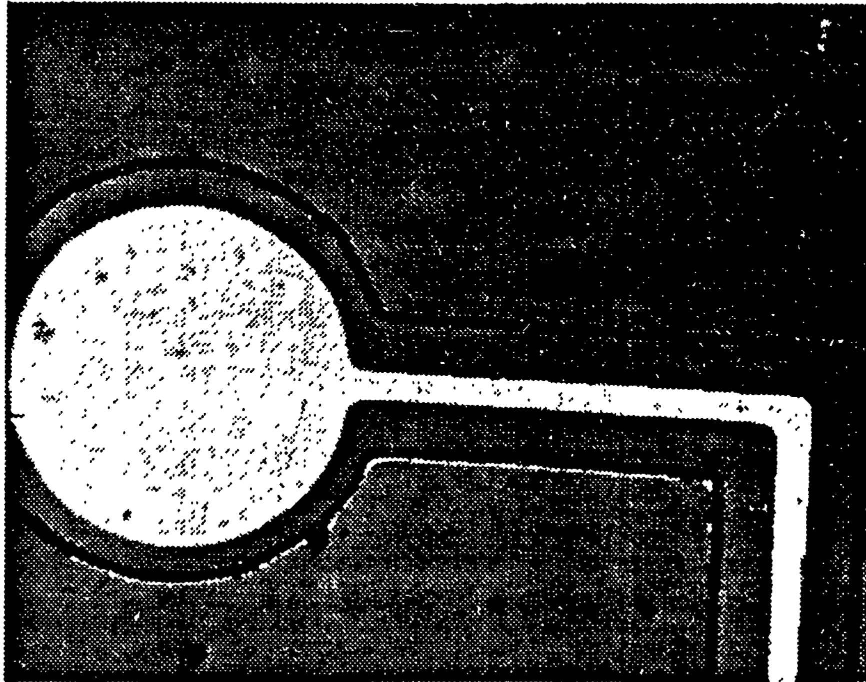

Figure 4.12. Photograph showing the glass wafer after metallization and ready for anodic bonding (x 50 magnification).

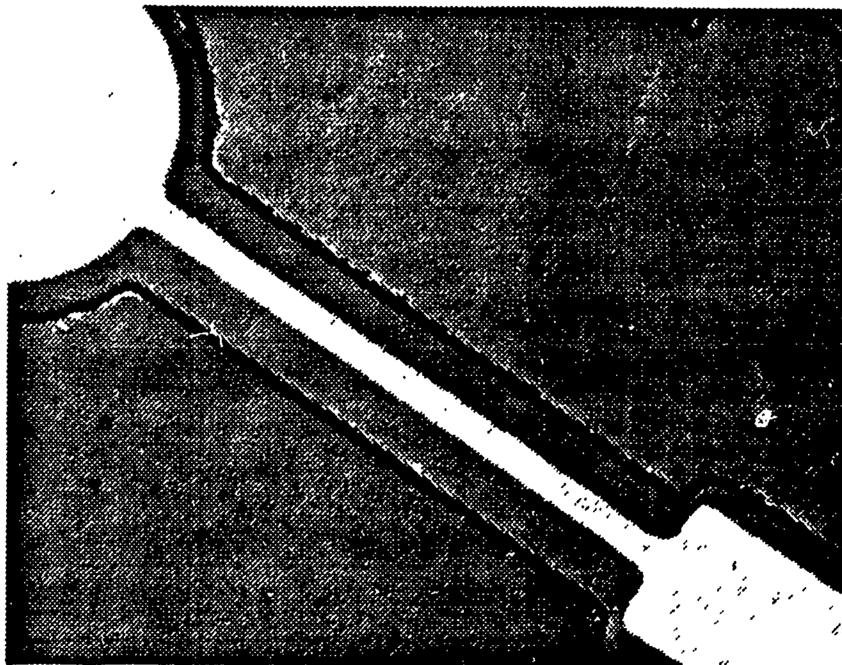

Figure 4.13. Photograph showing the bottom electrode and contact pad of a sensor element (x 50 magnification).

Figure 4.14. Photograph showing the metal pad on the glass wefer for electrode on the silicon wafer (x 100 magnification).

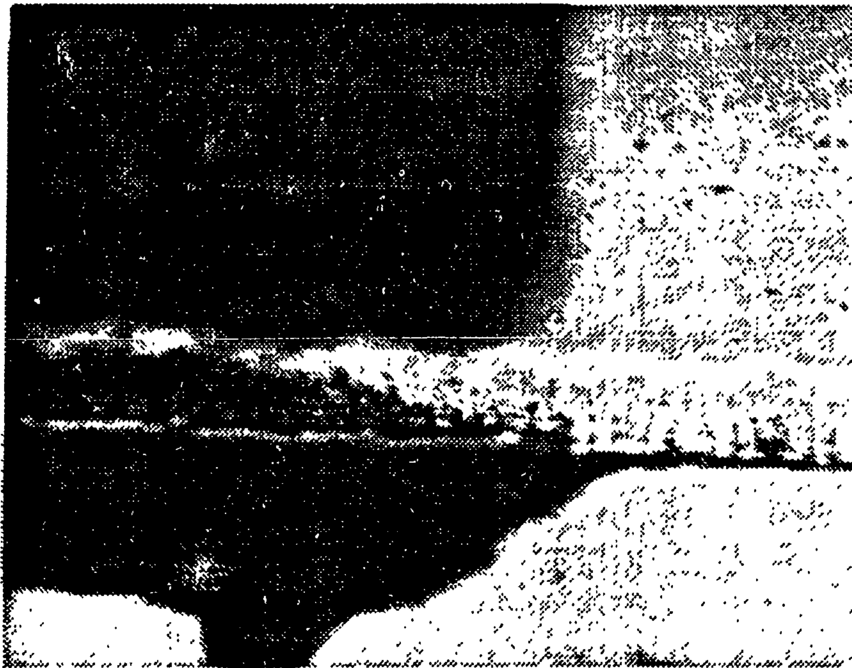

Figure 4.15. A magnified view of the photograph of Figure 4.14 showing the metal layer for the contact pad is continuous (x 500 magnification).

4.2.2.4 Anodic Bonding of Membrane with Glass

The glass and silicon wafers are now bonded using anodic bonding technique Anodic bonding provides proper packaging and protection of the tactile imager in environments that are often harsh and rough For the tactile sensor reported here, it is even more important to protect the boron-doped thin film silicon from touching other objects (since they carry control signals) and to enclose the capacitive gap so that particles do not get in between the two planes. These requirements can be achieved by covering the tactile imager with a thin deformable non-conducting polymer that can be replaced when required as shown step AB.1 of Figure 4.11. The non-conductive polymer should be fairly thin and flexible to minimize cross-talk between each individual sensor in the array and also minimize the loss in sensitivity. In this project, a layer of negative photoresist (~ 50μm) was spun on the silicon membrane which forms the protective skin for the tactile sensor.

Chapter - 5

Characterization of the Capacitive Pressure Micro Sensor

The characterization of the fabricated capacitive type pressure sensor is presented in this chapter. The experimental results presented here are based on the performance of first few prototype capacitive pressure sensors. The instruments used for testing and the test procedure are also discussed. Finally, the experimental results are tabulated and compared with analytical results.

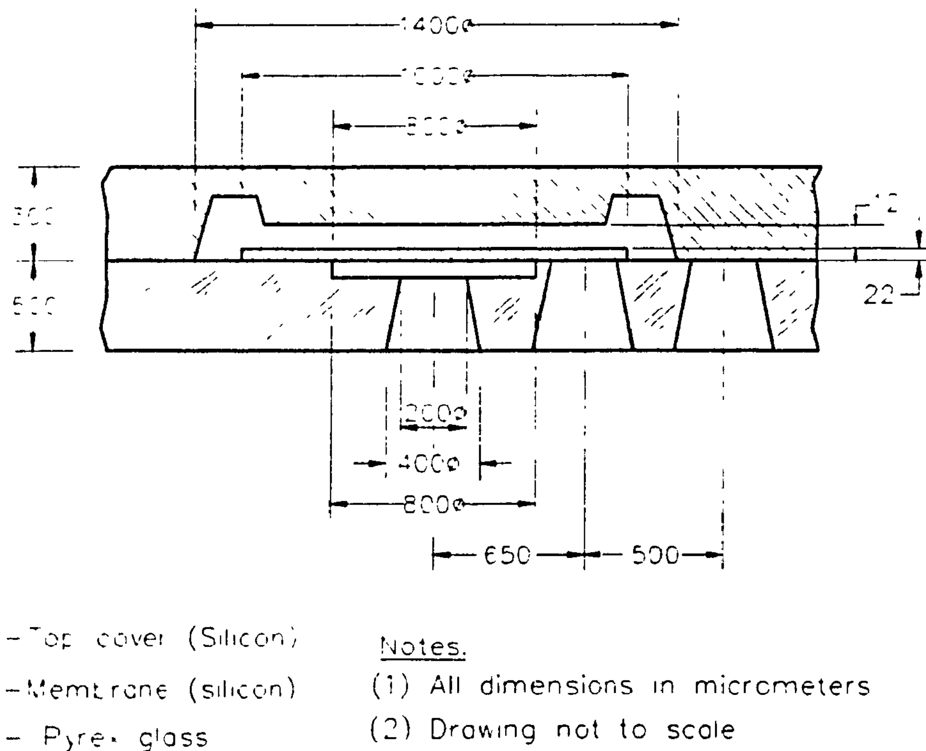

Figure 5.1 Cross-sectional view of fabricated capacitive pressure measurement sensor with achieved dimensions in microns.

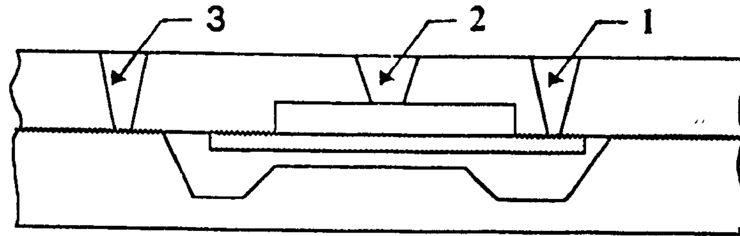

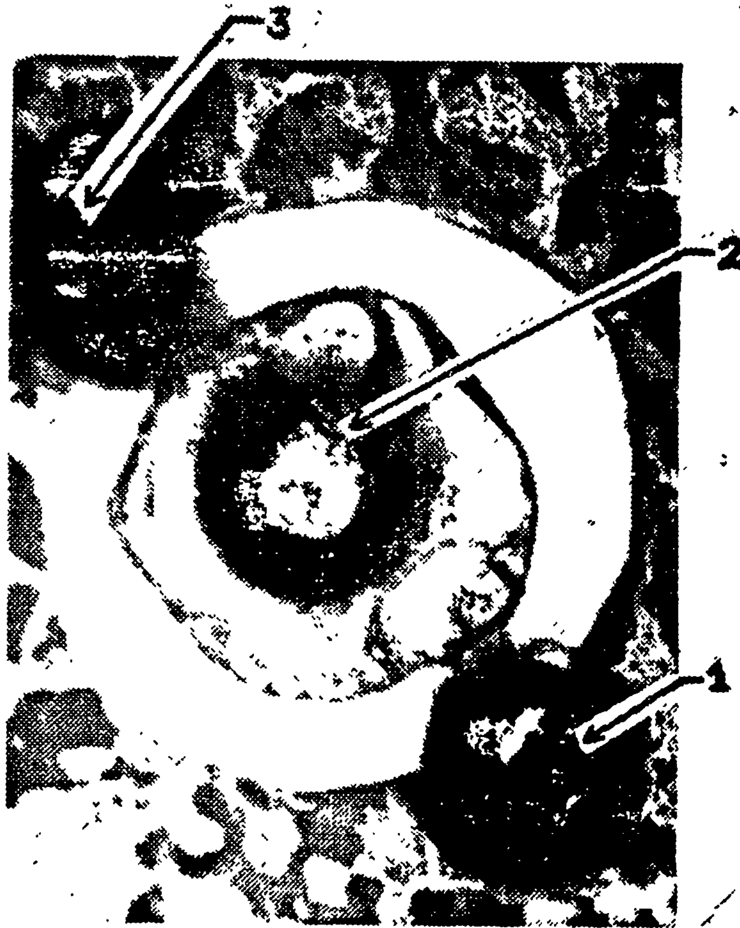

1. Electrical contact on silicon membrane   2 Pressure inlet hole

3. Electric Contact on top silicon cover

Figure 5.2 Photograph of the fabricated capacitive pressure measurement sensor (x 60 magnification).

The cross-sectional view of a single element of the fabricated pressure sensor with the achieved dimensions is illustrated in Figure 5.1. Figure 5.2 shows a photograph of a single element and Table 5.1 presents the designed and achieved dimensions of the sensor The dimensions of the fabricated sensor was measured using optical microscopy.

Table 5.1 Designed and achieved dimensions of capacitive pressure sensor

	Designed	Achieved
Diameter of silicon membrane (2a)	800 μm	800 μm
Thickness of silicon membrane (H)	20 μm	22 μm
Thickness of air gap (d)	10 μm	12 μm

5.1 Experimental Setup for Sensor Characterization

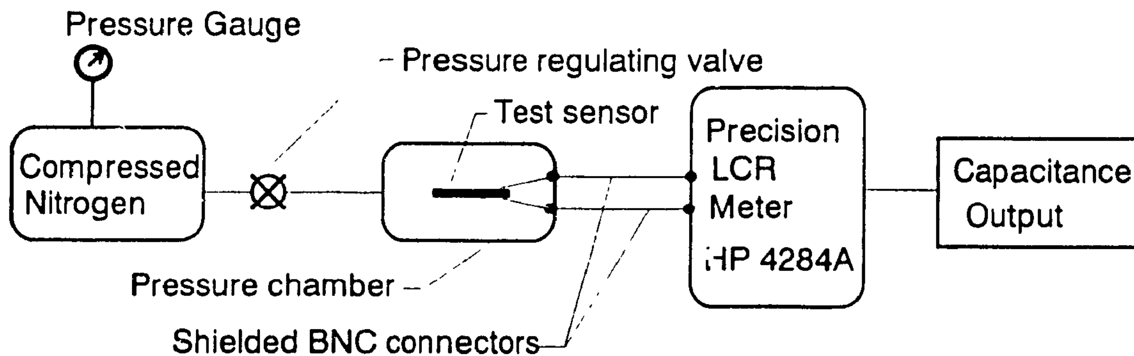

Figure 5.3 Block diagram of pressure measurement sensor testing system.

The fabricated capacitive type pressure sensor is characterized by applying a constant pressure and measuring the resulting change in capacitance. The experimental setup consists of a pressure chamber, pressure source and a precision LCR meter. Figure-5.3 illustrates the block diagram of the measuring and data analysis system.

The pressure chamber used here is a steel cylindrical vessel (10cm diameter and

15cm height) which is designed to withstand pressure up to 100 psig The chamber has a flat platform at the bottom to place the test device. The air tight pressure chamber forms a shield against the stray capacitance effects due to external noise Two electrical leads are provided on the chamber which connects the sensor to the capacitance measuring instrument. A nozzle is provided on the top of the pressure chamber which can be connected to a pressure source Here, we have used a compressed nitrogen cylinder with a pressure regulating valve as the pressure source The pressure gauge measures the pressure inside the test chamber. The pressure inside the chamber is regulated by means of a pressure regulating valve. An air leakage test was performed to ensure desired precision of the pressure chamber

The capacitance is read using a precision LCR meter (HP 4284 A) instrument which measures the capacitance of the device This measuring instrument has a resolution of 0.5 fF and the fluctuations in the measurements can be minimized at high input frequency. The sensor chip 's connected to a capacitance measurement instrument by means of calibrated leads BNC connectors and shielded cables which minimize the effect of external fields are used to connect the pressure chamber with the measuring instrument.

5.2 Experimental Procedure for Characterization of Pressure Sensor

The fabricated pressure sensor is placed inside the air tight pressure chamber Two electrical contacts, one from each of the two parallel plates are connected to the capacitance measurement instrument The compressed nitrogen cylinder is now connected to the chamber by means of a PVC tube. Nitrogen gas at regulated pressure is passed into the chamber through the pressure regulating valve. The two lead wires connected from the sensor to the precision LCR meter gives the capacitance of the sensor. Before testing the sensor, it is mandatory to determine the optimal frequency range in which the sensor

operates to obtain optimal sensitivity of the device. For this reason, the influence of factors like signal frequency, amplitude and DC bias voltage were studied and its effects are presented below.

5.2.1 Effect of Frequency on the Capacitance Measurement

The measuring instrument (HP 4284 A) has a operating frequency range from 20 Hz to 1 MHz. The sensor was characterized in ambient conditions. The capacitance reading of the test sensor placed inside the pressure chamber at normal atmospheric conditions were taken at different frequencies The zero pressure capacitance of the sensor was tested at different signal frequencies ranging from 20 Hz to 1 MHz It was observed that at low frequency the noise effect was predominant and therefore the reading was inconsistent Once the frequency was increased the effects due to stray capacitance minimizes and the capacitance measurements remain stable as illustrated in Figure 5.4. The quality, Q, of the stray or parasitic components influencing the circuit of the measuring instrument was tested for different frequencies and found that at high frequency (> 800 kHz) the quality of measurement is reliable and stable for low capacitance devices The reciprocal of quality (Q) gives the dissipation factor (D) of the measuring instrument The dissipation factor of the measuring instrument at 1 MHz was found to be negligible Figure 5.5 illustrates the dissipation factor as a function of signal frequency. The experimental study revealed that the fluctuation in the reading was less than 0.1 fF for 1 MHz frequency. For frequency above 800 kHz the fluctuations reduced considerably and therefore the ideal characterization frequency was selected as 1 MHz for this type of pressure sensors.

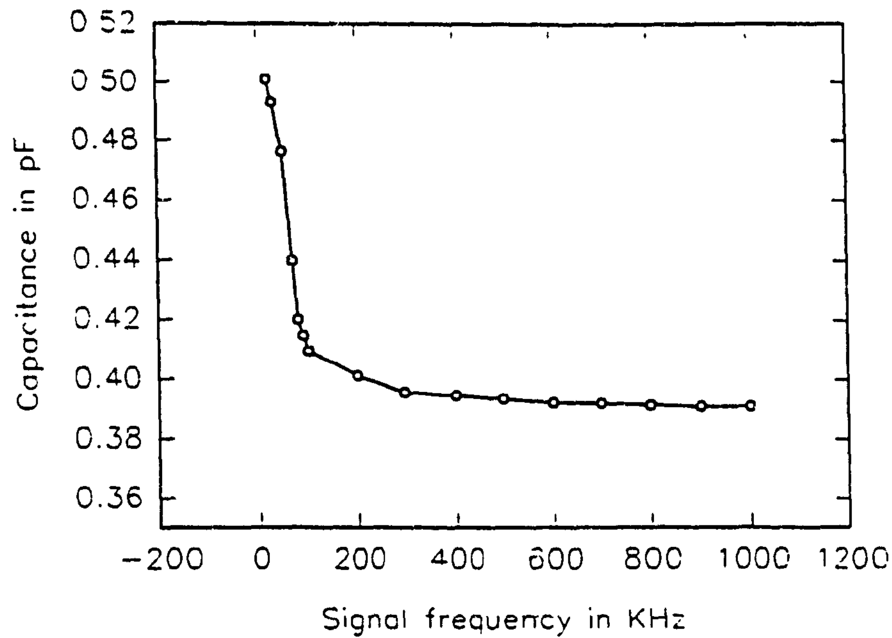

Figure 5.4 Experimental results of zero pressure capacitance as a function of signal frequency for each sensor element. (Level = 1V, Bias = No DC bias).

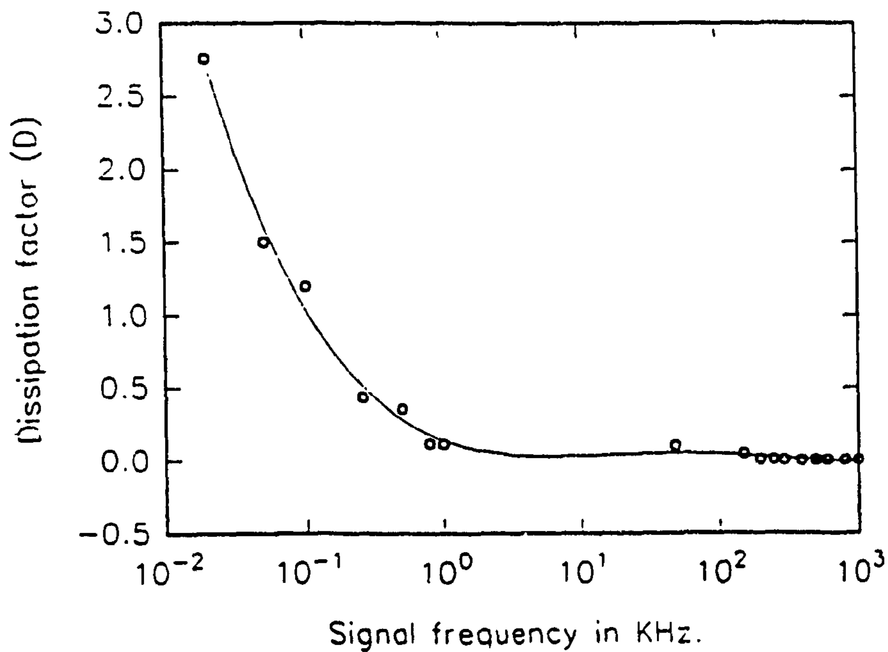

Figure 5.5 Dissipation factor (D) of the measuring instrument vs signal frequency.

5.2.2 Effect of Signal Amplitude and DC Bias on the Capacitance Measurement

The effect of amplitude of sinusoidal signal on the sensor response was studied in the range of 20 mV to 1 V and it was observed that the fluctuation was not significant In addition, the effect of DC bias in the range from -10 V to 10 V was also studied and found to be insignificant.

To summarize, the amplitude of sinusoidal signal and DC bias does not have significant effect on the capacitance response of the device whereas the fluctuation in frequency can be minimized above 800 kHz. Therefore, here we have selected 1MHz, input voltage of 1V and without DC bias as the settings for the precision capacitance measurement instrument.

5.2.3 Effect of Parasitic Capacitance on the Capacitance Measurement

The total sensor capacitance is a combination of different capacitances due to different dielectric effects present in the sensor The air dielectric between the two parallel plates contributes the major value of the sensor capacitance, C_x. Other effects like glass dielectric and silicon dielectric, called the parasitic capacitance (C_p) remains constant The equivalent circuit of the pressure measurement sensor is presented in Figure 5.6.

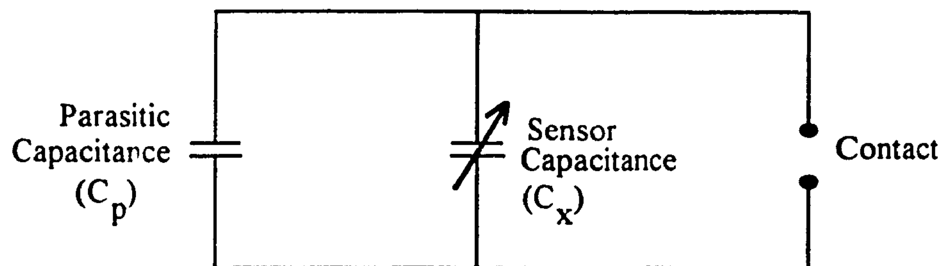

Figure 5.6. Equivalent circuit of the pressure measurement sensor.

Other factors which may effect the capacitance measurements include Brownian

noise, electrical noise and electrostatic force acting on the diaphragm [5] The effects of these factors were studied and found to be less than 2%. The principal causes of these effects are described below.

a) The Brownian noise is due to the discrete nature of the physical bombardment of molecules against the silicon diaphragm. The Brownian noise scale is mathematically written as:[5]

$$P_n^2 \ \alpha \ \frac{(P_{in} + P_{out}).BW.T^{0.5}}{a^2} \tag{5.1}$$

Where, P_n^2 is the mean square input pressure, P_{in} and P_{out} are the mean pressures on the two sides of the silicon diaphragm, BW is the bandwidth, a is the diaphragm radius and T is the temperature For the given device the Brownian noise has a value of the order of 10^{-4} µm Hg which is much smaller than the applied pressure.

b) The capacitance due to electrical noise is generated by the transducer element and the measuring instrument. For the pressure sensor the value for this noise is in the order of 50 µm Hg which is calculated from the equation [5]

$$P_n^2 = \frac{\left[1 + \frac{C_p}{C_0}\right] \frac{T}{V_{supply}^2} .H^6.d^3}{a^{10}} \tag{5.2}$$

c) The capacitance due to the pressure error caused due to the electrostatic force acting on the diaphragm with applied voltage is found to be negligible because the deflection of the pressure sensitive membrane considered to be small compared to the distance, d, between the parallel plates. This pressure error is calculated as [5]

$$P_{error} = \frac{e.V^2}{2.d^2} \tag{5.3}$$

where, e is the permittivity and V is the voltage across the capacitor plates.

The stray (parasitic) capacitance reduces the sensitivity, contributes to higher non-linearity and decreases the thermal stability. All leads must be shielded to reduce the effect of stray capacitance Errors like non-linearity and temperature co-efficients can be compensated using integrated circuitry. Therefore the total capacitance, C_{tot}, is written as

$$C_{tot} = C_x + C_p \tag{5.4}$$

where, C_x is the active capacitance

5.2.4 Capacitance Measurement with Applied Pressure

After measuring the zero pressure capacitance, the pressure chamber is closed and ensured to be air tight. The pressure inside the chamber is increased gradually up to a pressure of about 6 201 x 10^5 Pa (90 psig) The pressure differential across the diaphragm induces a change in capacitance The capacitance, at an input signal frequency of 1 MHz, is measured for different pressures Figure 5.7 shows the experimental and analytical results of the fabricated capacitive pressure sensor. The sensor was tested under the following conditions no DC bias, the amplitude and frequency of the input signal maintained at 1 V and 1 MHz respectively.

It was observed that the change in capacitance was steady as long as the pressure inside the chamber was maintained at a particular value. The pressure was increased in increments of 5 psi to a maximum of 90 psi (the pressure limit of the designed pressure chamber device) and the corresponding capacitance readings noted. Now the pressure inside the chamber was reduced in similar steps and the readings noted. The readings are plotted in Figure 5.8 which indicates that the variation in sensor capacitance (< 2fF) for a full cycle of applied pressure is stable and within the allowable tolerance (< 5% of the full scale) This indicates that the sensor has low hysteresis value

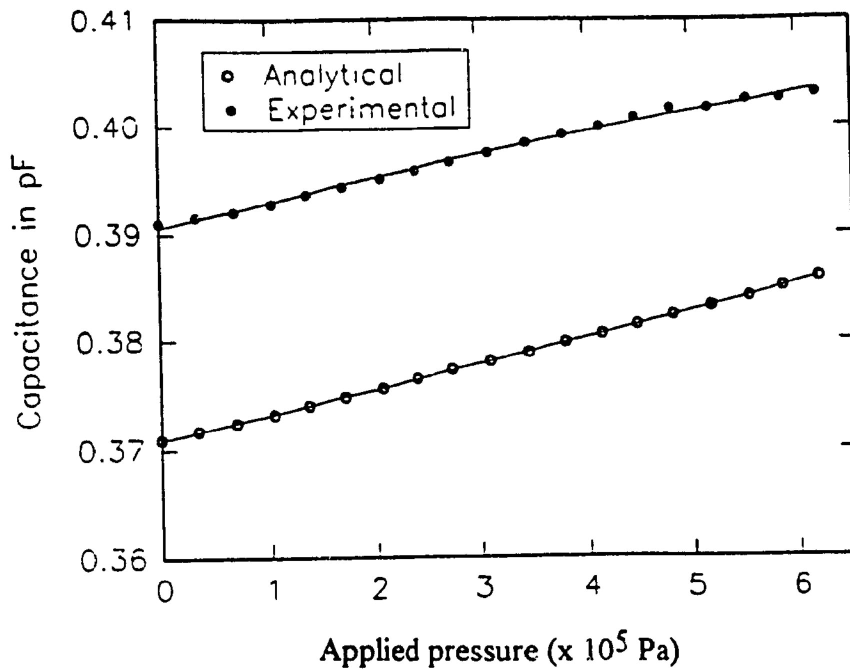

Figure 5.7 Capacitance as a function of pressure for each individual sensor element. (Frequency = 1 MHz, Level = 1V, Bias = No DC bias).

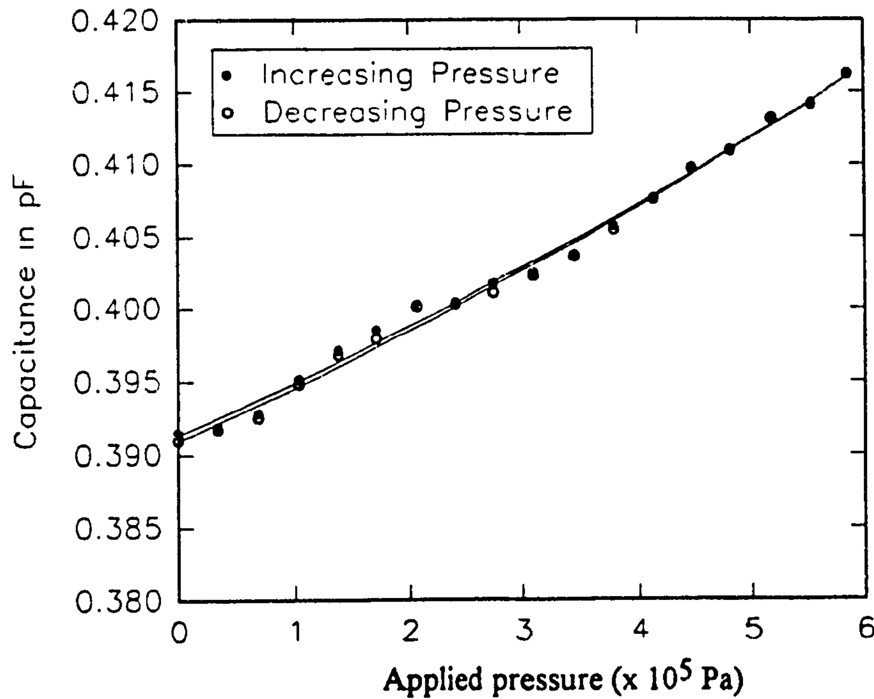

Figure 5.8 Experimental results of the capacitance vs pressure for a full cycle for an individual sensing element. (Frequency = 1 MHz, Level = 1V, Bias = No DC bias).

Figure 5.9 shows the experimental results of the high and low value of capacitance with respect to applied pressure for an individual sensing element measured at regular interval for two months. The upper curve represents the higher capacitance reading and the lower curve the low capacitance reading measured during the period for which the experiment was conducted. The low and high curves showed a deviation of about 2% from the mean value, indicating that it is likely, that the parasitic capacitance varied by about 5 fF over the period covered by this experiment.

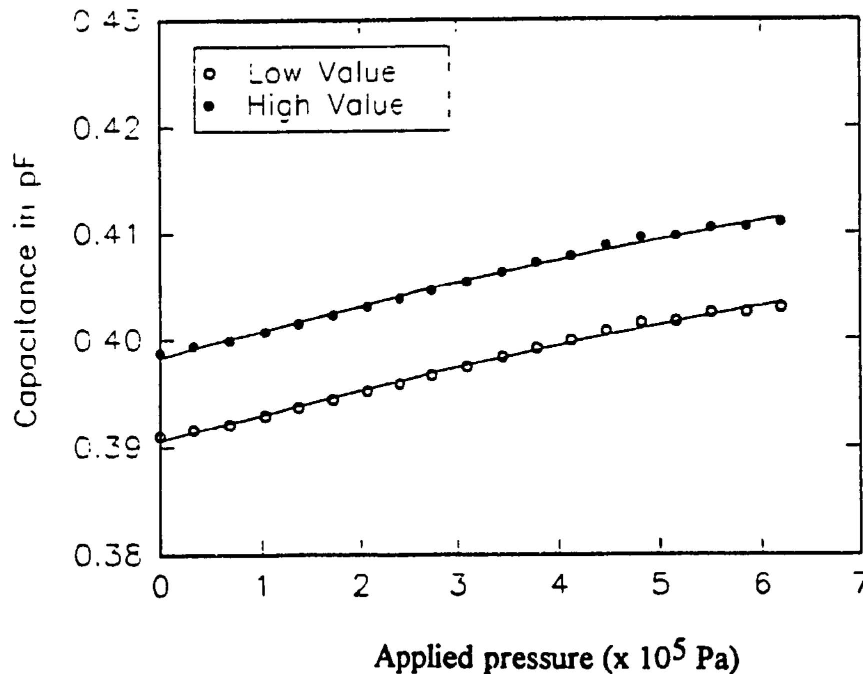

Figure 5.9 Experimental results of the high and low value of capacitance with respect to pressure for an individual sensing element measured at regular interval for two months. (Frequency = 1 MHz, Level = 1V, Bias = No DC bias)

5.3 Experimental Results of Pressure Micro Sensor

The fabricated pressure sensor output capacitance signal as a function of pressure

was measured yielding a very smooth linear plot The change in measured capacitance is within the designed performance limit for the achieved geometrical dimensions of the sensor. Table-5.2 shows the analytical and experimental performance characteristics of the sensor

Table 5.2 Comparison of the analytical and experimental performance characteristics of the 4 x 5 array pressure measurement sensor

	Analytical	Experimental
Zero Pressure Capacitance (C_0)	0 3709 pF	0 3910 pF
Max Pressure Capacitance (C_{max})	0 3859 pF	0 4030 pF
Sensitivity (S)	2 4189 fF/Bar	1.935 fF/Bar

The performance of the fabricated sensor depends on the achieved geometrical dimensions and the flatness of the pressure sensitive silicon membrane The zero pressure capacitance of the sensor depends on the radius and the distance between the parallel plates. The sensitivity and rupture pressure depends mainly on the thickness of the pressure sensitive membrane. Therefore, to correlate the actual performance of the fabricated sensor, a sensitivity analysis was performed with a variety of geometrical conditions pertaining to the sensor. The simulation takes into account different possible geometrical dimensions of the fabricated sensor (i e , radius and thickness of membrane and the distance between the parallel plate capacitor) and calculates the performance of the device. The sensor characteristics for lower and higher dimensional values achieved from the simulation are compared with the experimental values and summarized in Table 5.3. The table indicates that the sensitivity, zero and maximum capacitance values of the fabricated sensor lie within the range predicted by the simulations for varied sensor

geometries

Table 5.3 Comparison of simulated results for different sensor dimensions with experimental results.

	Sensor geometries and simulated response for two slightly varied cases		Achieved sensor characteristics.
	For higher sensitivity	For lower sensitivity	
Radius of silicon membrane (a)	405	398 μm	400 μm
Thickness of silicon membrane (H)	20	24 μm	22 μm
Thickness of air gap (d)	10	12 5 μm	12 μm
Zero Pressure Capacitance (C_O)	0 4562 pF	0 3525 pF	0.3910 pF
Max Pressure Capacitance (C_{max})	0 4889 pF	0 3626 pF	0 4030 pF
Sensitivity (S)	5 2733 fF/Bar	1 6288 fF/Bar	1.935 fF/Bar

The analytical response, for upper and lower geometrical range, and experimental response to applied pressure are plotted in Figure 5 10. It can be seen from the figure, that the experimental results are within this band of allowable dimensional tolerance It can also be observed that the slope of the actual performance curve is slightly lower than the designed performance curve (as illustrated in Figure 5.7) which can be accounted mainly due to the uneven membrane thickness (22 ± 0.5μm) Sensitivity increases with increase in diameter of the circular membrane (2a) and decreases with increase in distance between the two parallel electrodes (d) In addition, the surface roughness also plays an important role in the deflection characteristics of the membrane Sensitivity of the sensor decreases with higher surface roughness

To summarize, the comparison of simulated results for different geometrical dimensions of the sensor with the achieved geometry of the sensor leads to the conclusion that the important parameter affecting sensitivity of sensor is the membrane thickness Therefore, the pressure sensitive membrane should have smooth surface and uniform thickness to achieve optimal sensitivity.

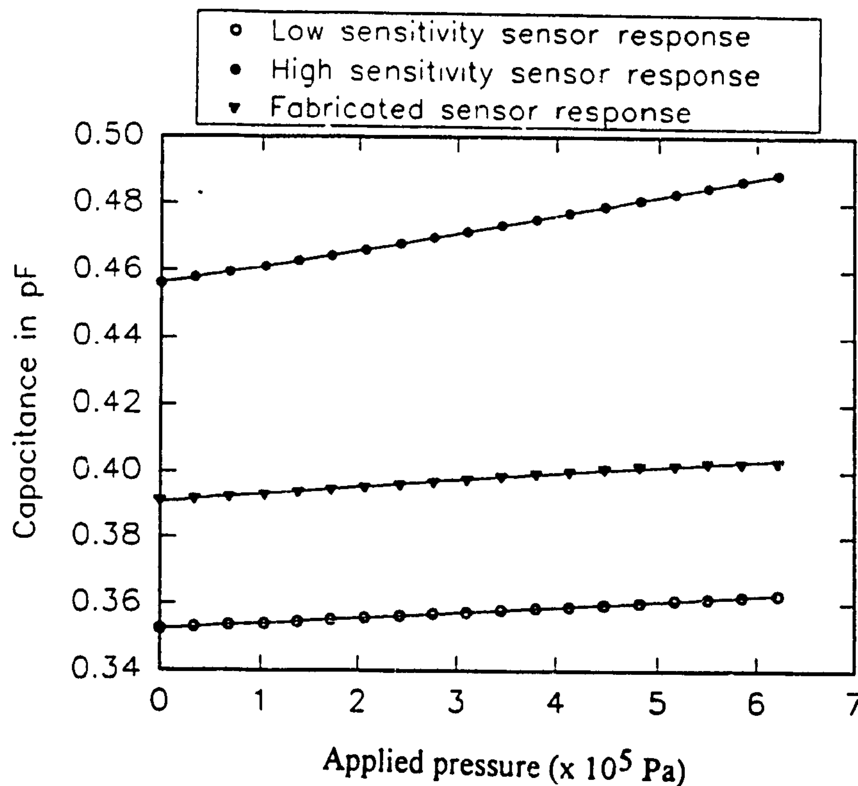

Figure 5.10 Comparison of simulated sensor performance for a range of geometrical dimensions with the experimental results. (Frequency = 1 MHz, Level = 1V, Bias = No DC bias)

5.4 Summary of Characteristics of Pressure Micro Sensor

The capacitive pressure sensor response characteristics indicates that the sensor is sensitive to pressure and the measured change in capacitance compared well with the

analytical results. The results of the experimental study performed on the pressure measurement sensor can be summarized as follows:

1. The sensitivity of the sensor for the pressure range of 0-6.2 bar/element is found to be 1.935 fF/Bar compared to the analytical value of 2 4189 fF/Bar. The sensitivity of the device is lower than the theoretical value mainly because the membrane was not flat which in turn affects the deflection and stiffness characteristics of the circular silicon membrane
2. The non linearity of the capacitance measurement circuit at frequency of 1 MHz is less than 1%. The dissipation factor of the measuring instrument at 1MHz was found to be 0.0045 Therefore, the sensor was characterized at 1MHz input signal frequency and the measured readings were stable and consistent.
3. The stability of the sensor response for a full cycle of applied pressure was measured to be less than 1% . Thus the sensor has low hysteresis value.
4. The repeatability of the sensor capacitance response with respect to applied pressure, measured for span of two months, was in the range of ±2 % . This indicates that the sensor chip was stable during the period covered by the experiment

Chapter - 6

Characterization of Capacitive Tactile Imaging Sensor

The characterization of the fabricated capacitive tactile imaging sensor is presented in this chapter. The 5 x 5 array tactile sensor with sensor number is illustrated in Figure 6.1. The instruments used for testing and the test procedure is similar to that of the pressure measurement sensor discussed in Chapter-4 This chapter presents the experimental results and its comparison with the analytical results of the tactile imaging sensor. Finally, a statistical regression analysis on the measured data is performed which provides a relationship among variables, like pressure vs capacitance, interdependence of capacitance variation between each element in the array and also variation in capacitance measurement with respect to time

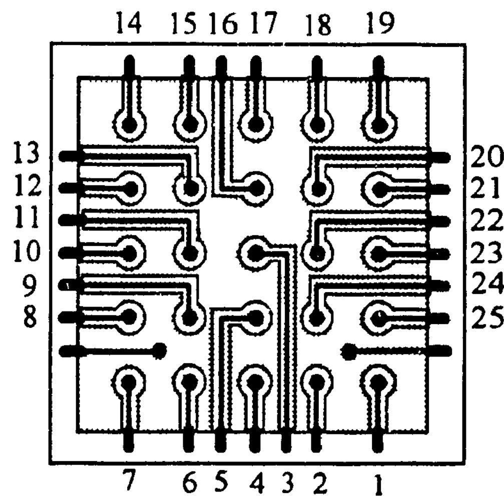

Figure 6.1. Tactile sensor with sensor number illustrated for characterization purpose.

Figure 6.2a. Photograph showing a single element of the fabricated tactile imaging sensor (x 60 magnification).

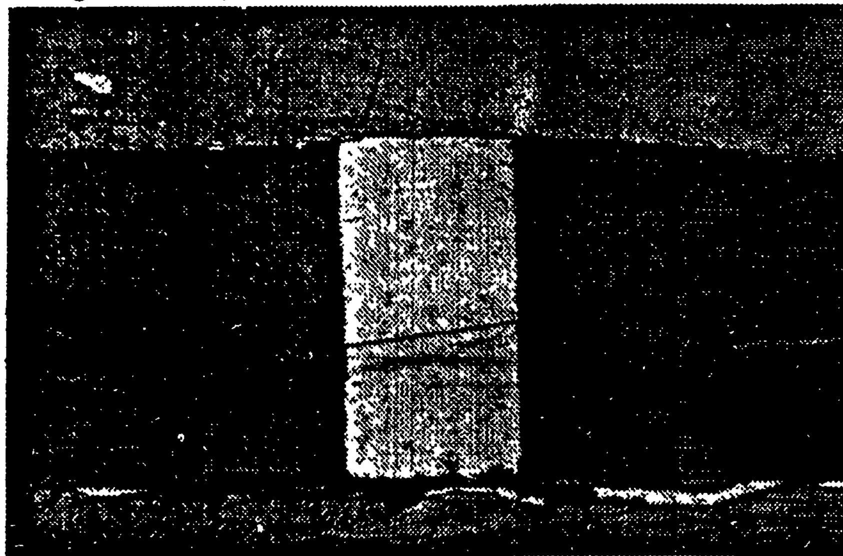

Figure 6.2b. Photograph showing the bottom electrode pad of a single element of the fabricated tactile imaging sensor (x 100 magnification).

6.1 Experimental Setup for Tactile Imaging Sensor

Figure-6.2 shows a photograph of the fabricated tactile imaging sensor Figure-6 3 illustrates the block diagram of the measuring and data analysis system. The sensor is placed on the testing platform of the probe box which is lined with metal and maintained at ground potential to avoid stray signals from interfering the test results. The probe box is a light proof black-box which minimizes the effect of light on the capacitor and prevents any unwanted carriers from being generated. The box should be dry and clean to prevent any leakage of current. The zero pressure capacitance of each sensor in the array is measured by bringing the probe wire in contact with the electrodes of the sensor.

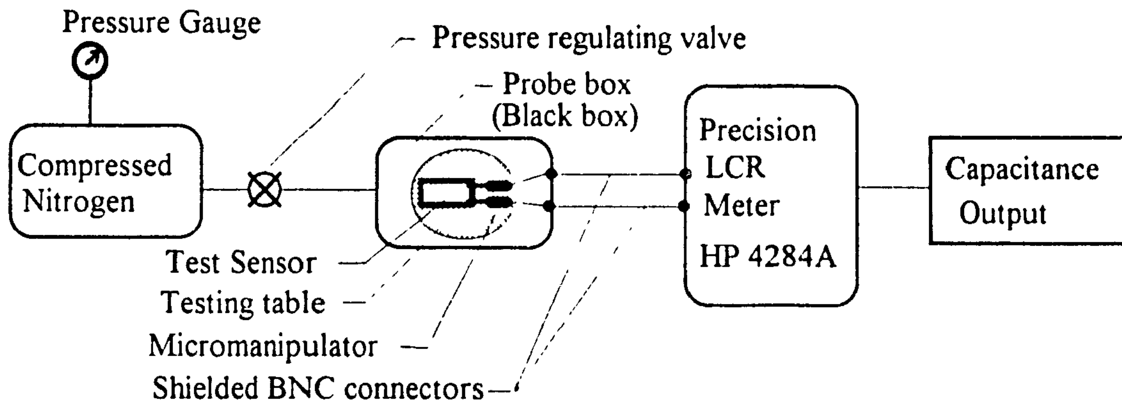

Figure 6.3 Block diagram of sensor testing system.

The test probe (micromanipulator) is composed of a magnetized insulated base which prevents shorting the probe wire to ground. The micromanipulator has a control arm which allows the wire to be moved into precise position by using the control arm adjustment knobs. The probe wire positioned on the tip of the probe control arm provides the physical connection between the measuring equipment and the testing sensor.

The testing platform is a circular disk on which the sensor is laid for testing. The platform is equipped with the ability to heat or cool the device for measuring the temperature stresses affecting the test device. A hole provided at the center of the stage

secures the device to the testing platform by connecting it to a vacuum pump. The platform is also encircled with a cooling ring which provides a cooled buffer to prevent undue heating of surrounding parts. Two platforms are provided on opposite side of the testing platform on which the micromaniputor probes are positioned. These platforms are made of stainless steel and are isolated from the ground.

The fabricated tactile imaging sensor is tested to determine its response characteristics with respect to applied force and pressure Two type of tests were performed on the sensor

(a) Geometric shape analysis of objects placed on the sensor

(b) Determination of sensor response characteristics with respect to applied pressure

For geometrical shape analysis, three different geometrical objects (i e , cube, cylinder and sphere) were selected The objects were placed on the sensor and the capacitance of each sensor element in the array measured Secondly, for the pressure response test a plexi-glass cap was fabricated and used as a pressure chamber The chamber is glued on top of the sensor A nozzle, provided on top of the pressure chamber, is connected to the pressure source using a flexible tube. Here, a compressed nitrogen cylinder is used as the pressure source A pressure gauge placed on the nitrogen cylinder measures the pressure inside the test chamber The pressure inside the chamber is regulated by means of a pressure regulating valve placed on the nitrogen cylinder

The capacitance is measured using a precision LCR (Inductive Capacitive Resistive) meter (HP 4284 A) instrument which measures the capacitance of the device This instrument is used for evaluating LCR components of semi-conductor devices over a wide range of frequencies (20 Hz to 1 MHz) and for testing under different signal levels in the range from 5mV to 2Vrms The optimal operating characteristics of this instrument is as explained in Chapter-5. The sensor chip placed on the testing platform is connected to the connector panel which is located at the rear of the probe box. The control panel serves

as an interface to connect the probe box with the capacitance measurement instrument by means of calibrated leads BNC connectors and shielded cables which minimizes the effect of external fields are used as connectors

6.2 Experimental Procedure for Characterization of Tactile Imaging Sensor

Two devices were fabricated for this project, the measurements taken for one of the device is presented in this chapter for the characterization of tactile imaging sensors fabricated using micromachining technology. For the selected device, it was observed that sensor numbers 6,14 and 21 were not responding to the desired design due to errors incurred during fabrication These sensors did not function satisfactorily mainly due to the following reason· (a) The masks prepared in the laboratory was not perfect and (b) the fabrication process like etch time and photolithography were manually operated and controlled. Due to the aforementioned problems the metal electrodes of these sensors were not continuous. These problems can be solved once the technology is established and the process becomes automated Therefore, the reading for these sensors were eliminated in the following experimental data tables

The fabricated tactile array sensor is placed on the testing platform of the probe box The vacuum pump is switched on, to hold the sensor to the platform Two probes, one from each of the two parallel plates of the sensor are connected to the capacitance measurement instrument through the leads in the probe box. Initially, the capacitance of each sensor, at ambient conditions is measured using the capacitance measuring instrument. This value gives the reference capacitance (zero deflection capacitance) for a particular input signal frequency. The zero pressure capacitance of each sensor element was tested at different signal frequency ranging from 20 Hz to 1 MHz and the

experimental results tabulated in Table 6 1.

Table 6.1 Experimental results of zero pressure capacitance of each element in the tactile array sensor with respect to different signal frequency.

Sensor	Capacitance (pF) at different input frequency							
No	20 Hz	100 Hz	1000 Hz	100 kHz	250 kHz	500 kHz	800 kHz	1000 kHz
1	0.5722	0.49112	0 34874	0 34680	0 34640	0.34590	0.34589	0 34580
2	0.5619	0 48913	0 33921	0 3390	0 33812	0.3381	0 3374	0.3371
3	0 5912	0.5115	0.3552	0.3550	0.3542	0 35398	0.35395	0 35381
4	0.5662	0.4815	0.33128	0 33122	0 3312	0.33118	0 33113	0 33105
5	0 5698	0 5187	0 3518	0 3511	0 3506	0 3503	0 3503	0.3502
7	0 5691	0 5162	0 3559	0.3558	0.3553	0 3551	0 3550	0 3549
8	0 5661	0 5143	0.3533	0.3533	0.3531	0 3528	0 3525	0 3525
9	0 5817	0.5016	0 3619	0 3618	0.3615	0 3615	0 3614	0.3611
10	0 5689	0.5158	0 3551	0 3551	0.3548	0 3546	0.3541	0 3541
11	0.5877	0 5044	0 3660	0 3655	0 3654	0 3651	0.3651	0 3365
12	0 5629	0 4882	0 3388	0 3383	0.3383	0 3381	0.3379	0 3375
13	0 5699	0 4834	0.33955	0 33951	0 3[illegible]950	0 33950	0 33949	0.33947
15	0 5611	0.5072	0 33885	0 33881	0 [illegible]3879	0 33879	0 33876	0.33872
16	0 5818	0 4812	0 3542	0 3541	0 3541	0 3539	0.3538	0 3535
17	0 5592	0 48112	0 3329	0 33281	0 3326	0 3324	0.3321	0 3321
18	0.5643	0 49002	0 3369	0 3369	0 3367	0.3366	0 336[illegible]	0.3361
19	0 5567	0 4942	0 3373	0 3371	0 3367	0.3367	0 33665	0.3366
20	0 5593	0 4985	0 3383	0 3380	0 3377	0.3377	0 3376	0 3375
22	0 5834	0 5062	0.3671	0 33671	0.33667	0 33665	0 33661	0 3366
23	0 5637	0.4909	0.3347	0.3345	0.3344	0.3344	0 3341	0 3341
24	0 5862	0 5073	0 3682	0.3682	0.36811	0.36809	0.36805	0 368
25	0.5641	0 4911	0 3362	0.3361	0.33581	0 33579	0.33579	0.33578

Figure 6 4 illustrates a typical reading of the zero pressure capacitance of a sensor element with respect to signal frequency. It was observed that at low frequency the noise effects were predominant and therefore the reading was inconsistent. Once the frequency

is increased the stray effects are reduced and the capacitance value is stable as illustrated in Figure 6.4. Figure 6.5 shows the distribution of zero pressure capacitance of each sensor in the array at 1 MHz frequency. It can be observed from the figure that the variation of zero pressure capacitance of each sensor element from the mean value is less than ±5% of the mean value for the device. This variation in capacitance is most likely due to the dimensional variations in the shape and diameter of the bottom electrodes of each capacitor during the fabrication process.

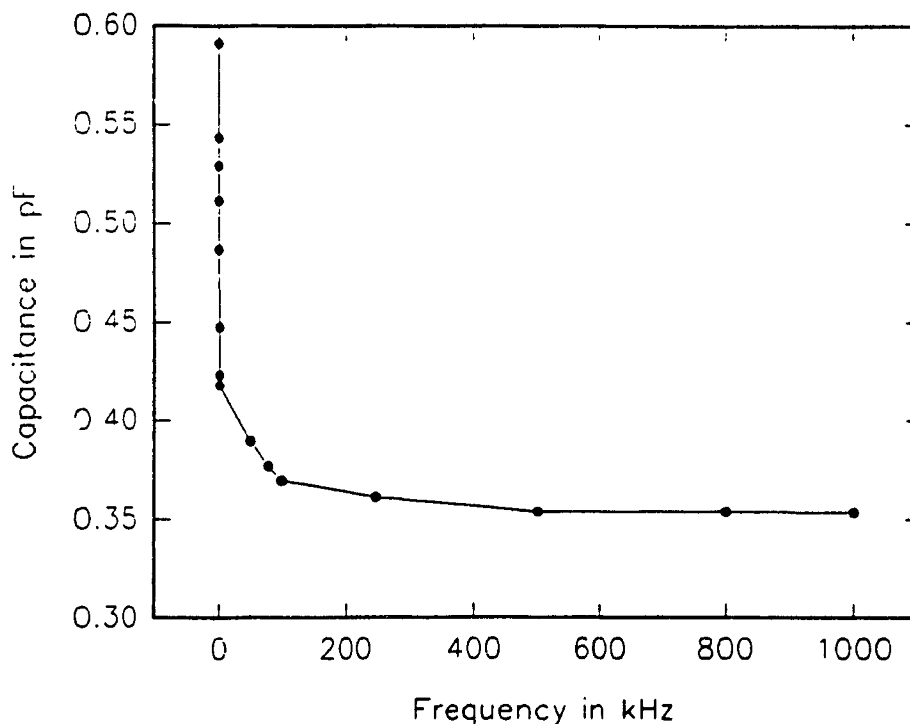

Figure 6.4 Experimental results of zero pressure capacitance as a function of signal frequency for each sensor element (level = 1V, bias=no DC bias).

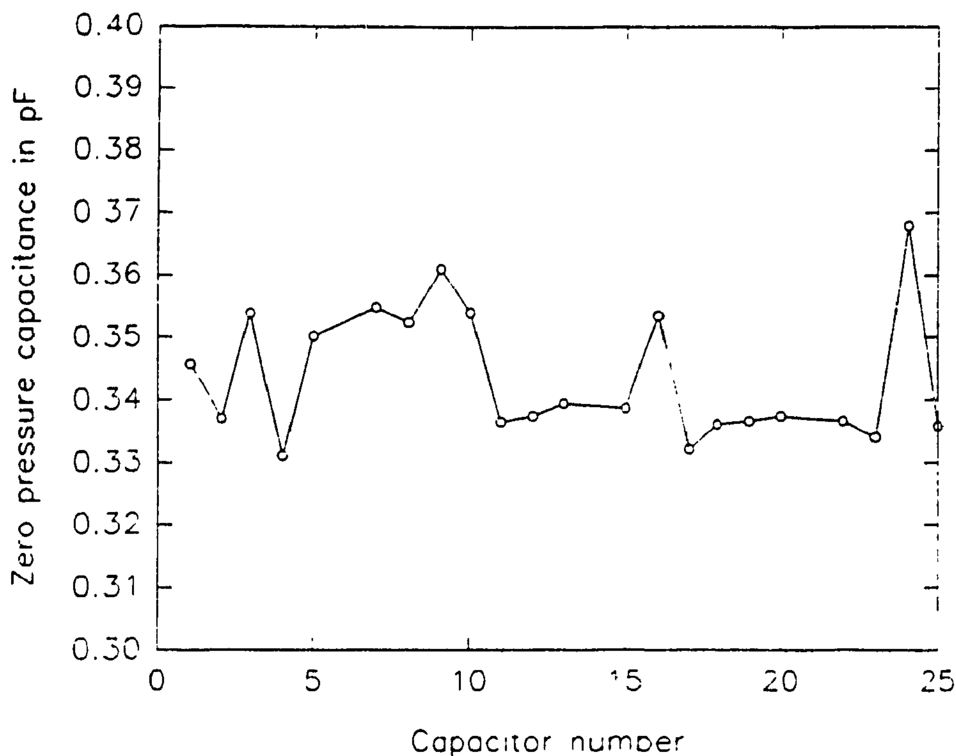

Figure 6.5. Distribution of zero pressure capacitance for each sensor element in the array (frequency=1MHz, level=1V, bias=no DC bias).

The dissipation factor of the measuring instrument decreases with increase in signal frequency and was equal to 0.0045 at 1 MHz. Therefore, at high frequency the quality of the capacitance measurement is stable and consistent. Figure 6.6 illustrates the dissipation factor as a function of signal frequency. After measuring the zero pressure capacitance of each sensor element in the device, the geometrical shape identification and pressure response characteristics tests were performed on the sensor chip. The experimental procedure for these tests are presented below.

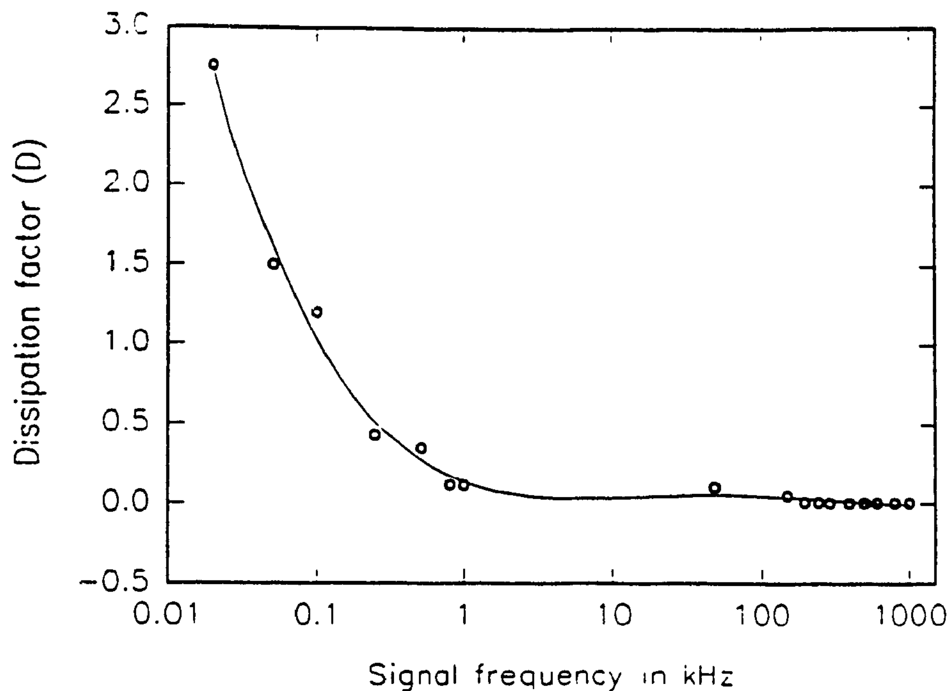

Figure 6.6. Dissipation factor (D) of the measuring instrument as a function of signal frequency. (semi-log scale).

6.2.1 Touch Understanding - Geometrical Shape Analysis

Touch understanding sensor basically consists of tactile sensing which extracts the features of an object's surface when the sensor comes in contact with it[13]. Geometrical shape analysis is an essential preliminary step in identifying three dimensional objects during grasping, inspection and assembly operations. The design problem of these type of sensors is related to the sensor structure and the sensing element which generally senses three dimensional object partially at the point of contact.

In this project, the capacitance data obtained when different geometrically shaped objects placed in contact with the sensor array is presented. The desirable feature of the fabricated tactile sensor array at this stage of the research is to perform a low-level processing of the objects placed on its surface by measuring the capacitance data of sensor elements which have values above a preset threshold. The element readings below the threshold (<0.5fF) are assumed to correspond to areas where there is no contact between the sensor and the object. These data predicts the viability of the technology

which can be developed so that the sensor identifies three dimensional object. The capacitive response characteristics of the sensor chip with respect to applied load is presented in this section.

Three objects with different geometrical shapes were selected, to analyze the response characteristics of the sensor when these objects are placed on the tactile sensor Here, we have selected stainless steel material with geometric shapes of cube, cylinder and sphere as the objects. The dimension of the selected objects is smaller than the sensor chip which helps in analyzing its total load effect on the sensor chip in a single set of reading The weight of these objects were determined using a sensitive digital balance. The load acting on each sensor should be less than the rupture load of the touch sensitive silicon membrane A layer of negative photoresist (~ 50μm thick) was used as the non-conducting polymer which forms the elastic skin for the sensor. The purpose of the skin is two fold, it serves as a mechanical protection to the pressure sensitive silicon membrane and secondly it distributes the load on the sensor when it comes in contact with point objects Table 6 2 presents the analytical value of sensor capacitance of each element in the sensor array for different loads acting on it The capacitance due to the metal lining connecting the contact pad and the bottom electrode also contribute to the zero pressure capacitance The design calculation takes into account this value of capacitance which is found to have a mean value of 9.5% of the zero pressure capacitance. This capacitance is considered to be constant because the membrane deflects only in regions which lie above the circular recessed parts of the glass substrate.

Table 6.2 Analytical capacitance of each element in the tactile sensor chip for different loads placed on it.

Capacitance in pF at different loads									
0 gmf	1 gmf	2 gmf	3 gmf	4 gmf	5 gmf	8 gmf	10 gmf	12 gmf	15 gmf
0.3755	0 3767	0.3779	0 3791	0 3803	0 3816	0 3854	0.388	0 3907	0.3948

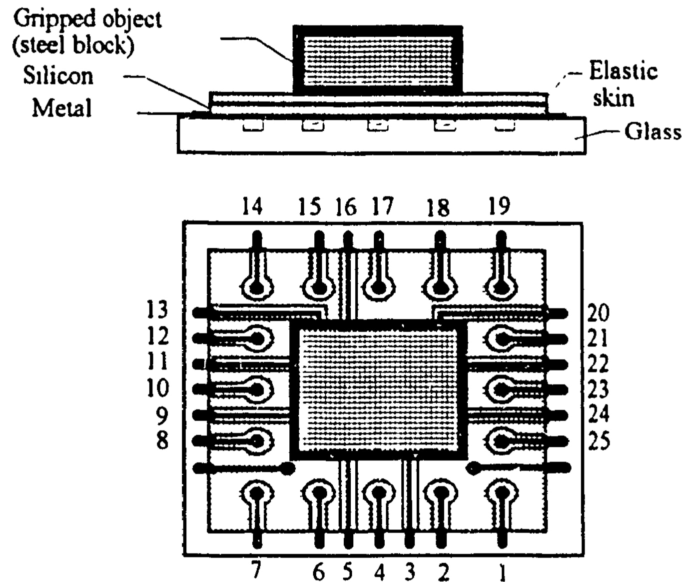

Figure 6.7 Sensors below the hatched area are affected when the rectangular block (12x12x40 mm) is placed on the sensor.

Table 6.3 Experimental data of capacitance when rectangular block is placed on tactile imaging sensor for geometrical shape analysis.

ΔC = Change in capacitance , Mass-1 = Mass of steel block = 5 gmf/element

(* Sensors which showed major change in capacitance)

Sensor No.	No load (pF)	Mass-1 (pF)	ΔC (fF)	Sensor No	No load (pF)	Mass-1 (pF)	ΔC (fF)
1	0.34580	0 34550	-0.3	**16 ***	**0.35350**	**0.35870**	**5.2**
2	0 33710	0.33740	0.3	17	0.33210	0 33250	0 4
3 *	**0.35381**	**0.35901**	**5.2**	18	0 33610	0 33640	0.3
4	0 33105	0 33135	0 3	19	0 33660	0.33620	-0.4
5 *	**0.35020**	**0.3550**	**5.0**	**20 ***	**0.33750**	**0.34260**	**5.1**
7	0.35490	0.35440	-0.5	**22 ***	**0.33660**	**0.34180**	**5.2**
8	0.35250	0.35230	-0.2	23	0.33410	0 33430	0 2
9 *	**0.36110**	**0.36610**	**5.0**	**24 ***	**0.36800**	**0.37300**	**5.0**
10	0.35410	0.35450	0 4	25	0.33578	0 33548	-0 3
11 *	**0.33650**	**0.34160**	**5.1**				
12	0.33750	0.33710	-0.4				
13 *	**0.33947**	**0.34857**	**9.1**				
15	0 33872	0 33832	-0.4				

The fabricated tactile sensor is placed on the testing platform of the probe box and the vacuum pump is switched on, to hold the device to the platform. The capacitance, at an input signal frequency of 1 MHz, is measured when different objects are placed on the sensor The response when a rectangular block is placed on the touch sensitive sensor surface is tabulated in Table 6.3. Table 6.4 presents the sensor response when a cylindrical block of known weight is placed on the sensor. Similarly, sphere balls of different weights were placed on the sensor and the capacitance of each element in the array measured and presented in Table 6.5. The response of those sensor elements which were pressed by the objects showed a change in capacitance The change in capacitance for sensor elements below 0.5 fF were considered negligible and tabulated as no change It was observed that the sensors which lie below the objects showed a considerable change in capacitance which indicates that the geometric profile of the object surface can be identified using these observations Figure 6.7, Figure 6.8 and Figure 6.9 illustrates the sensors which lie under the hatched area are affected when objects like cube, cylinder and sphere respectively are placed on its surface The weights placed on the sensor skin transmits an uniformly distributed load on the sensor elements which lie under it.

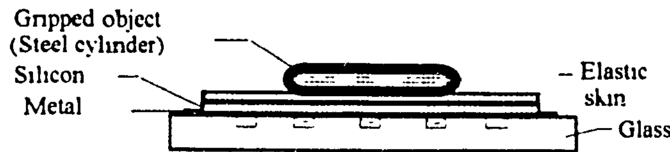

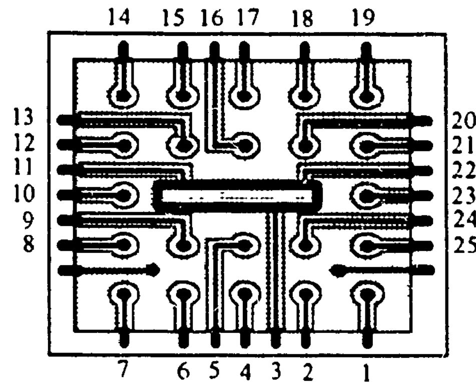

Figure 6.8 Sensors lying below the hatched area are affected when the cylinder (12 mm radius and 12 mm long) is placed on the sensor.

Table 6.4 Experimental value of capacitance when cylindrical block is placed on tactile imaging sensor for geometrical shape analysis.

ΔC = Change in capacitance , Mass-2 = Mass of steel cylinder = 4 gmf/element

(* Sensors which showed major change in capacitance)

Sensor No	No load (pF)	Mass-2 (pF)	ΔC (fF)	Sensor No	No load (pF)	Mass-2 (pF)	ΔC (fF)
1	0 34580	0 34520	-0 6	16	0 3535	0 3533	-0 2
2	0.33710	0 3372	0 1	17	0 33210	0 33240	0.3
3*	**0.35381**	**0.3811**	**4.3**	18	0 33610	0 33660	0 5
4	0 33105	0 3312	0 15	19	0 33660	0 33640	-0.2
5	0 35020	0 3503	0 1	20	0.33750	0 33720	-0 3
7	0 35490	0 3544	-0 5	**22***	**0.3366**	**0.34050**	**3.9**
8	0 35250	0 3521	-0 4	23	0 33410	0.33440	0.3
9	0.36110	0 3614	0 3	24	0 36800	0.368300	0 3
10	0 35410	0 3541	0 0	25	0 33578	0 33524	-0 54
11*	**0.3365**	**0.3406**	**4.1**				
12	0 33750	0 3373	-0 2				
13	0.33947	0 33952	0 05				
15	0.33872	0.33832	-0 4				

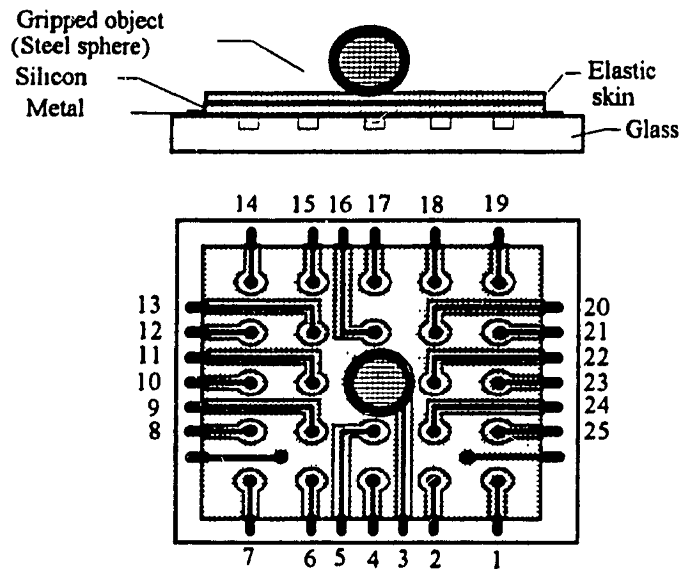

Figure 6.9 Sensor lying below the hatched area is affected when the sphere is placed on the chip.

Table 6.5 Experimental results of each sensor element in the tactile imaging sensor when spherical objects of different weights are placed on the sensor for geometrical shape analysis.

Sensor No.	Capacitance in pF for different weights				
	0 gmf	2.0 gmf	3 gmf	4 gmf	5 gmf
1	0 34580	0 3477	0.3489	0.3503	.3511
2	0.3371	0 3392	0.3401	0 3416	0.3423
3	0.35381	0.35582	0 3569	0 3581	0.3588
4	0.33105	0.333	0.3342	0.3355	0.3364
5	0.3502	0.3519	0.3533	0.3543	0.3556
7	0 3549	0 3561	0 3578	0.3596	0 3601
8	0 3525	0 3544	0 3557	0.3571	0 3578
9	0 3611	0.3624	0 3644	0.3653	0.3664
10	0.3541	0 3566	0.3572	0.3596	0.3599
11	0 3365	0.3382	0.3396	0 3409	0 3414
12	0.3375	0 3394	0.3401	0 3417	0.3422
13	0 33947	0.34145	0 3427	0.3438	0 3441
15	0 33872	0 3405	0 3412	0 3431	0 3439
16	0 3535	0 3559	0.3566	0 357	0 3583
17	0 3321	0.3344	0 3354	0.3365	0.3371
18	0 3361	0.3384	0 3389	0.3409	0.3418
19	0 3366	0 3382	0 3394	0 3411	0 3419
20	0.3375	0 3391	0 3408	0 3415	0 3424
22	0 3366	0.3387	0.3394	0.3403	0.3417
23	0.3341	0.3360	0 3375	0.3385	0.3392
24	0.368	0.3698	0.371	0 3726	0 3734
25	0 33578	0.3375	0.3389	0 3403	0 3416

6.2.2. Pressure Response Test

The fabricated tactile imaging array sensor is sensitive to both force and pressure applied on the sensitive thin silicon membrane A pressure response test is conducted by applying predetermined pressure on selected sensor elements on the chip The pressure

measurement test ensures a uniform load on the selected sensor elements and therefore the response characteristics of these elements can be studied. For this purpose, a plexi-glass pressure chamber was constructed for testing the sensor chip. The fabricated sensor is placed on the testing table of the probe box and the pressure chamber is glued air tight on to the sensitive silicon surface. A pressure leakage test was conducted, for the experimental setup, to ensure that the chamber is air tight. Two probes, one from each of the two parallel plates of the sensor element are connected to the capacitance measurement instrument. A compressed nitrogen cylinder is then connected to the chamber

Table 6.6 Experimental and analytical response of capacitive tactile imaging sensor with respect to applied pressure

Pressure ($x\ 10^5\ N/m^2$)		0	0 3445	0.689	1.034	1 378	1.723	2.067	2.412
Analytical Capacitance (pF)		0 3755	0.3782	0.3809	0.3837	0 3866	0.3895	0 3926	0 3957
Experimental value of Capacitance for sensor number (pF)	3	0 3538	0.3563	0.3598	0 3623	0 3641	0.3659	0 3689	0.3708
	5	0.3502	0 3528	0 3555	0 3590	0 3605	0.3619	0.3644	0.3664
	9	0 3611	0 3633	0 3658	0.3696	0 3710	0.3722	0.3749	0.3777
	11	0 3365	0.3391	0.3421	0 3455	0.3469	0 3482	0.3510	0 3540
	13	0.3395	0 3422	0 3455	0 3483	0.3498	0.3516	0.3541	0.3564
	16	0 3535	0 3561	0 3586	0.3616	0.3631	0.3646	0 3672	0 3703
	20	0.3375	0 3396	0 3418	0.3466	0 3468	0.3495	0 3524	0.3549
	22	0 3366	0 3390	0 3414	0.3452	0.3471	0.3491	0 3512	0.3957
	24	0 3680	0.3699	0.3725	0 3768	0.3786	0.3802	0.3831	0.3854

A regulated pressure from the nitrogen cylinder is fed into the chamber through the pressure regulating valve. The two lead wires connected from the sensor to the pressure LCR meter gives the capacitance of the sensor The pressure inside the chamber is

increased gradually up to a pressure of about 2.41x 10^5 N/m^2 (35 psig). The pressure differential across the diaphragm induces a change in capacitance. The capacitance, at an input signal frequency of 1 MHz, is measured for different pressures. The experimental and analytical values are tabulated in Table 6.6. Figure 6.10 shows the experimental and analytical pressure response results of the fabricated capacitive tactile imaging sensor. The response of the each sensor element in the array is linear with respect to change in pressure. In effect each sensitive site in the array is a separate force/pressure sensor. Ideally, the performance of each element in the array should match every one of the other but practically this is not the case.

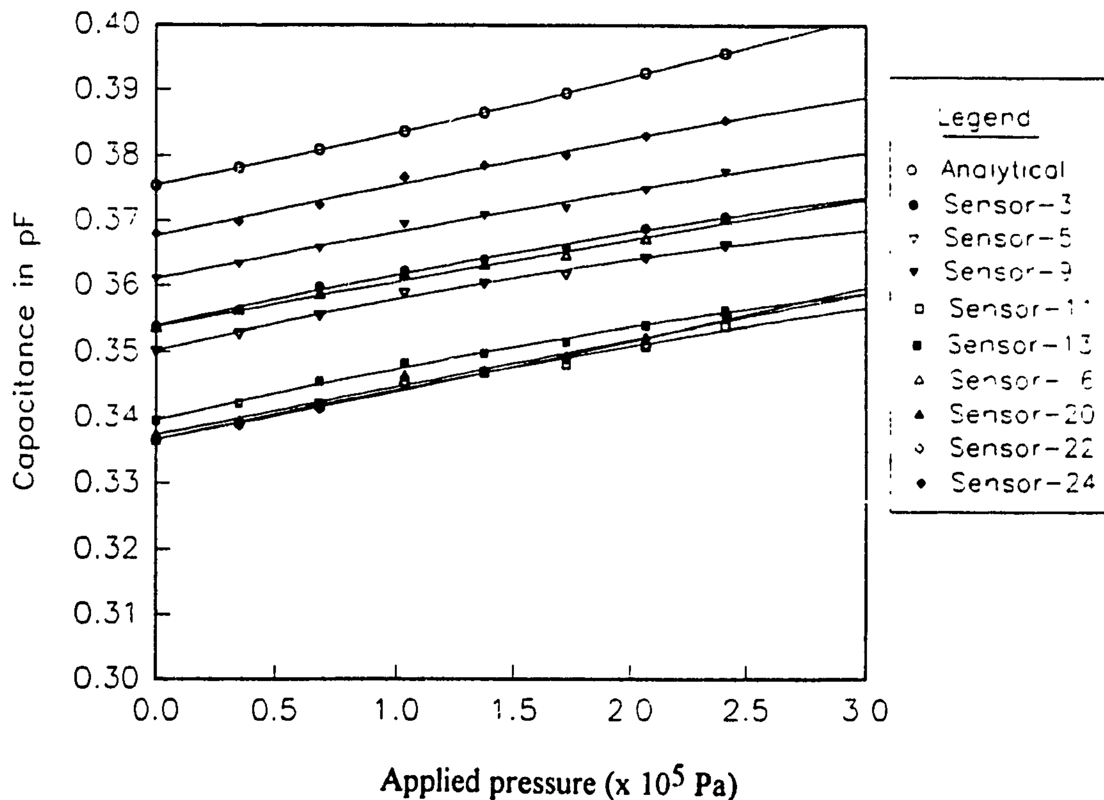

Applied pressure (x 10^5 Pa)

Figure 6.10 Capacitance as a function of pressure for selected sensor element (frequency=1MHz, level=1V, bias=no DC bias).

6.3 Statistical Analysis of Performance of Tactile Imaging Array Sensor

A statistical regression analysis was performed on the experimental data obtained for the tactile imaging array sensor. The regression analysis provides a conceptual method for investigating statistical relationship among variables, like pressure vs capacitance, interdependence of capacitance variation between each element in the array and the change in capacitance with respect to time This analysis helps in evaluating the consistency of the fabrication process and the precision of measuring instrument. The standard approach in this method is to use the measured data to compute an estimate of the proposed relationship and evaluate the best fit using statistics It also helps in understanding the interrelationship among the variables and the constants.

The zero pressure capacitance of each sensor element in the tactile array measured at regular interval for 45 day is tabulated in Table 6.7 It is obvious from the table that the variation in measurements are within the tolerable limits (± 5%) of the mean value Table 6 8 presents the summary of statistical analysis of zero pressure capacitance of each element taken at regular interval for 45 days The standard deviation of the measured capacitance for the period covered by the experiment is below 0.1fF, which is within the precision of the measuring instrument (0.5fF).

The correlation between each sensor element and the measured data for zero pressure capacitance is presented in Table 6.9 The correlation helps in evaluating the interrelation between the selected variable. For correlation coefficient $|r| < 30\%$, indicates a strong independence between the variables, $30\% < |r| < 70\%$ indicates a relationship between the variables and $|r| > 70\%$ indicates a strong relationship between the variables From Table 6 9, it is obvious that there is no relation (strong independence) between the sensor capacitance with respect to time The summary of the statistical analysis from the above mentioned tables indicates that the sensor chip was stable, during the characterization period covered by the experiment, as illustrated in Figure 6 11.

Table 6.7 Experimental results of zero pressure capacitance of tactile imaging sensor measured at regular interval for 45 days.

Sensor	Sensor capacitance in pF for the following days									
No.	0	5	10	15	20	25	30	35	40	45
1	0 3453	0 3457	0 3451	0 3459	0 3448	0 3454	0 3458	0 3452	0 3449	0 34580
2	0 3363	0 3378	0 3374	0 3369	0 3377	0 3372	0 3378	0 3366	0 3376	0 3371
3	0 3531	0 3544	0 3539	0 3536	0 3532	0 3539	0 3543	0 3538	0 3536	0 35381
4	0 3314	0 3312	0 3301	0 3317	0 3314	0.3319	0 3318	0 3312	0 3314	0 33105
5	0 3506	0 3502	0 3497	0 3504	0 3508	0 3493	0 3498	0 3503	0 3504	0 3502
7	0 3543	0 3548	0 3557	0 3544	0 3554	0 3548	0 3543	0 3555	0 3553	0 3549
8	0 3529	0 3521	0 3518	0 3528	0 3522	0 3533	0 3529	0 3527	0 3533	0 3525
9	0 3618	0 3616	0 3606	0 3613	0 3614	0 3604	0 3615	0 3612	0 3609	0 3611
10	0 3534	0 3543	0 3548	0 3539	0 3544	0 3536	0 3543	0 3542	0 3544	0 3541
11	0 3369	0 3358	0 3365	0 3363	0 3372	0 3361	0 3357	0 3368	0 3374	0 3365
12	0 3371	0 3379	0 3368	0 3366	0 3379	0 3358	0 3374	0 3377	0 3359	0 3375
13	0 3397	0 3388	0 3395	0 3395	0 3387	0 3392	0 3385	0 3394	0 3398	0 33947
15	0 3395	0 3383	0 3394	0 3384	0 3396	0 3382	0 3387	0 3394	0 3385	0 33872
16	0 3531	0 3539	0 3528	0 3533	0 3538	0 3527	0 3535	0 3528	0 3543	0 3535
17	0 3328	0 3326	0 3312	0 3320	0 3316	0 3323	0 3324	0 3316	0 3327	0 3321
18	0 3368	0 3362	0 3357	0 3365	0 3363	0 3369	0 3358	0 3366	0 3355	0 3361
19	0 3369	0 3362	0 3375	0 3366	0 3363	0 3374	0 3363	0 3377	0 3365	0 3366
20	0 3371	0 3374	0 3383	0 3377	0 3378	0 3381	0 3379	0 3382	0 3376	0 3375
22	0 3368	0 3362	0 3375	0 3364	0 3363	0 3369	0 3372	0 3374	0 3365	0 3366
23	0 3347	0 3338	0 3348	0 3347	0 3336	0 3345	0 3338	0 3336	0 3348	0 3341
24	0 3684	0 3678	0 3686	0 3673	0 3682	0 3675	0 3683	0 3675	0 3683	0 3680
25	0 3351	0 3364	0 3359	0 3353	0 3365	0 3354	0 3362	0 3363	0 3359	0 33578

Table 6.8 Summary of statistical analysis of zero pressure capacitance of each sensor element taken at regular interval for 45 days.

Sensor No	Mean	Median	S	Min	Max.	Q1	Q3
1	0.34539	0.34535	0.00040	0.34480	0.34590	0.34505	0.34580
2	0.33724	0.33730	0.00052	0.33630	0.33780	0.33683	0.33773
3	0.35406	0.35385	0.00072	0.35310	0.35540	0.35360	0.35452
4	0.33132	0.33140	0.00051	0.33010	0.33190	0.33116	0.33173
5	0.35017	0.35025	0.00045	0.34930	0.35080	0.34977	0.35045
7	0.35496	0.35485	0.00054	0.35430	0.35570	0.35438	0.35551
8	0.35265	0.35275	0.00050	0.35180	0.35330	0.35217	0.35300
9	0.36118	0.36125	0.00044	0.36040	0.36180	0.36083	0.36152
10	0.35414	0.35425	0.00041	0.35340	0.35480	0.35382	0.35440
11	0.33652	0.33650	0.00057	0.33570	0.33740	0.33602	0.33697
12	0.33706	0.33725	0.00077	0.33580	0.33790	0.33643	0.33775
13	0.33926	0.33945	0.00045	0.33850	0.33980	0.33878	0.33955
15	0.33887	0.33870	0.00055	0.33820	0.33960	0.338[illegible]	0.33942
16	0.34977	0.35305	0.00754	0.33510	0.35430	0.34850	0.35357
17	0.33213	0.33220	0.00053	0.33120	0.33280	0.33160	0.33263
18	0.33624	0.33625	0.00047	0.33550	0.33690	0.33577	0.33665
19	0.33680	0.33660	0.00055	0.33620	0.33770	0.33630	0.33742
20	0.33776	0.33775	0.00038	0.33710	0.33830	0.33748	0.33812
22	0.33678	0.33670	0.00046	0.33620	0.33750	0.33637	0.33725
23	0.33474	0.33460	0.00151	0.33360	0.33880	0.33375	0.33480
24	0.36799	0.36810	0.00044	0.36730	0.36860	0.36750	0.36832
25	0.33588	0.33590	0.00048	0.33510	0.33650	0.33537	0.33632

Q1 = First quartile, Q3 = Third quartile and S = Standard deviation

Table 6.9 Correlation between each sensor element and the measured data for zero pressure capacitance taken at regular interval for 45 days

Sensor No	Correlation *	Sensor No	Correlation *	Sensor No	Correlation *
1	-0.014	11	0.201	22	0.111
2	0.141	12	-0.133	23	-0.502
3	-0.153	13	0.091	24	-0.137
4	0.164	15	-0.212	25	0.242
5	-0.102	16	0.204		
7	0.294	17	-0.059		
8	0.393	18	-0.319		
9	-0.357	19	0.020		
10	0.196	20	0.262		

* correlation between zero pressure capacitance versus time.

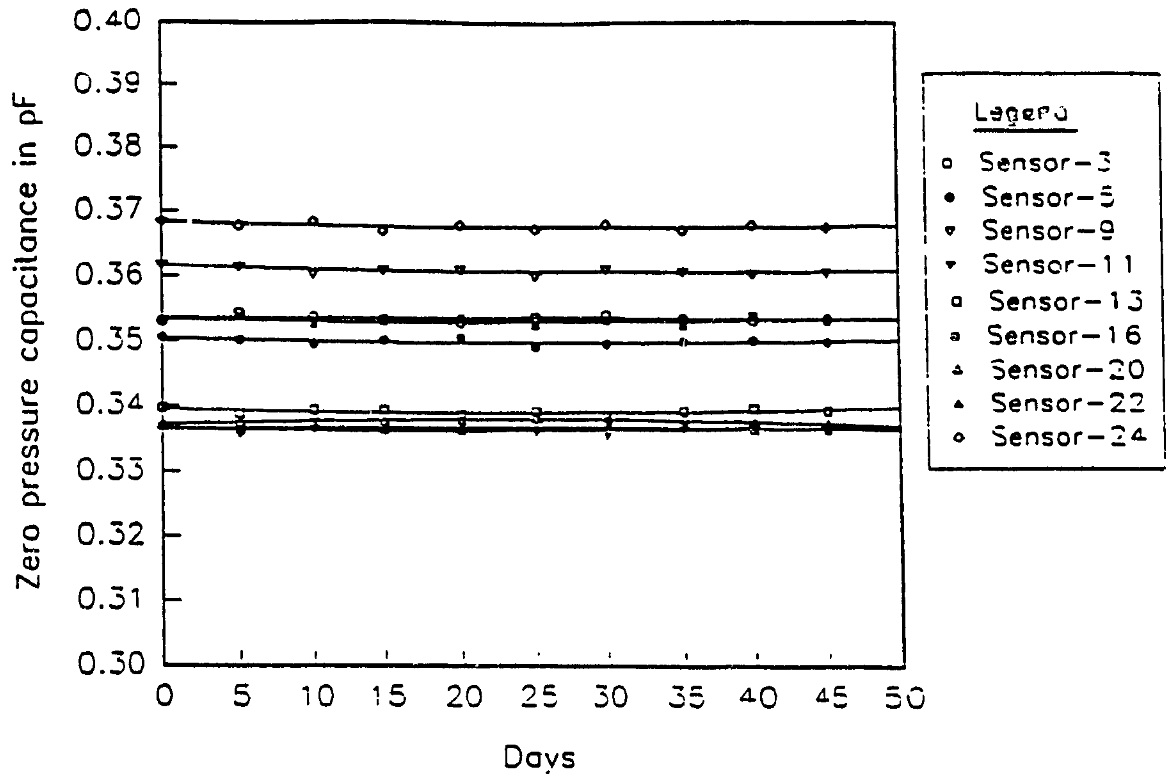

Figure 6.11. Zero pressure capacitance measured at regular interval for selected sensor elements to verify long term stability of device (frequency=1MHz, level=1V, bias=no dc bias).

A regression analysis was performed to study the variation of each sensor element with respect to applied pressure. The summary of the regression analysis is presented in Tables 6.10a. The correlation coefficients are used to calculate the regression equation, C_r, which is written as:

$$C_r = b_0 + b_1 (P) \tag{6.1}$$

where, b_0 and b_1 are the mean of the zero pressure capacitance and the slope of the function curve respectively and P is the applied pressure.

The multiple coefficient of determination, R^2, the adjusted multiple coefficient of determination R^2(adj) and the regression equation with respect to pressure is tabulated in Table 6.10b. From this table it is obvious that the capacitance of the selected sensor

elements have a strong relation with respect to applied pressure To substantiate the regression analysis a correlation between the sensor elements and the applied pressure was performed and the results are presented in Table 6.11. It is obvious for Table 6.11 that there is a strong correlation between each sensor elements and the applied pressure. This correlation also establishes that each element can perform as an individual sensing element with the same efficiency.

Table 6.10a. Summary of regression analysis of sensor element with respect to applied pressure.

Sensor No.	Correlation co-efficient		Standard deviation (S)		Standard deviation of residuals (s)
	Const. (b_0)	Pressure (b_1)	Const	Pressure	
3	0 354317	0 00048119	0 000359	0 00001717	0 0005564
5	0 350833	0 00045738	0.000444	0 00002124	0.0006882
9	0 361333	0 00046381	0.000437	0.00002087	0 0006764
11	0.337008	0.00048024	0 000460	0 00010220	0.0004802
13	0 340192	0 00047048	0 000403	0 00001927	0 0006245
16	0 353850	0 00045857	0 000349	0 00001668	0 0005405
20	0 337425	0.00049786	0 000518	0 00002477	0 0008025
22	0.336508	0 00052310	0 000448	0 00002141	0 0006939
24	0 36795	0 00050643	0 000433	0.00002068	0 0006702

Table 6.10b. Summary of regression analysis of sensor element with respect to applied pressure.

Sensor No	R^2 (%)	R^2 (adj) (%)	Regression equation of capacitance with pressure
3	99 2	99.1	C = 0.354 +0.000481 Pressure
5	99 2	99.1	C = 0 354 +0.000481 Pressure
9	98.8	98.6	C = 0 361 +0.000464 Pressure
11	98 8	98.5	C = 0.337 +0.000480 Pressure
13	99 0	98.8	C = 0.340 +0.000470 Pressure
16	99.2	99 1	C = 0.354 +0.000459 Pressure
20	98 5	98 3	C = 0.337 +0.000498 Pressure
22	99.8	98.8	C = 0.337 +0.000523 Pressure
24	99 0	98 8	C = 0.368 +0 000506 Pressure

R^2 = multiple coefficient of determination
R^2(adj) = adjusted multiple coefficient of determination

Table 6.11 Correlation between capacitance of sensor elements and applied pressure

Sensor No.	correlation coefficient *	correlation coefficient (capacitance Vs capacitance)							
		3	5	9	11	13	16	20	22
3	0.996								
5	0.994	0.998							
9	0.994	0.996	0 998						
11	0.994	0.998	0.998	0.999					
13	0.995	0.999	0.999	0.997	0.999				
16	0.996	0.997	0.997	0.999	0.999	0.998			
20	0.993	0.993	0.995	0 997	0 995	0.994	0.995		
22	0.995	0.992	0.993	0.997	0 996	0.993	0.998	0.994	
24	0.995	0 996	0 998	0 999	0 997	0.996	0 996	0 997	0 995

* correlation between capacitance Vs pressure.

6.4 Experimental Results of Tactile Imaging Sensor

The performance characteristics of these type of tactile imaging array sensors are indeed encouraging The experimental mean value of no-load or zero load capacitance of each element is about 0 3437 pF compared to the analytical value of 0 3755 for the same geometrical dimensions of the fabricated sensor. The sensor response to applied pressure compared well with the analytical results Table-6 12 shows the analytical and experimental performance characteristics of an element (Sensor-3) of the 5x5 array tactile imaging sensor.

Table 6.12 Comparison of analytical and experimental performance characteristics of an element (Sensor-3) in the 5 x 5 array tactile imaging sensor.

	Analytical	Experimental results (for Sensor number 3)
Zero Pressure Capacitance (C_O)	0.3755 pF	0.3538 pF
Max. Pressure Capacitance (C_{max})	0.3957 pF	0.3708 pF
Max. operating Pressure	4.32×10^5 (N/m^2)/element	2.41×10^5 (N/m^2)/element
Sensitivity (S)	8 375 fF/Bar	7.048 fF/Bar

From the obtained experimental data it can be observed that Sensor-24 and Sensor-4 has the lowest and highest sensitivity respectively The variation in sensitivity can related to the changes in the geometrical dimension of each sensor element occurred during the fabrication. To determine the range of dimensional variation of each sensor element a simulation using different possible geometrical dimension was performed and the summary of the results is presented in Table-6 13 Therefore it can be concluded that the dimensional variation of the sensor is within the limit of ±5%.

Table 6.13 Comparison of simulated results for different geometrical dimensions with the experimental results.

	For lower sensitivity		For higher sensitivity	
	Analytical	Experimental (Sensor -24)	Analytical	Experimental (Sensor-4)
Radius of membrane (μm)	500	498	495	503
Thickness of membrane (μm)	16.5	15	15	15
Thickness of air gap (μm)	15	15	17	16
Zero pressure capacitance C_o (pF)	0 3755	0 3680	0 3240	0.3311
Max. pressure capacitance C_{max} (pF)	0.3960	0.3854	0.3612	0 3595
Sensitivity (S) (fF/Bar)	7 13	7.22	15.44	11.81

6.5. Summary of Characterization of Tactile Imaging Sensor

The response characteristics of the sensor is not dependent on the no-load capacitance (C_o) but in the change in capacitance of each element in the array. The primary function of the device is to measure the displacement of touch sensitive material into conveniently processed electrical signal rendering the impressions on the touch surface. The summary of the experimental study performed on the tactile imaging sensor are presented below.

1. The fabricated sensor chip can be used as a geometrical shape recognition sensor. The experimental results compared well with the analytical results. The measured data of capacitance when different geometrically shaped objects are placed on the sensor is very raw and therefore it should be further processed to get the exact geometric shape of the object.

2. The sensitivity of the sensor, for the pressure range of 0-2.41 bar/element, is found to be 7.048 fF/Bar compared to the analytical value of 8.375 fF/Bar. The sensitivity of the device is lower than the theoretical value mainly because of the variation in the geometry of the sensor incurred during fabrication and the precision limit (0.5fF) of the measuring instrument

3. The non-linearity in the capacitance output is caused by the capacitance in the non-active area (stray capacitance or parasitic capacitance - C_D) of the variable capacitor. Figure 6.12 shows the equivalent circuit of the tactile imaging sensor. The stray capacitance reduces the sensitivity, contribute to higher non-linearity and decrease the thermal stability. All leads must be shielded to reduce the effect of stray capacitance. Errors like non-linearity and temperature co-efficients can be compensated using integrated circuitry. Therefore the total capacitance (C_T) is written as

$$C_T = C_x + C_D \tag{6.2}$$

where, C_x is the active capacitance

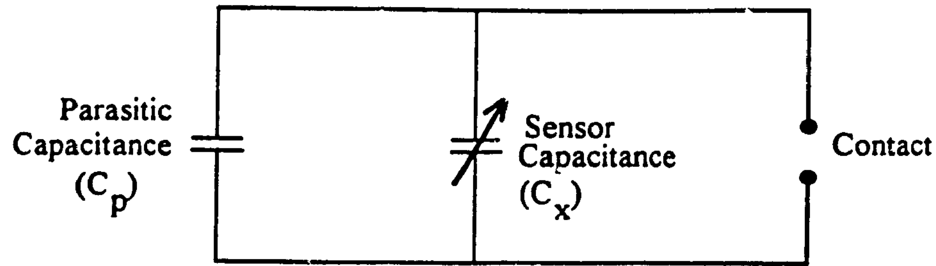

Figure 6.12. Equivalent circuit of the tactile imaging sensor.

4. The stability of the sensor chip for capacitance measurement with respect to applied pressure for a full cycle is illustrated in Figure 6.13. From the figure it is observed that the variation in capacitance is less than 5%, indicating low hysteresis effect for the sensor chip

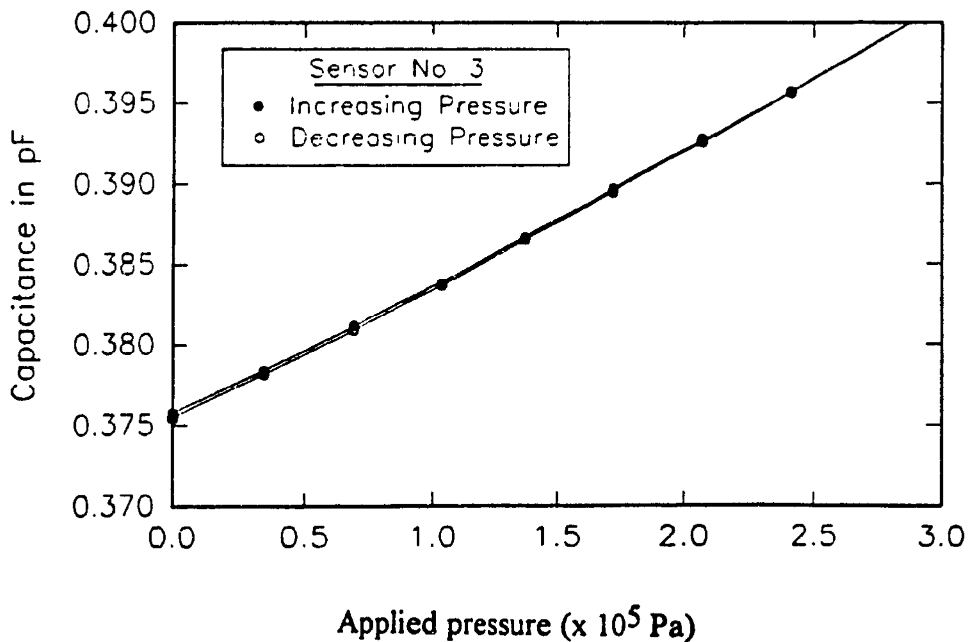

Figure 6.13. Experimental results of capacitance Vs pressure for a full cycle for an individual sensing element (frequency=1MHz, level=1V, bias=no dc bias).

5. The dimensional repeatability of each element in the sensor array is less than ± 5%. This error occurs during the fabrication process and can be eliminated once the technology is established.

6. The repeatability of the sensor capacitance response with respect to applied pressure measured for a span of 45 days was close to ± 2%. Figure 6.14 shows a typical repeatability curve of the sensor The upper curve represents the high reading and the lower curve the low reading measured during the span of the experiment The observed deviation is likely to be due to the effects of parasitic capacitance of the measuring instruments and the surroundings

7. The results from the statistical and regression analysis performed on the experimental data of the sensor chip is summarized as follows

   (a.) The zero pressure capacitance of each sensor element is within 10% of the mean value of the sensor chip The standard deviation is below 0.1fF which is within the precision of the measuring instrument (0.5fF)

   (b) The correlation between sensor capacitance at zero pressure and the position of the each sensor element shows that there is strong independence between them. The range of correlation is from -0 357 to 0.242 which indicates negligible dependence and each element in the array acts as individual sensor

   (c.) The regression analysis of capacitance versus pressure proves that their is a strong dependence of capacitance with applied pressure. The multiple coefficient of determination, R^2, is about 99%

(d.) The results of the analysis of correlation between capacitance with time shows a very strong independence, for a period of 45 days. The very low multiple coefficient of determination, R^2, indicates the stability of the sensor chip for the period of time covered by the experiment.

(e.) There is a strong correlation between each sensor element with respect to applied pressure. This indicates that all capacitor in the sensor array have the same sensitivity. The correlation establishes that each element can perform as an individual sensing element with the same efficiency. This also proves that batch processing technique can be applied to achieve high density array sensor chip.

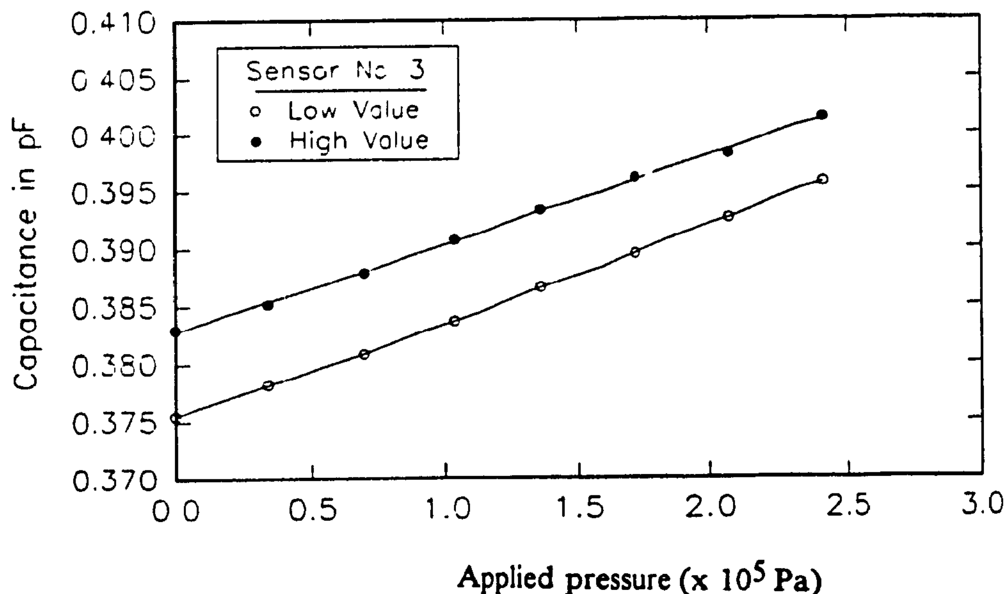

Figure 6.14. Experimental results of the high and low value of capacitance for an individual sensing element measured at regular interval for 45 days (frequency=1MHz, level=1V, bias=no dc bias).

Chapter - 7

Conclusions and Suggestions for Future Work

Two miniature capacitive pressure sensors one for pressure measurement and the other for tactile sensing, have been designed and fabricated using micromachining technology The fundamental performance of both sensors has been evaluated and the sensor chips have demonstrated satisfactory sensitivity to applied pressure In addition, several experiments were performed to study and characterize micromachining techniques like anodic bonding, electrochemical glass drilling and anisotropic silicon etching using KOH etchant. This chapter presents the conclusions of the research work performed for this dissertation thesis and the suggestions for future work

The primary objective of this dissertation research is to contribute to the field of Micromechatronics by presenting a novel method for the design and fabrication of capacitive type miniature silicon/glass sensors The fabrication process is substantially different from any previously reported capacitive sensors The highlights of the present research work are summarized as follows

I. A 4 x 5 array capacitive pressure measurement sensor have been designed, fabricated and characterized. The designed pressure sensor has the following fabrication features

   i. It has four non-aligning and two aligning masking steps

   ii. Anodic bonding is used for bonding the silicon membrane with glass substrate

   iii. The top silicon cover is also anodically bonded to the glass wafer

   iv. Electrochemical discharge drilling technique is used to drill holes in glass substrate for metal contacts and pressure inlet vent

II A novel 5 x 5 array capacitive tactile imaging sensor has been designed, fabricated and

characterized The fabricated capacitive tactile imaging sensor can be used as a touch sensor to measure the force and pressure applied on it. The designed sensor has the following fabrication features:

i. Prefabricated silicon thin wafer having uniform thickness (variation $\pm 0.1 \mu m$) is used as the touch sensitive membrane. No masking steps are required for this membrane.

ii. The glass wafer has two masking steps, of which one is an alignment masking step

III. Characterization of the boundary conditions of anodically bonded silicon-glass structures.

IV. Design and realization of an electrochemical glass drilling apparatus and determining the drilling time for glass with different thickness

V. Design and setting up of a constant temperature KOH etching apparatus and experimentally determining the etch rate at different temperature and different KOH concentration

7.1 Conclusions

The following conclusions are drawn from the analytical and experimental studies performed in this dissertation research.

1. The experimental and analytical results of the fabricated capacitive sensors reveals that slight changes in the geometrical parameters of the sensor (thickness and diameter of membrane) introduce large variations in the capacitance of the device. Therefore, precision design and machining of micro-electro-mechanical-systems (MEMS) plays an important role in realizing high accuracy measurement devices.
2. The sensitivity of the fabricated capacitive pressure measurement sensor is 1.935

fF/Bar compared to the analytical value of 2.42 fF/bar for a pressure range of 0-6 2 Bar/element. The performance characteristics of the sensor chip showed good linearity and low hysteresis value for the range of measured pressure. The yield and uniformity in performance were satisfactory

3. The capacitive type micromachined pressure measurement sensor can be used for measuring different ranges of pressure depending on the size of the sensor. The pressure measurement sensor fabricated for this research work had a membrane thickness of 22 μm. Although the membrane thickness was not uniform, due to the problems faced during fabrication, acceptable characteristics of the sensors have been achieved.
4. The variable capacitive type tactile sensor can be used as a potential device for providing force feedback signals and sensing information of the sensing element The preliminary work demonstrates the feasibility of a micromachined tactile sensor The fabricated capacitive tactile sensor is useful for pressure measurements within the range of 0-2.41 bar for a membrane thickness of 15μm. The first results of the silicon tactile sensor looks promising, however, much research has to be done with respect to yield and reliability.
5. The sensitivity of capacitive sensors can be increased by reducing the membrane thickness and increasing the diameter of the membrane The surface of the membrane should be flat and uniform to achieve optimum sensitivity.
6. The rupture pressure of the silicon membrane determines the operating pressure range of the sensor. The rupture pressure increases with the diaphragm thickness and decreases with the diaphragm diameter.
7. The sensor is very susceptible to environmental noise and their application is restricted

to very well shielded environments. This effect is minimized by operating the sensor at high signal frequency (>800 kHz).

8. Anodic bonding solves major problems like packaging and long term stability of miniature pressure transducer. The optimal bonding parameters obtained from experimental study is, 350°C (hot plate temperature) and 1000V (applied voltage) The characterization of boundary conditions of anodically bonded silicon-glass sandwich structures showed that this type of sealing is superior compared to epoxy glued structures. Cantilever silicon strips anodically bonded to glass for different range (22.2 - 3.4 mm) of bond length had the same natural frequency. However silicon cantilever strips bonded to glass using epoxy bonding showed significant changes in the natural frequency (decrease of 4.5% for 12.2 mm decrease in bond length) with change in bond length
9. The principle of electrochemical discharge drilling of glass can be used to make leak free electrical contact points and vent holes for micromachined sensors. The experimental study performed on the assembled drilling apparatus yielded the optimal operating parameters and the time for drilling through holes in glass having different thickness. The optimal process parameters for drilling are: (a) concentration of electrolyte (NaOH) = 35% (weight), (b) applied voltage = 36V (DC), (c) force applied on the needle = 0.2 N.
10. The experimental study of etch rate of HF on glass revealed that, for the first minute the etch rate is 9 μm/min. and it gradually stabilizes to 4 μm/min. after 6 minutes of etching.
11. The experimental results obtained for etching silicon in KOH, using the assembled constant temperature etching apparatus, compared well with those from the literature.

The etch rates were lower by 5% from those found in literature However, a uniform etch rate was attained using the constant temperature apparatus (for example., a etch rate of 1.6μm/min at 85°C) for different temperature and different KOH concentration.

Silicon is an excellent sensing material from the electrical and mechanical point of view. Therefore, it has been used in a wide assortment of sensing application. Due to the increasing demand for silicon-compatible sensors and transducers, and the corresponding success in demonstrating various micromachining techniques like bonding, drilling and etching in this dissertation thesis, it is likely that silicon will be increasingly called upon not only in its traditional electronic role, but also in a wide range of mechanical applications where miniaturized, high precision, high reliability, and low-cost mechanical components and devices are required, performing functions not ordinarily associated with silicon Thus we begin to realize that silicon isn't just for circuits anymore

The main advantage of micromachining technology is that such sensors can be fabricated using batch processing techniques. Batch processing helps in improving the sensitivity characteristics and lowering the cost of the device Thus high density array sensors with different geometrical shapes can be fabricated on a single chip using this technique. The size of the sensor makes it suitable for a large range of applications like bioengineering, space, robotics, automotive industry, etc.

7.2 Suggestions for Future Work

Future work to extend the results obtained in this thesis can be carried out in several directions. Some of the possible directions are to improve the quality and sensitivity of the sensor. The initial measured results indicate that the fabricated sensor

output can be converted to a usable signal using off-chip electronics which can be housed in close proximity to the sensor But, future sensors should be designed with on-chip circuitry to minimize parasitic and improve the performance of the sensor. Micromachined devices integrated with electronic circuitry results in high precision capacitance measurement sensors The reliability of the device is expected to be high once the technology is established

The future trends can also be directed to fabricate multiple devices like temperature, pressure and flow devices in one package. Presently, microprocessors are being designed into almost all the new appliances such as microwave oven, washing machines and dish washers As the trend continues, these devices will require sensors to get feedback from the analog world Another advantage is that, these products can be made more efficient with lower power consumption by implementing micro mechatronic devices into their operating system

The future trends for these type of sensors will be to improve the performance to meet the practical requirements in space and robotics applications The process is simple and reproducible and therefore the next generation of sensors will be constructed with on-chip integrated circuitry. Proper packaging and protection of the tactile imager is very important for its successful operation in environments that are often harsh or destructive. The gap between the plates should be enclosed so that dust particles will not get in between them these requirements can be achieved by covering the tactile imager with a thin deformable insulating sheet that can be replaced when needed Although capacitive sensors have a constant problem of stray capacitance, the problem can be minimized by proper shielding and feedback techniques and by placing the measuring circuit in close proximity to the sensor.

The operating range of the sensor can be increased by covering the diaphragm area with a boss. This design helps in keeping the two electrodes as parallel as possible. The capacitive sensors with slip detectors offers the most encouraging field as miniature tactile sensors to replace the lost touch sensation on human hand. If the glass thickness is reduced, this approach is also expected to be compatible with curved array surfaces which mimic the finger tip for robotics application The integration of sensors, computing circuits, and actuators in a single fabrication process is a challenge that requires practical thinking in all phases of production of a useful system [52].

APPENDIX - I

Derivation of Relation Between Pressure and Capacitance

The pressure micro-transducer essentially consists of two circular parallel plates separated by a gap *d* to form a variable capacitor. The lower plate is rigid while the upper plate is flexible and clamped at the edge. Thus under a uniformly distributed load the top plate is free to deflect downwards until it touches the lower plate. The bending of the upper plate is considered to be axi-symmetric. The maximum deflection will be at the center

The deflection at any point at a radial distance r from the center is

$$w = \frac{P}{64D}(a^2 - r^2)^2 \qquad \text{(A1.1)}$$

where, w = deflection and

D = flexural rigidity of the plate written as

a = radius of the plate

$$D = \frac{EH^3}{12(1-\nu^2)} \qquad \text{(A1.2)}$$

where, E = modulus of elasticity of the material

H = thickness of the plate

ν = Poisson's ratio

Equation -A1.1 is derived from the relation [14]

$$w = C_1\frac{r^2}{4} + C_2\log\frac{r}{a} + C_3 + \frac{Pr^4}{64D} \qquad (A1.3)$$

The boundary conditions are

$$w = 0 \quad \text{at } r = a$$

$$\left.\frac{dw}{dr}\right|_{r=0} = 0$$

$$\left.\frac{dw}{dr}\right|_{r=a} = 0$$

Applying these conditions in Equation - A1.3, we get $C_2 = 0$ and

$$C_1 = -\frac{Pa^2}{8D} \qquad (A1\ 4)$$

$$C_3 = \frac{Pa^4}{64D} \qquad (A1.5)$$

The maximum deflection is given by

$$w_{max} = \frac{Pa^4}{64D} \qquad (A1.6)$$

The deflection of the plate can be divided into two different regimes, REGIME I and REGIME II, the first being described by the expression A1.3, where the upper plate bends until it touches the lower plate.

The following expression describes the bending in the second regime (REGIME II):

$$w = C_1 + C_2 \log r + C_3 r^2 + C_4 r^2 \log r + \frac{Pr^4}{64D} \tag{A1.7}$$

where, r, is the distance of any point from the center of the plate. The area of contact has a radius of b, which will depend on d, the gap between the plates, D the flexural rigidity of the plate material and P is the applied pressure.

The constants of integration C_1, C_2, C_3, C_4 are obtained by applying the boundary conditions, which are given by

$$w = 0, \quad \frac{dw}{dr}\Big|_{r=a} = 0 \quad \text{at,} \quad r = a$$

$$w = \delta, \quad \frac{dw}{dr}\Big|_{r=b} = 0 \;, \quad M_r\Big|_{r=b} = 0 \quad \text{at,} \quad r = b$$

The parameters are normalized as follows:

$$\bar{r} = \frac{r}{a}$$

$$\bar{b} = \frac{b}{a}$$

$$\bar{d} = \frac{d\,D}{P_o\,a^4}$$

$$\bar{w} = \frac{w\,D}{P_o\,a^4}$$

$$\overline{P} = \frac{P}{P_o}$$

where, P_o is the atmospheric pressure.

Using the normalized parameters in equation (A1.7) we obtain,

$$\overline{w}(\overline{r}) = C_1 + C_2\log(\overline{r}) + C_3\overline{r^2} + C_4\overline{r^2}\log(\overline{r}) + \frac{\overline{P}\overline{r^4}}{64D} \quad \text{(A1 8)}$$

The boundary conditions, using the normalized parameters are

$$\overline{w}(1) = 0, \quad \overline{w'}(1) = 0$$

$$\overline{w}(\overline{b}) = \overline{\delta}, \quad \overline{w'}(\overline{b}) = 0$$

$$\overline{M_r}(\overline{b}) = 0, \text{where} \quad \overline{M_r} = (\overline{w}'' + \frac{\nu}{r}\overline{w'})$$

applying the boundary conditions in equation (4) we obtain

$$C_1 + C_3 = -\frac{\overline{P}}{64} \quad \text{(A1.9)}$$

$$C_2 + 2C_3 + C_4 = -\frac{\overline{P}}{16} \quad \text{(A1.10)}$$

$$C_1 + C_2\log\overline{b} + C_3\overline{b^2} + C_4\overline{b^2}\log\overline{b} = -\frac{\overline{b^4}}{64}(\overline{P}) + \overline{\delta} \quad \text{(A1.11)}$$

$$\frac{C_2}{\overline{b}} + 2C_3\overline{b} + C_4\overline{b}(2\log\overline{b} + 1) = -\frac{\overline{b^3}}{16}(P) \quad \text{(A1.12)}$$

$$\frac{C_2(\nu-1)}{\overline{b}^2} + 2C_3(\nu+1) + C_4\left[3 + 2\log(\overline{b}) + 2\nu\log(\overline{b}) + \nu b\right] = -\overline{P}\frac{\overline{b^2}}{16}(3+\nu) \tag{A1.13}$$

In order to find the stresses it is necessary to know the moments. The moments are given by the relation,

$$M_r = -D\left(\frac{d^2w}{dr^2} + \frac{\nu}{r}\frac{dw}{dr}\right) \tag{A1.14}$$

$$M_t = -\frac{D}{r}\left(\frac{dw}{dr} + \nu\frac{d^2w}{dr^2}\right) \tag{A1.15}$$

The maximum stress at the center is given by

$$\sigma_{max} = \frac{6M}{h^2} \tag{A1.16}$$

Note that the stress is maximum at h/2 Therefore, using A1 14 and A1.15 we have,

$$\sigma_{r(max)} = \frac{6D}{h^2}\left(\frac{d^2w}{dr^2} + \frac{\nu}{r}\frac{dw}{dr}\right) \tag{A1.17}$$

Substituting for D from Equation - A1.2, we get

$$\sigma_{r_{max}} = \frac{Eh}{2(1-\nu^2)}\left(\frac{d^2w}{dr^2} + \frac{\nu}{r}\frac{dw}{dr}\right) \tag{A1.18}$$

Normalizing the above expression we can write

$$\sigma_r = -\frac{Eh}{2(1-\nu^2)}\left(\frac{P_0\,a^4}{D\,a^2}\right)\left[\frac{\overline{d^2w}}{\overline{dr^2}} + \frac{\nu}{\overline{r}}\frac{\overline{dw}}{\overline{dr}}\right] \tag{A1.19}$$

where,

$$\overline{\sigma_r} = \left[\frac{d\overline{w}^2}{d\overline{r}^2} + \frac{\nu}{\overline{r}}\frac{d\overline{w}}{d\overline{r}}\right] \tag{A1.20}$$

$$r = a\overline{r}$$

$$\frac{d}{dr} = \frac{1}{a}\frac{d}{d\overline{r}}$$

$$\frac{d^2}{dr^2} = \frac{1}{a^2}\frac{d^2}{d\overline{r}^2}$$

$$\left[\frac{d^2w}{dr^2} + \frac{\nu}{r}\frac{dw}{dr}\right] = \frac{1}{a^2}\left[\frac{d^2\overline{w}}{d\overline{r}^2} + \frac{\nu}{\overline{r}}\frac{d\overline{w}}{d\overline{r}}\right]$$

$$\overline{\sigma_r} = \left[\frac{h^2}{6P_o a^2}\right]\sigma$$

A1.1 Capacitance calculation

$$C_{air} = 2\pi\varepsilon_o\varepsilon_r \int \frac{rdr}{d} \tag{A1.21}$$

where,

ε_o is the vacuum permittivity = 8.854×10^{-12} F/m

ε_r is the relative permittivity $= \varepsilon_{material} / \varepsilon_o$

For the region not in contact the capacitance is given by the expression

$$C_{air} = 2\pi\varepsilon_0\varepsilon_r \int \frac{rdr}{d - w(r)} \quad \text{for the air gap} \tag{A1.22}$$

$$C_{in} = 2\pi\varepsilon_0\varepsilon_r \int \frac{rdr}{H_{in}} = \frac{\pi\varepsilon_0\varepsilon_r}{H_{in}}(a^2 - R^2) \tag{A1.23}$$

where **R** is the radius of the area in contact and H_{in} is the thickness of the insulation layer

The effective capacitance C_e of the area is given by

$$C_e = \frac{C_{in} * C_{air}}{C_{in} + C_{air}} \tag{A1.24}$$

For the area in contact the capacitance C_c is given by

$$C_c = 2\pi\varepsilon_0\varepsilon_r \int \frac{rdr}{H_{in}} = \frac{\pi\varepsilon_0\varepsilon_r R^2}{H_{in}} \tag{A1.25}$$

Thus the total zero pressure (no load) capacitance is

$$C_0 = C_e + C_c \tag{A1.26}$$

APPENDIX - II

Cleaning Procedure for Silicon and Glass Wafer

Cleaning the wafers is performed before every micromachining or photolithography process. This Appendix presents the standard cleaning procedure used for silicon and glass wafers

1. Boil the wafer in a mixture of $H_2SO_4 + H_2O_2$ (1:1) for 5 minutes and then rinse in de-ionized (DI) water having a resistivity 15 - 18 MΩ-cm.
2. Boil the wafer in a mixture of $HCl + H_2O_2 + H_2O$ (1:1:5) for 5 minutes and then rinse in DI water.
3. Clean the wafer in $HF + H_2O$(1:50) (10 Sec) to remove the native oxides from the silicon surface.
4. Clean the wafer (without boiling) in a mixture $NH_4OH + H_2O_2 + H_2O$ (1:1:5) for 5 Minutes and then rinse in DI water.

Note: (a) The steps 3 and 4 is performed only for clean silicon wafers

(b) Silicon wafers with SiO_2 as mask is not dipped in HF

APPENDIX - III

Photolithography

Photolithography plays an important role in the fabrication of all micromechatronic devices. It is conducted in a yellow room so that the exposure is not damaged by other light sources. The photosensitive material is not influenced by the yellow light. In this process, photoresist (PR) is applied on the wafer, spun on a chuck, dried in an oven, exposed to UV light and then developed in the developer. The PR is a means to protect chosen regions of the wafer for the subsequent micromachining processes. A schematic diagram of the process of photolithography is shown in Figure A3.1

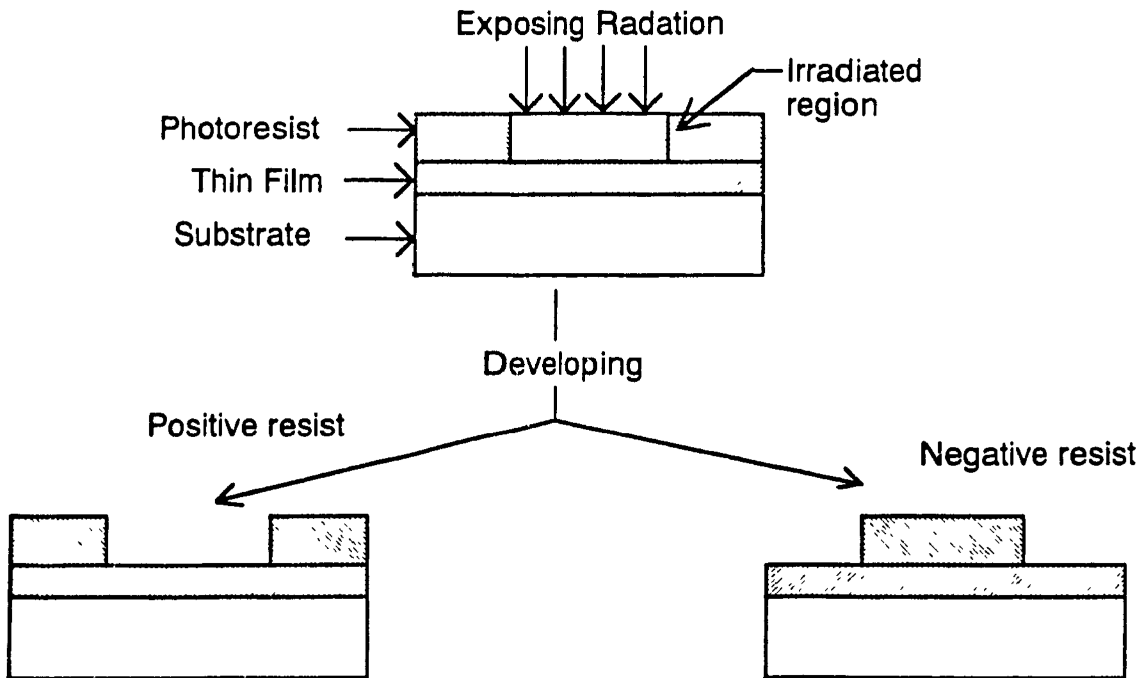

Figure A3.1 Photolithography [66].

There are two types of photoresists namely:

(a) Positive photoresist, which when exposed to UV light through a mask, develops the region which are not opaque.

and,

(b) Negative photoresist, which when exposed to UV light through a mask develops the region which are opaque.

A3.1 The photolithography procedure

i. The sample silicon wafer is centered on the spinner chuck and secured with vacuum The dust particles are blown off with purified compressed N_2 Then using a syringe equipped with "minisart" 0.45 micron filter, apply 2-3 drops of photoresist ("shipley" type 1350J for positive photoresist and HNR-120 Resist-OCG-microelcetronics materials Inc for negative photoresist) to the slice. The slice is then spun immediately on the spinner (at 3000 rpm for 30 sec. for the positive photoresist and for the negative photoresist initially at 500 rpm for 3 sec. then at 2000 rpm for 15 sec.)

ii. The wafer is *"Soft baked"* in a forced air convection oven at 95°C for 30 min. for positive photoresist or 20-25 minutes for negative photoresist. Then it is allowed to cool in ambient for 15 min.

iii. The wafer is placed on the mask aligning instrument and then aligned using the X-Y table. The wafer is then exposed to UV-light (for 10 seconds for positive photoresist or 65 seconds for negative photoresist.) which is placed under the mask

iv. The wafer is developed in the developer (for positive photoresist use a solution of "microposit developer" concentrate and for negative photoresist use "negative resist

developer") for 45 sec and then rinsed in DI water for positive photoresist or in negative resist rinser for negative photoresist. Then the wafer is dried in purified, filtered N_2 which is set at a pressure of 20 psi.

v. The wafer is "Hard baked" in a forced air convection oven (at 115°C for 30 min. for positive photoresist or at 145°C for 10-20 minutes for negative photoresist).

vi. The photolithography procedure is completed and the wafer is now ready for the next processing step

A3.2 Stripping of Photoresist

i. The negative photoresist is stripped off from the wafer by dipping it in a solution of "microstrip negative resist remover" for some time (~ 5 minutes)

ii. The positive photoresist is removed from the wafer by dipping it in acetone for ~1 minute.

Appendix - IV

Mask Drawings for Micromachined Capacitive Pressure Micro Sensor

The mask drawings for the micromachined capacitive pressure micro sensor is presented in this Appendix. Mask -1 is used to etch cavity in the glass wafer The Mask-2 is used to pattern the silicon wafer to realize the membrane. Mask-3 is used to pattern the top silicon cover. Mask-4 is used to pattern a ring shaped structure in the top silicon cover. Mask-5, the negative of Mask-3, patterns the top silicon cover to deposit SiO_2 in the already recessed region when the device is used as a static pressure measurement sensor. Finally, Mask-6 helps in patterning the glass wafer to deposit metal for electrical contact

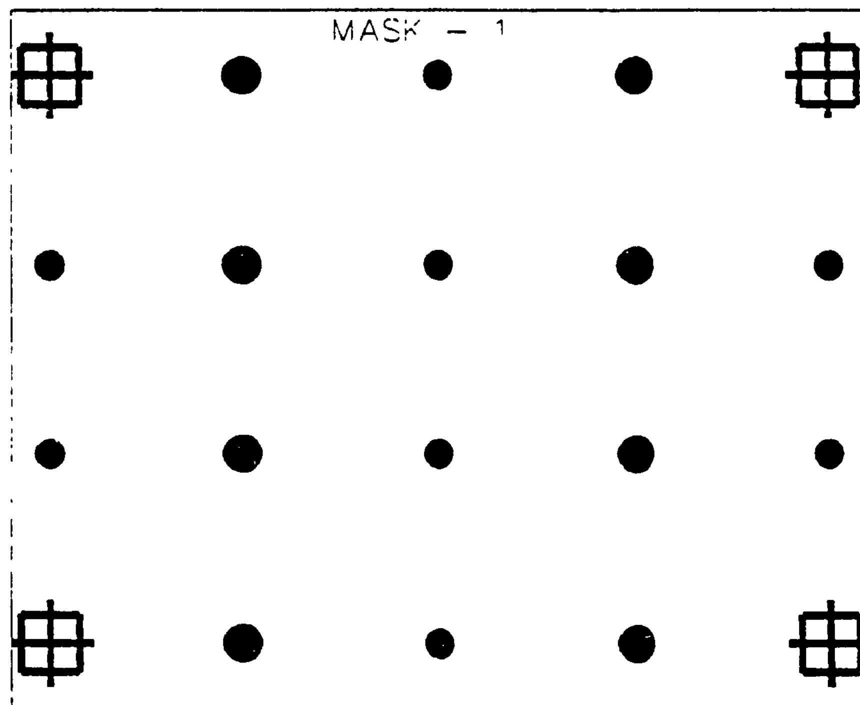

Figure A4.1 Mask - 1 (Scale 1:5).
Diameter of larger circle = 1000μm,
Diameter of smaller circle = 800μm
Center to center distance between the alignment marks = 20mm .
Center to center distance between two adjacent sensors = 5 mm

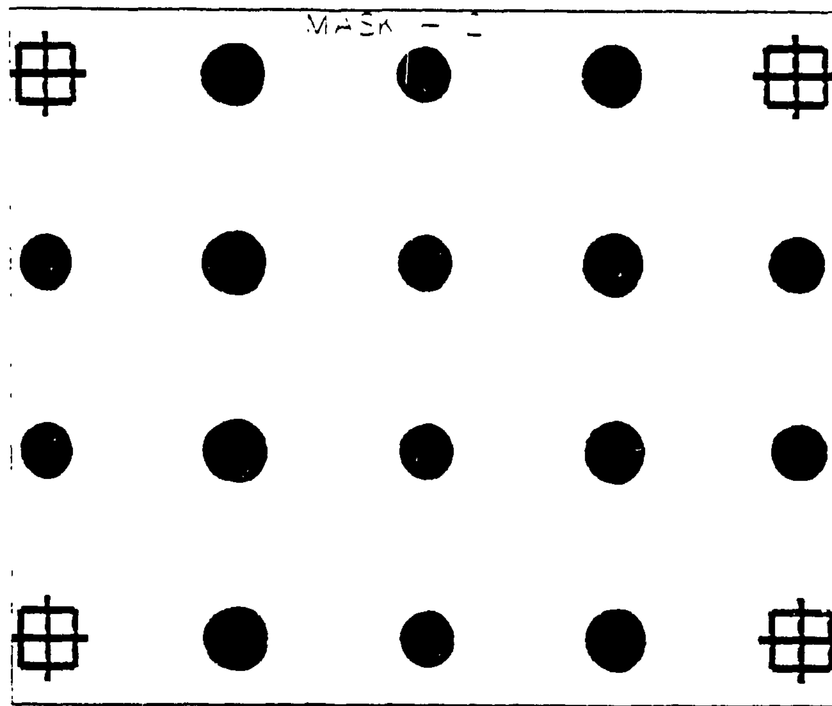

Figure A4.2 Mask - 2 (Scale 1:5).

Diameter of larger circle = 1700μm,

Diameter of smaller circle = 1500μm

Center to center distance between the alignment marks = 20mm .

Center to center distance between two adjacent sensors = 5 mm

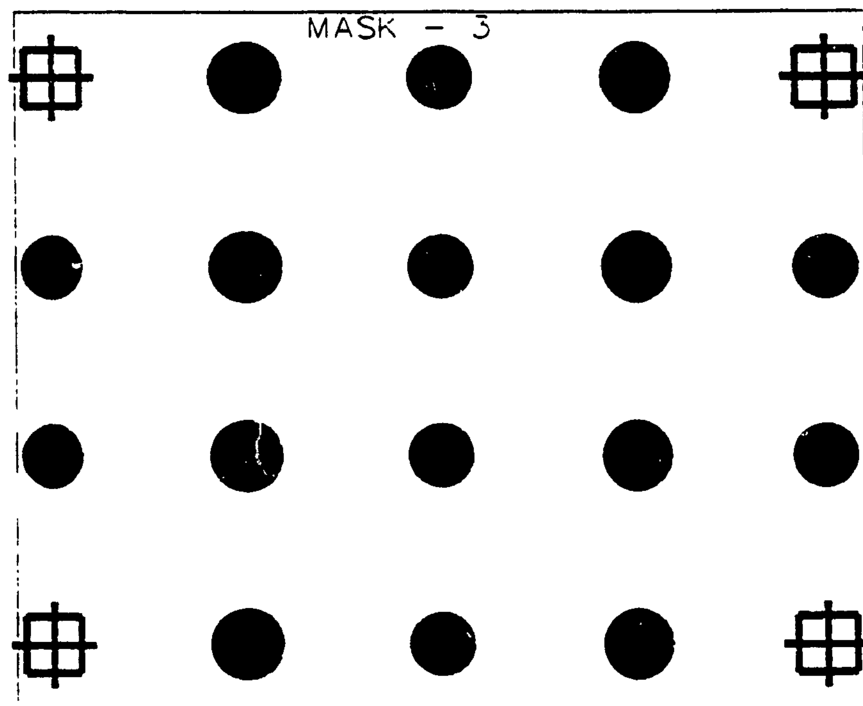

Figure A4.3 Mask - 3 (Scale 1:5).
(Mask -5 is the negative of Mask -3)
Diameter of larger circle = 1900µm,
Diameter of smaller circle = 1700µm
Center to center distance between the alignment marks = 20mm .
Center to center distance between two adjacent sensors = 5 mm

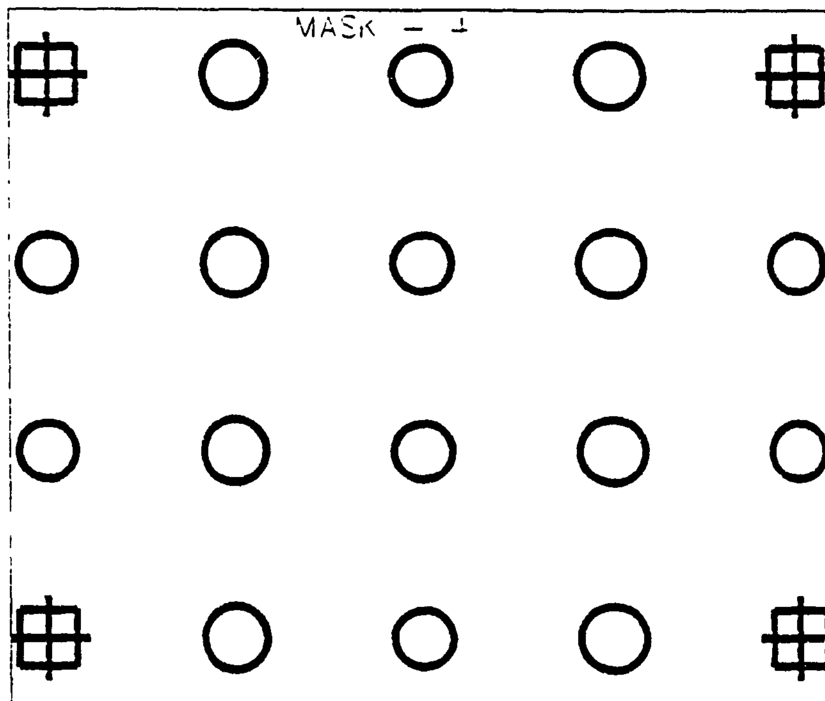

Figure A4.4 Mask - 4 (Scale 1:5).

Inner and outer diameter of larger ring = 1900μm and 1500μm

Inner and outer diameter of smaller ring = 1700μm and 1200μm

Center to center distance between the alignment marks = 20mm .

Center to center distance between two adjacent sensors = 5 mm

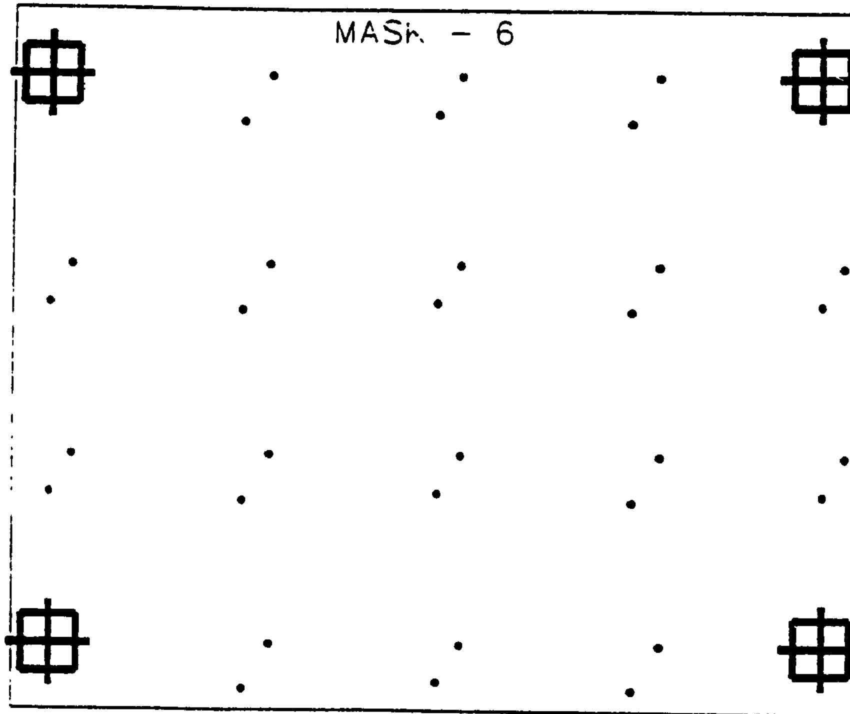

Figure A4.5 Mask - 6 (Scale 1:5).
Diameter of circle = 200μm
Center to center distance between the alignment marks = 20mm .

Appendix - V

Mask Drawings of Capacitive Tactile Sensor

The capacitive tactile imaging sensor has two masking steps, the mask drawings of the sensor are presented in this Appendix. Figure A5.1 illustrates the Mask-1 which is used to pattern the chromium coated glass wafer in selected regions. Mask-2 (see Figure A5.2) patterns the glass wafer for metal deposition which forms the electric contacts for the sensor. In this project, a single bottom electrode for each sensor element in the array was used as the metallization mask. An alternate mask (see Figure A5 3) was designed, having multiple (four) electrodes as bottom electrode for each sensor element. The advantage of using multiple electrodes is to sense both normal and shear force acting on the tactile sensor. This mask can be used for future improvement of the tactile sensor performance.

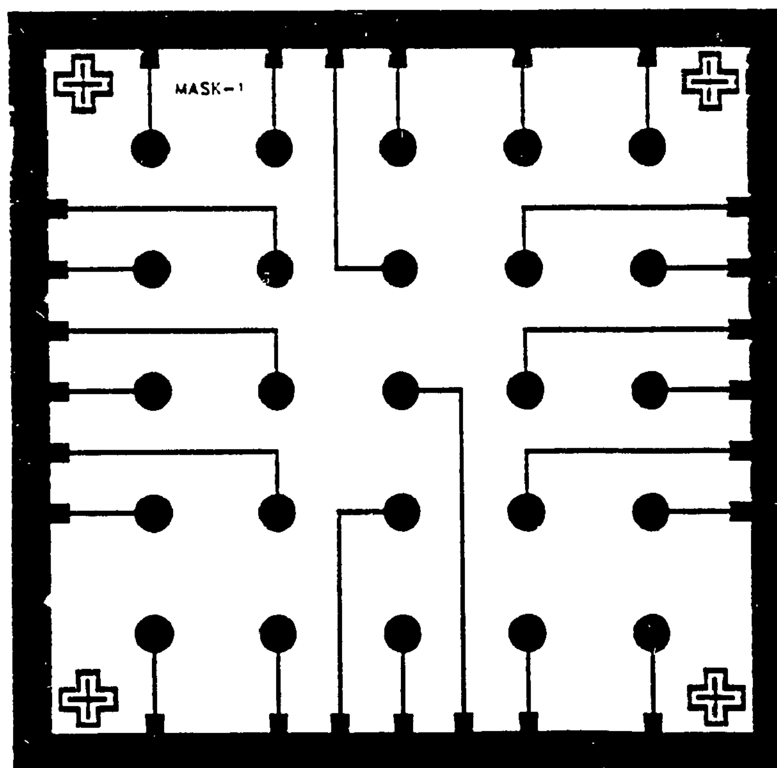

Figure A5.1 Mask - 1 (Scale 1:5).
Diameter of circle = 1000μm
Thickness of channel = 100μm
Length of side = 20mm (square)
Center to center distance between two adjacent sensors = 3.2mm

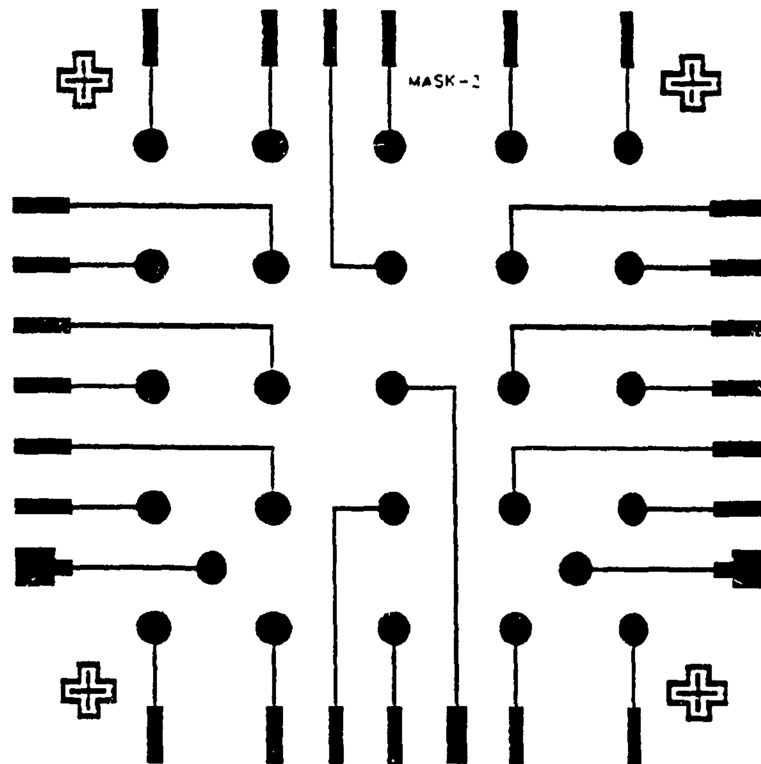

Figure A5.2 Mask - 2 (Scale 1:5).
Diameter of circle = 900μm
Thickness of electrode = 90μm
Length of side = 20mm (square)
Center to center distance between two adjacent sensors = 3.2mm

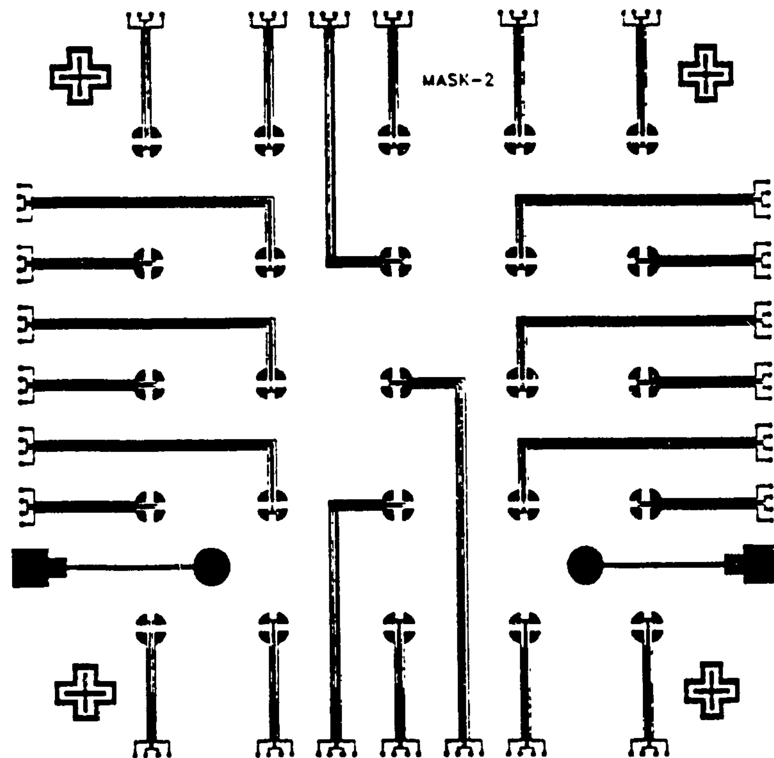

Figure A5.3 Mask - 2 (Alternate) (Scale 1:5).
Diameter of circle enclosing all four electrodes of one sensor element = 900μm
Thickness of electrode = 15μm
Length of side = 20mm (square)
Center to center distance between two adjacent sensors = 3.2mm

Appendix - VI

Anisotropic Silicon Etching Using KOH Etchant

Anisotropic etching is one of the major step in micromachining process to realize thin silicon membrane. Wet chemical etching of semiconductor surface is the result of the dissolution of the semiconductor in the etchant. The rate of etching is determined by the type of semiconductor (Si or GaAs), type of crystal orientation (<100>, <110> or <111>), type and concentration of impurity atoms (n-type or p-type), flow of etchant solution over the semiconductor surface and the temperature of the etchant solution. This Appendix presents the implementation of an apparatus which can be used as a constant temperature bath for etching silicon using KOH etchant (anisotropic etchant) The experimental results of the rate of silicon etching in KOH etchant using the designed etching apparatus is also presented and compared with those found in literature

A6.1 Anisotropic Etching of silicon in KOH

The existence of selective and anisotropic etching of silicon has formed the basis of many micromachining devices The anisotropic nature of wet chemical etchants helps in etching silicon at a faster rate in one particular crystal plane than the other planes [1,57,70] Figure A6.1 illustrates some examples of silicon crystallographic planes [69]

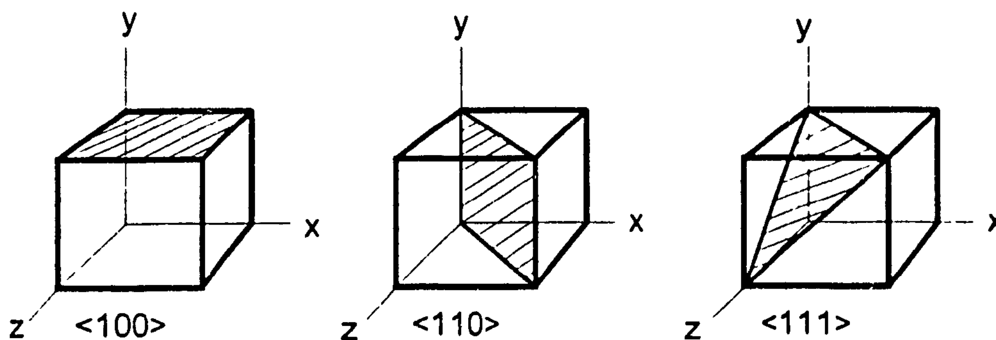

Figure A6.1. Silicon crystallographic planes.

The etch action of the alkaline solution may be described by the equation proposed by Palik et al. [12].

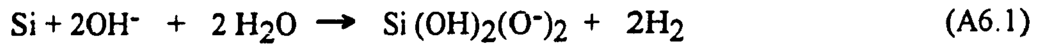

$$Si + 2OH^- + 2H_2O \rightarrow Si(OH)_2(O^-)_2 + 2H_2 \quad (A6.1)$$

From the above equation it can be seen that the etch products are formed by the reaction which is a product of the OH^- ion and the free water molecule concentration Seidel et al [57] performed extensive study of anisotropic etching of crystalline silicon in alkaline solutions and their findings on KOH etchant are presented in Tables A6.1, A6.2 and A6 3 In KOH solution, <110> etches about 60% faster than <100>, with nearly identicai activation energies of 0 61 eV and 0.59 eV respectively. The activation energy of <111> is approximately 0 7 eV. The etch rate ratio of <110> · <100> · <111> was found to vary from 50.30 1 at 100^oC to about 160 100:1 at room temperature [57] For very high concentration exceeding 15 w/o (weight %) the silicon etch rate decreases with the concentration For the full range of concentration the best fit for the temperature dependence etch rate (R_e) for $KOH.H_2O$ etchant was obtained as [57]

$$R_e = k_0[H_2O]^4[KOH]^{\frac{1}{4}}e^{-\frac{E_a}{kT}} \quad (A6\ 2)$$

Where, E_a is the activation energy, k the Boltzmann's constant (8.62×10^{-5}eV/K), T is the temperature in Kelvin and k_0 is a constant

$KOH\ .\ H_2O$ is an orientation dependent etchant which has a large differential etch ratio. The principle feature of such etching behavior in silicon is that <111> surface is attacked at a much slower rate than all other crystallographic planes [1]. Anisotropic etching results in a uniform etch-rate ratio or each directions. The dangling bonds available per surface unit cell depends on the crystal orientation of the exposed silicon surface The dangling bond is lowest for a <111> surface with one bond per unit cell, whereas there are two on <100> or <110> surfaces [58] It is especially useful for V-grooves on <100> silicon or U-grooves on <110> silicon wafers since the large

differential etch ratio permits deep, high aspect ratio grooves with minimal undercutting of the masks. It is also useful as an boron etch stop etchant to realize heavily doped p-type. thin membranes and beams in silicon. The high dopant concentration decreases the width of space charge layer on the silicon surface. Price [60] reported a significant reduction of the dissolution rate for boron doped silicon above 5×10^{18} cm^{-3} in KOH etchant and the etch rate R_e) is expressed as

$$R_e = 2\ 5 \times 10^{24}\ C_B^{-1\ 3} \qquad \text{(A6.3)}$$

where, C_B is the concentration of boron in silicon substrate.

Table A6.1 <100> silicon etch rates in (μm/h) for various KOH concentrations and etch temperatures as calculated from Eq. A6.2 by setting E_a=0.595 eV and K_0=2480 μm/h. (mol/liter)$^{-4.25}$.[57]

% KOH	Temperature (°C)								
	20°	30°	40°	50°	60°	70°	80°	90°	100°
10	1.49	3.2	6 7	13 3	25.2	46	82	140	233
15	1.56	3.4	7.0	14 0	26 5	49	86	147	245
20	1 57	3 4	7.1	14 0	26 7	49	86	148	246
25	1.53	3.3	6 9	13 6	25 9	47	84	144	239
30	1.44	3 1	6 5	12 8	24 4	45	79	135	225
35	1 32	2 9	5 9	11 8	22 3	41	72	124	206
40	1 17	2 5	5.3	10 5	19 9	36	64	110	184
45	1.01	2.2	4 6	9 0	17 1	31	55	95	158
50	0 84	1.8	3 8	7.5	14.2	26	46	79	131
55	0.66	1 4	3 0	5.9	11.2	21	36	62	104
60	0.50	1.1	2.2	4 4	8.4	15	27	47	78

Table A6.2 <110> silicon etch rates in ($\mu m/h$) for various KOH concentrations and etch temperatures as calculated from Eq. A6.2 by setting E_a=0.60 eV and K_0=4500 $\mu m/h. (mol/liter)^{-4.25}$.[57]

% KOH	Temperature (°C)								
	20°	30°	40°	50°	60°	70°	80°	90°	100°
10	2 2	4 8	10.1	20 1	38	71	126	216	362
15	2 3	5 1	10 6	21.2	40	74	132	228	381
20	2.3	5.1	10.7	21 3	41	75	133	229	383
25	2 3	5 0	10 4	20 6	39	73	129	222	372
30	2 1	4 7	9 8	19 4	37	68	121	209	350
35	2 0	4 3	8 9	17 8	34	63	111	192	321
40	1.7	3 8	8 0	15.9	30	56	99	171	285
45	1 5	3 3	6 9	13 7	26	48	85	147	246
50	1 2	2 7	5 7	11 3	22	40	71	122	204
55	1 0	2 2	4 5	9 0	17	31	56	96	161
60	0 7	1 6	3 4	6 7	13	24	42	72	121

Table A6.3 Calculated silicon etch rates of thermally grown silicon dioxide in (nm/h) for various KOH concentrations and etch temperatures. E_a=0.85 eV. [57]

% KOH	Temperature (°C)								
	20°	30°	40°	50°	60°	70°	80°	90°	100°
10	0 40	1 22	3 5	9 2	23	54	123	266	551
15	0 63	1 91	5.4	14.4	36	85	193	416	862
20	0 88	2 66	7.5	20.0	50	118	268	578	1200
25	1 14	3 46	9.8	26 0	65	154	348	752	1560
30	1.42	4.32	12 2	32 5	81	193	435	940	1950
35	1 44	4 37	12 4	32.8	82	195	440	949	1970
40	1.33	4 03	11 4	30 3	76	180	406	876	1820
45	1.21	3 67	10.4	27.5	69	163	369	767	1650
50	1 08	3 28	9 3	24 6	62	146	330	713	1480
55	0 95	2 87	8 1	21 6	54	128	289	624	1290
60	0 81	2 45	6 9	18 4	46	109	246	532	1100

A6.1.1 KOH Etching Apparatus

A constant temperature beaker-in-beaker apparatus was used for etching silicon in KOH solution The schematic drawing of the etching apparatus is illustrated in Figure A6.2. The apparatus consists of two beakers. a 250 ml. Pyrex beaker placed inside a 600 ml Pyrex beaker. The inner beaker is held on plexi-glass support placed inside the larger beaker. The two beakers are placed in an enclosed electric heater. The heater is a constant temperature heat bath with a temperature range from -90 ^{o}C to 900 ^{o}C and a controlling capability of $\pm 0.1^{o}C$.

A Teflon multiple wafer holder was fabricated to hold the wafers in a fixed horizontal position inside the etchant Figure A6 3 illustrates the wafer holder used for etching apparatus The wafers are placed inside the grooves of the holder and tightened by means of the Teflon screws. The wafer holder is then placed inside the smaller beaker and the etchant with predetermined concentration is poured into it The apparatus is now ready for etching

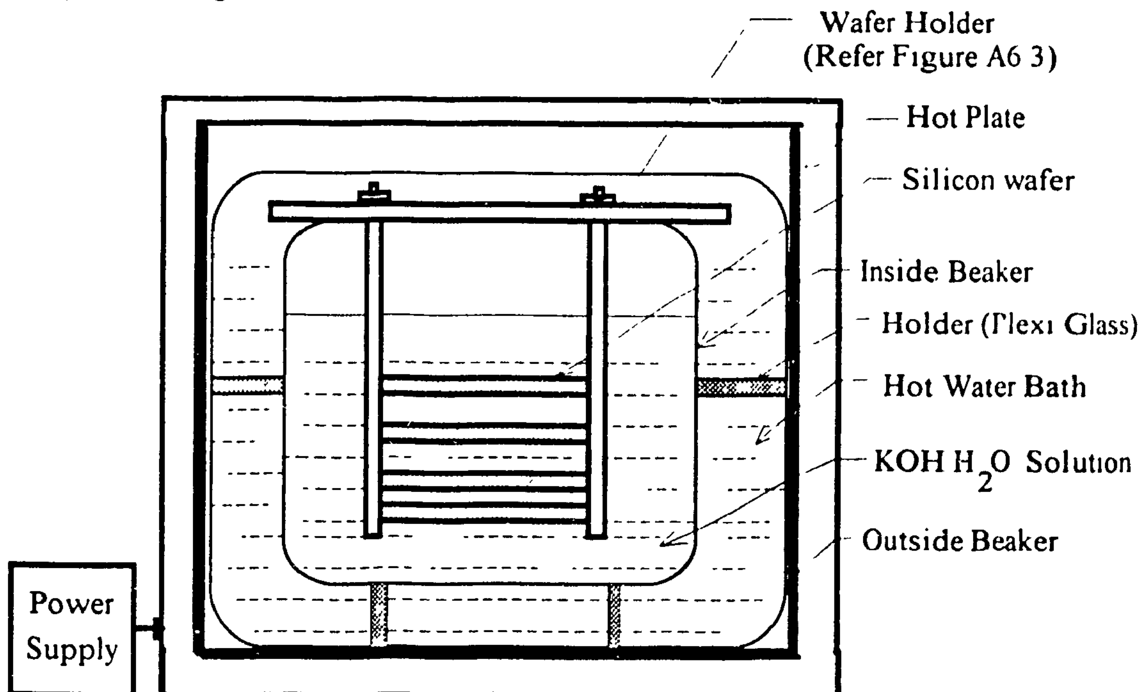

Figure A6.2 Schematic representation of a constant temperature KOH etching apparatus.

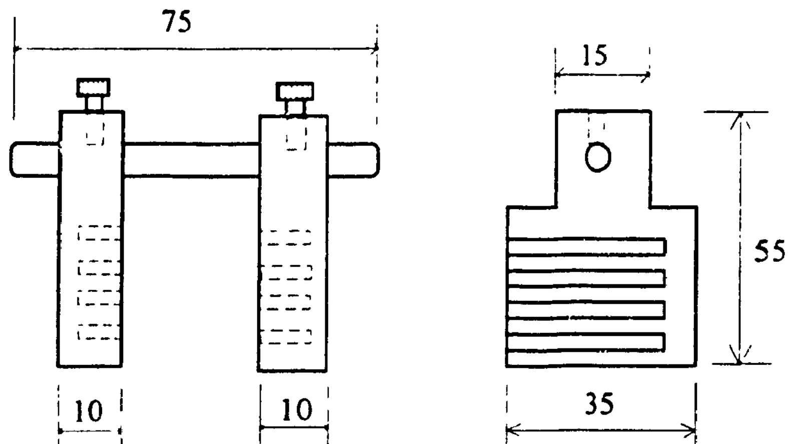

Notes: 1) All dimensions in millimeters
2) Drawing is not to scale
3) Material used = Teflon

Figure A6.3 Silicon wafer holder used for KOH etching apparatus.

A6.1.2 Experimental Procedure

The sample used for this study were p-type <100> silicon wafers Most experiments were performed during the fabrication of the pressure measurement micro sensor The samples were chemically cleaned as mentioned in Appendix-II and rinsed in de-ionized water The etching experiments were carried out in the fabricated etching apparatus The samples were etched from 0 5 to 2 hours in KOH solution After etching, the sample surfaces were observed under an optical microscope to study the etch rate and patterns formed on the wafer

The etchant was prepared by diluting electronic grade KOH solution with de-ionized water The temperature of the bath was maintained at 85°C. The concentration of the etchant was varied from 10% to 60% and the etch rate was determined Figure A6 4 compares the experimental and theoretical results of silicon etch rate as a function of KOH concentration at 85°C From the figure it is observed that the experimental etch rate is slightly lower than the analytical value but closely related to it for the full range of temperature Another experiment was performed to determine the silicon etch rate as a

function of temperature at 35% KOH concentration. The experimental and analytical results of this experiment is presented in Figure A6.5.

A6.1.2 Experimental Results

The experimental results using the assembled constant temperature etching apparatus compared well with the analytical results except that the etch rate was lower by 5% The disadvantage of KOH is that SiO_2 is etched at a rate (14 Å/min.) which precludes its use as a mask in many application. However a thick layer can be used to overcome the aforementioned problem Generally, Si_3N_4 is the preferred masking material for KOH The experiments conducted using heavily boron doped silicon membranes were not satisfactory because of the formation of brown stains on silicon while etching

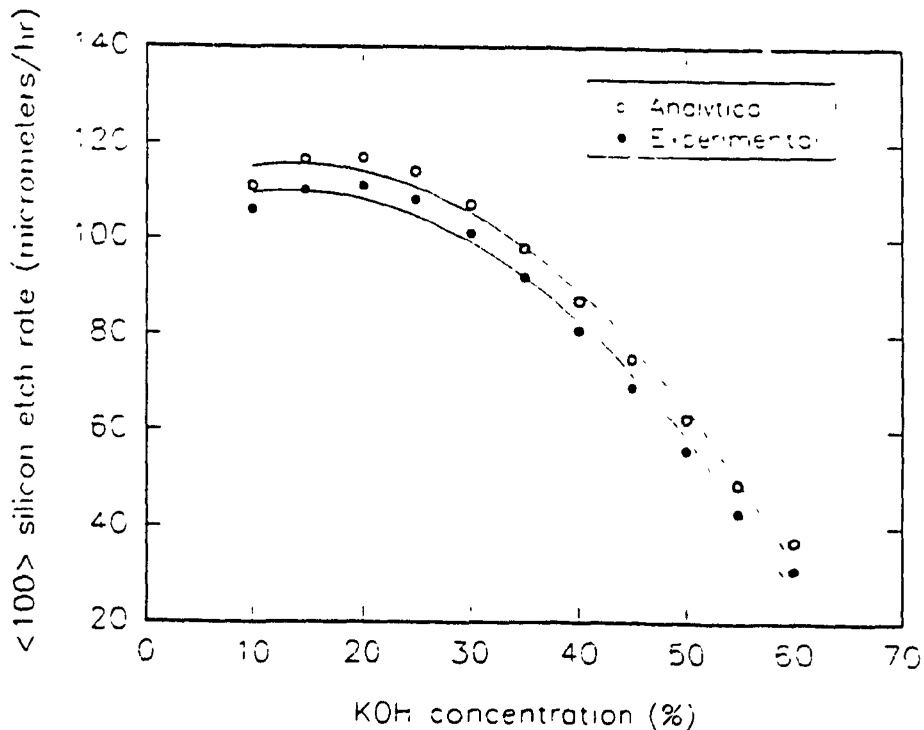

Figure A6.4 Silicon etch rate as a function of KOH concentration at 86⁰C.

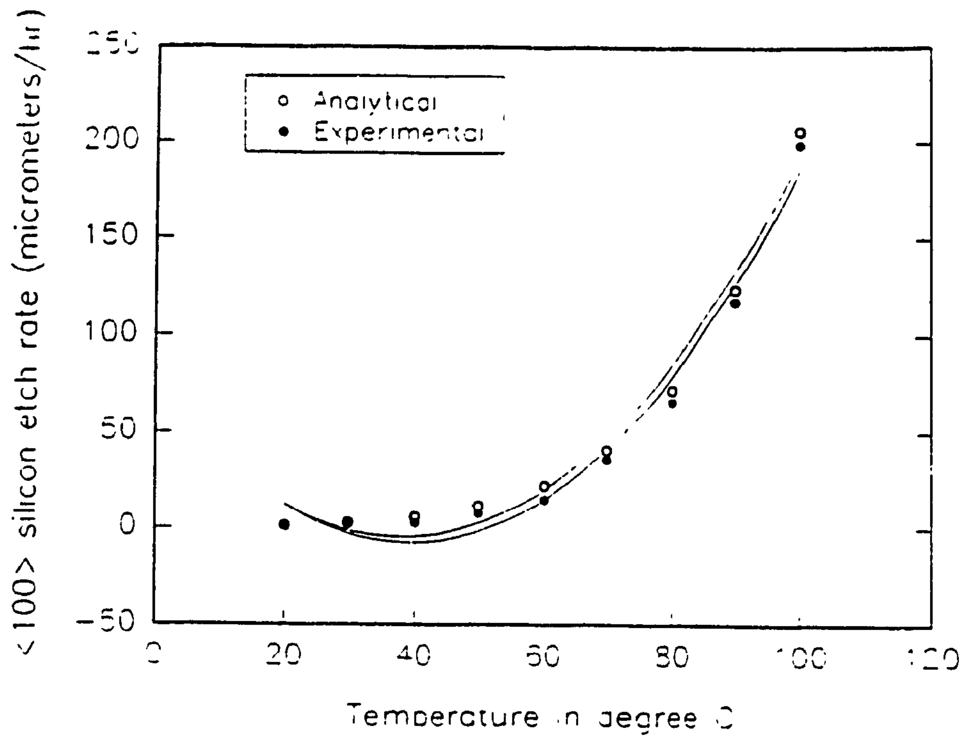

Figure A6.5 Silicon etch rate as a function of temperature at 35% KOH concentration.

Appendix - VII

Mask Making Using Photographic Techniques

A7.1. Preparation of Glass Masks

The mask patterns shown in Appendices IV & V are initially prepared on computer using drafting software (Auto CAD) Computer aided drafting equipment (printer) transfers these patterns onto transparency papers. The dimensions of the patterns on the transparent sheets are 10 times larger than the actual size The patterns are then transferred on to photosensitive glass masks with the help of a camera having 1 10 reduction. The glass masks are processed as follows:

A7.1.1 Preparation of Developer

The developer consists of two parts i e part-A (Kodak super RT developer-net weight 675 g) and part-B (Kodak super RT developer -net weight 657 g) Each of part-A and part-B are mixed separately with 4000 ml of di-ionized (DI) water before the developing process.

A7.1.2 Preparation of Fixer

The fixer consists of two parts. part-A (946 ml) and part-B (104 ml) Parts-A and part-B are mixed with 1900 ml of DI water.

A7.1.3 Preparations for Taking Photograph of Masks

The glass masks are photographed in a dark room and therefore it is mandatory to prepare the chemicals before the start of the process. Initially, three dishes (A,B and C)

are cleaned in DI water. Dish A is filled with 1000 ml of developer, dish B with a mixture 1000 ml DI water + 500 ml fixer and dish C with 1000 ml of DI water.

A7.1.4 Process Technology for Mask Making

The transparency, with the mask drawing on it, is placed on an opaque glass at a suitable distance (focal length) from the photographic lens. The distance between the opaque glass and the lens is so adjusted that the pattern on the photographic film is reduced four times. Now, the camera is loaded with a photographic film and exposed to the transparent paper for a few seconds (~ 4-5 sec) The film is then taken out of the camera and dipped first in dish A for 5 minutes and second in dish B for 5 minutes and then finally in dish C for 5 minutes It should be noted that, the light inside the room should not be turned on until the film is fully developed. The film is now dried in atmosphere After drying, this film is now placed on the opaque glass and the above procedure is repeated using a glass photosensitive film. The exposure for the glass film is 5-6 seconds Thus, the final mask obtained is reduced 10 times the original pattern The glass mask is dried and stored in boxes in the clean room The above procedure is repeated to prepare all the masks required for the capacitive pressure measurement sensor and tactile imaging sensor

Appendix - VIII

Thermal Oxidation Using Wet Oxidation Process

Thermal oxidation is a process of growing oxide on silicon surface at elevated temperatures by reactive sputtering, anodic deposition or pyrolytic deposition of oxysilane compounds The method used here is wet oxidation which involves formation of an SiO_2 layer on silicon by passing oxygen gas through a heated saturator filled with de-ionized (DI) water which is maintained at a temperature (96-100°C) below the boiling point of water to prevent undue depletion of water molecules on the surface of silicon wafer. For the growth of an oxide film of thickness x_0, a layer of silicon of thickness $0.45x_0$ is consumed. The saturator is connected to a heater located at the oxidation furnace inlet which serves the purpose of vaporizing any liquid H_2O from entering the furnace The chemical reaction undergoing during wet oxidation is written as

$$Si + 2H_2O \rightarrow SiO_2 + 2H_2 \qquad (A8\ 1)$$

The silicon wafers are cleaned as mentioned in Appendix II, except for buffered HF (HF.NH_4F) dip. The wafers are dried with purified nitrogen and loaded on the quartz oxidation boat. The oxidation boat is placed at the mouth of the quartz oxidation furnace for 5 minutes. The wafers are now slowly moved to the center of the furnace and the oxidation time is started. At the end of the oxidation time, the furnace is allowed to cool for one hour. The wafers are removed from the furnace and stored in DI water to prevent atmospheric contamination until further processing

Oxidation of silicon is one of the important micromachining process steps where SiO_2 is used as a mask for Si, while etching in etchants like KOH (potassium hydroxide) or TMAH (tetra methyl ammonium hydroxide). In this project we have used KOH as the etchant for etching silicon. However, KOH etches SiO_2 at a lower rate than it does for Si

The etch rate of Si and SiO_2 in KOH is approximately 1.4 μm/min and 14Å/min respectively [1] To overcome the aforementioned problem a thick layer of SiO_2 was used to protect the areas where the etching is undesirable. A sample calculation to determine the oxidation time is presented below.

Thickness of Silicon dioxide (X_o) = 1 μm

Temperature of the oxidation furnace (T) = 1100°C (= 1373 K)

The oxidation time (t) is given by the following equation

$$t = \frac{X_0^2}{B} + \frac{X_0}{\left(\frac{B}{A}\right)} \quad \text{(A8.2)}$$

The parabolic reaction rate (B) is given by

$$B = C_1 e^{\frac{-E_1}{kT}} \quad \text{(A8.3)}$$

where, C_1 = 2 14 x 10^2 μm^2/hr

E_1 = Activation energy (0 71 eV)

k = 8 62 x 10^{-5} eV/K

T = 1373 K

The linear reaction rate constant (B/A) is written as

$$\frac{B}{A} = C_2 e^{\frac{-E_2}{kT}} \quad \text{(A8.4)}$$

where,

C_2 = 8.95 x 10^7 μm/hr

E_2 = Activation energy (2 eV/K)

T = 1373 K

Substituting equation (3.2) and equation (3.3) in equation (3.1) we get the oxidation time (t) as **t = 2 hr 7 minutes**

Appendix - IX

Chromium Deposition Evaporator

The chromium film has a good adhesion on glass substrate This Appendix presents the process parameters required for chromium deposition in a chromium deposition evaporator. The experimental data on chromium-glass interface summarized by Frieser [68] shows that the glass surface is oxidized during the evaporation process and the chromium penetrates into the glass during this process Attempts to peel chromium film (~ 1000 Å or less) from the glass substrates invariably resulted in a layer of glass coming off with the chromium [68] This property of chromium on glass can be used as a mask and also as an electrode on glass substrate in micromachining processes

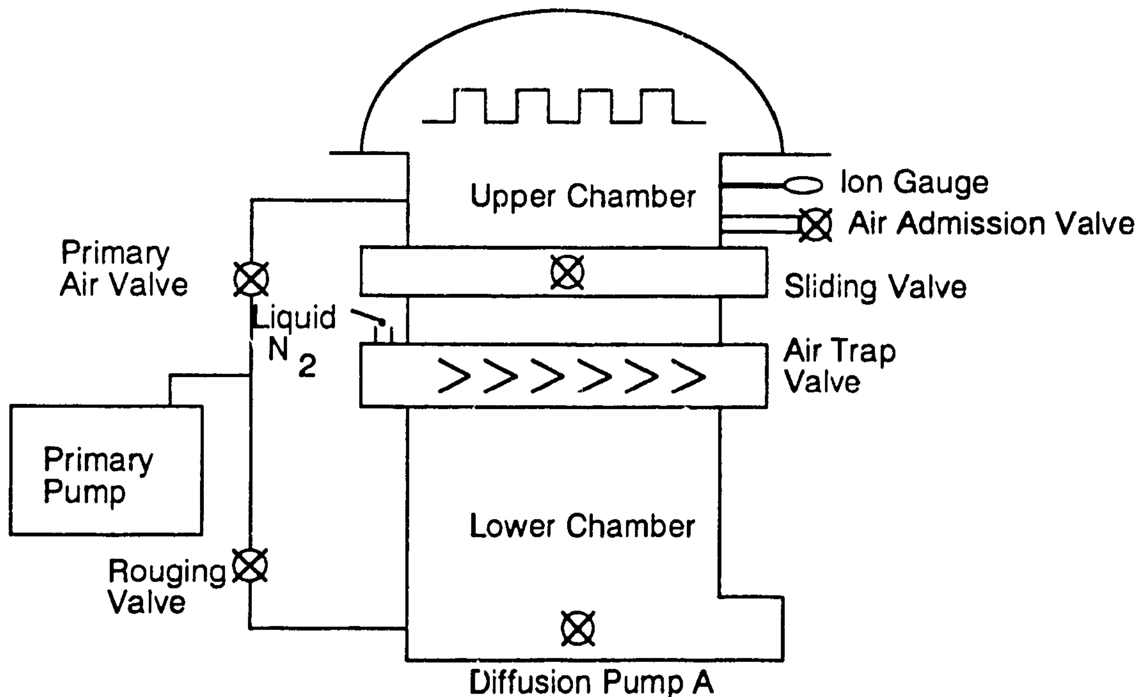

Figure A9.1 Chromium Evaporator.

A schematic drawing of a chromium evaporator is shown in Figure A9.1. The evaporator has two chambers a lower chamber and an upper chamber. The two chambers are separated by a sliding valve which is opened only during evaporation Generally, the diffusion pump A which runs continuously maintains the pressure of the lower chamber at 50 mtorr The upper chamber is held tightly below atmospheric pressure so that it remains clean

Initially, the upper chamber is released by opening the air release valve and letting in N_2 gas N_2 gas is used because it is inert and does not contaminate the chamber. The upper chamber is cleaned and the chromium pellets are placed on a tungsten boat The glass wafers, on which chromium is to be deposited, are placed on a platform above the tungsten boat A revolving flap is placed in between the glass wafers and the tungsten boat which can be moved when the evaporator is ready for deposition. Now the upper chamber is closed and the pressure inside is reduced to 50 mtorr using the primary pump Liquid nitrogen is filled into the nitrogen tank which helps in maintaining the required pressure inside the lower chamber Once the pressure in the upper chamber stabilizes to 50 mtorr the sliding valve is slowly opened Now the upper and lower chambers are allowed to stabilize at a pressure of 2×10^{-6} torr The low pressure maintained inside the chamber plays an important role for the metal deposition At low pressure (10^{-5} - 10^{-6} torr) the evaporated atoms undergo a collisionless transport towards the target substrate and secondly, it avoids oxidizing the heated source material. Figure A9.2 shows the photograph of a deposited film of chromium peeling off from the glass substrate during subsequent micromachining process This phenomenon occurs due to high evaporation pressure inside the evaporator The photograph in Figure A9.3 show the chromium deposited at the appropriate evaporation pressure. therefore, it is mandatory to maintain the required pressure (10^{-5} - 10^{-6} torr) inside the chamber to get good metal deposition

Once this pressure inside the chamber stabilize, an electric current of 50 A is

supplied to the tungsten boat. The heat produced at this current combined with the low pressure inside the chamber leads to the evaporation of chromium pellets. The flap covering the glass wafers from the tungsten boat is moved aside when the evaporation rate stabilizes to 4-5 Å/sec. A computer connected to the sensor placed inside the chamber is used to monitor the thickness of the deposited chromium film. The current supply is turned off once the required thickness of chromium is achieved. Now the evaporator is allowed to cool for about 45 minutes and then the glass samples are removed from the evaporator.

Figure A9.2 Photograph showing defective chromium deposition due to high evaporation pressure inside the evaporator (x 200 magnification).

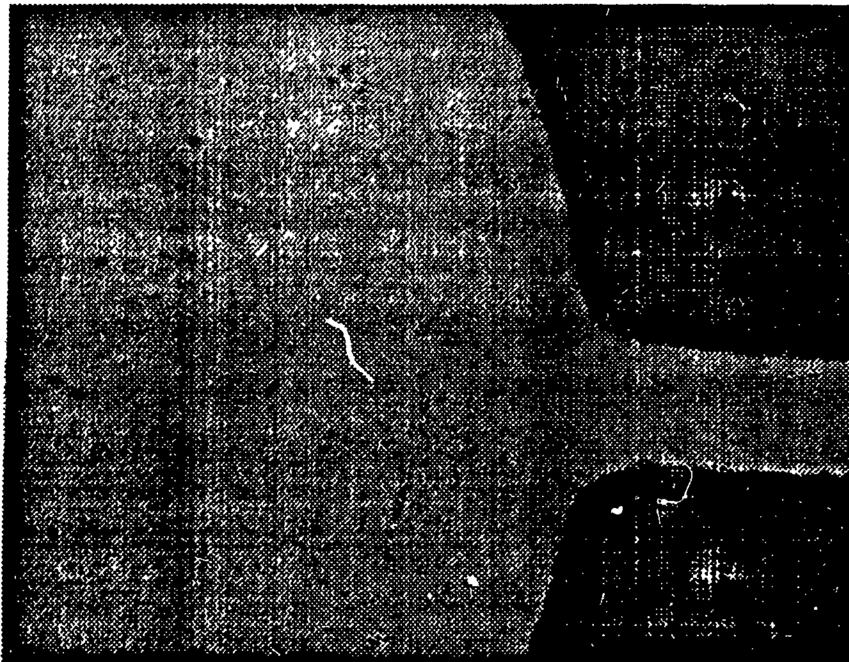

Figure A9.3 Photograph showing a well deposited metal pad (chromium) on glass wafer (x 200 magnification).

BIBLIOGRAPHY

[1] K. E. Petersen, "Silicon as a mechanical material" Proc. IEEE, Vol 70, no. 5 pp. 420-457, May 1982.

[2] R. Puers, "Capacitive sensors: when and how to use then",Sensors and Actuators, A.37-38(1993) 93-105.

[3] W.H. Ko, M.H. Bao and Y.D. Hong, "A high sensitivity integrated circuit capacitive pressure transducer", IEEE Trans. Electronic Devices, Ed.-29 (1982), pp 48-56

[4] S K. Clark and K.D. Wise, "Pressure sensitivity in anisotropically etched thin-diaphragm pressure sensors", IEEE Trans Electron Devices, Ed -26 (1979), pp.1887-1896.

[5] H.L. Chau and K D Wise "Scaling limits in batch-fabricated silicon pressure sensor", 1985, IEEE, pp.174-177.

[6] S. Shoji and M. Esashi, "Photoetching and electrochemical discharge drilling of pyrex glass", Technical Digest of the 9th Sensor Symposium 1990, pp 27-30

[7] M. Guckel and D. Burns, "Planar processed polysilicon sealed cavities for pressure transducer arrays", IEDM Tech. Digest, 1984, pp.223-225.

[8] R. A. Russell, Robot tactile sensing, Prentice hall, New York-1991 ed

[9] Society of Manufacturing Engineers Technical Report no. MSR80-03, Dearborn, MI, 1980.

[10] P. David, D.De. Rossi, C. Domenici, R Francesconi, "Ferroelectric polymer tactile sensors with anthropomorphic features", IEEE 1984, International Conference on Robotics.

[11] J..G. Webster, "Tactile sensors for robotics and medicine", John Wiley and Sons 1988 ed.

[12] W. H. Ko, "Solid state capacitive pressure transducer", Sensors and Actuators, 10(1986) pp 303-320.

[13] G. Kinoshita and K Hattori, "Tactile sensor design and tactile sensing on 3-D objects", Journal of Robotic Systems 2(1), 41-52(1985).

[14] S. Timoshenko and S. Woiwsky-Krieger, Theory of plates and shells, McGraw Hill, New York Second Edition, 1959, page 308-311.

[15] C. Sandeer, J. Knutti and J. Meindl, "A monolithic capacitive pressure sensor with pulse period output", IEEE Trans Electron Devices, Ed-17 (1980) pp. 927-930.

[16] Y. Lee and K D. Wise, "A batch-fabricated silicon capacitive pressure transducer with low temperature sensitivity", IEEE Trans Electron Devices, Ed-29 (1982) pp. 42-48.

[17] W.H. Ko, B X. Shao, C.D. Fung, W.J.Shen and G J Yeh "Capacitive pressure transducers with integrated circuits", Sensors and Actuators 4 (1983).pp 403- 411.

[18] M Smith, M Prisbe, J. Shott and J Meindl, "Integrated circuits for a capacitive pressure sensor", Proc. IEEE frontiers Engin Comp. in Health Care, 1984, pp 440-443.

[19] A Hanneborg, T.E. Hansen, P.A Ohlckers, E. Carlson, B. Dahl and O. Holwech, "An integrated capacitive pressure sensor with frequency modulated output", Sensors and Actuators, vol. 9 (1986) pp. 345-351.

[20] A. Hanneborg and P. Ohlkers,"A capacitive silicon pressure sensor with low TCO and high term stability", Senors and Actuators, A21-A23 (1990) pp 151-154.

[21] M J.S. Smith, L Bowman and J.D. Meindl, "Analysis, design and performance of a capacitive pressure sensor IC", IEEE Transactions on Biomedical Engineering, Vol. BME-33 No 2, February 1986, pp - 163 -174.

[22] H. Chau and K Wise, "Scaling limits in batch fabricated silicon pressure sensors", 3rd International Solid State Sensors and Actuators (Transducers '87) Philladelphia, PA, USA, June 7-11, 1985, pp.174-177.

[23] S. Miyoshi, H Akiyama, H. Shinkaku, Y.Inami and M.Hijikigawa, "A new fabrication process for capacitive pressure sensor", 4th International Solid State Sensors and Actuators (Transducers '87), Tokyo, Japan, June 2-5, 1987, pp. 309-311

[24] S. Shoji, T. Nisase, M. Esashi and T Matsuo, "Fabrication of an implantable capacitive type pressure sensor", Proc 5th Int. Conf. Solid State Sensors and Actuators (Transducers '87), Tokyo, Japan, June 2-5, 1987, pp 305-308.

[25] K Furuta, M. Esashi, S. Shoji and Y Matsumoto, "Catheter-tip capacitive pressure sensor", Tech Digest, 8th Sensor Symp , Japan, 1989, pp 25-28.

[26] B. Puers, E. Peeters and W. Sansen, "CAD tools in mechanical sensor design", Sensors and Actuators, 17 (1989) pp. 423-429.

[27] Y. Backlund, L. Rosengren, B Hok and B. Sweddbergh, "Passive silicon transensor intended for biomedical, remote pressure monitoring", Sensors and Actuators, A21-A23 (1990) pp. 58-61

[28] M. Kandler, J. Eichholz, Y. Manoli and W. Mokwa "CMOS compatible capacitive pressure sensor with read-out electronics", in H.Reich, (ed) Microsystems Springer, New York, 1990, pp 574-580.

[29] Y. Matsumot, S. Shoji and M Esashi, "A miniature integrated capacitive pressure sensor", Tech Digest, 9th Sensor Symp., Japan 1990, pp.43-46.

[30] B. Peurs, E. Peeters, A. V. Bossche and W.Sansen, "A capacitive pressure sensor with low impedence output and active suppression of parasitic effects", Sensors and

Actuators, A21-A23 (1990) pp 108-114.

[31] B. Puers, A V D. Bossche, E Peeters and W.Sansen, "An implant pressure sensor for use in cardiology", Sensors and Actuators A21-A23 (1990) pp 944-947.

[32] V. Artyomov, E. Kudryashov, V. Shelenshkevich and A. Shugla, "Silicon capacitive pressure transducer with increased modulation depth",Senors and Actuators, A28 (1991) pp. 223-230.

[33] J Ji, S Cho, Y. Zhangg, K Najafi and K. Wise, "An ultraminiature CMOS pressure sensor for a multiplexed cardiovascular catheter", 6th int. Conf Solid State Sensors and Actuators (Transducers '91) San Francisco, CA, USA, June 24-28, (1991) pp 1018-1020.

[34] T. Kudoh, S. Shoji and M Esashi, "An integrated miniature capacitive pressure sensor", Sensors and Actuators, Philedelphia, 1985 pp.60-63.

[35] J Kung and H Lee, "An integrated air-gap capacitor process for sensor applications", Proc. 6th Conf. Solid State Senors and Actuators (Transducers '91) San Francisco, CA, USA, June 24-28, (1991) pp. 1010-1013.

[36] H Terabe, T Fukaya, S. Sakurai, O. Tabata, S. Sugiyama and M. Esahi, "Capacitive pressure sensor for low pressure measurements with high overpressure tolerence", Technical digest of the 10th sensor symposium, 1991, pp 133-136.

[37] L. Rosengren, J Soderkvist and L. Smith, "Micromachined sensor structures with linear capacitive response" Sensors and Actuators A31 (1992).pp 200 - 205

[38] F.V. Schnatz, U. Schoneberg, W. Brockherde, P. Kopystynski, T. Mehlhorn, E Obermeier and H. Benzel, "Smart CMOS capacitive pressure transducer with on-chip caliberation capability", Sensors and Actuators A23 (1992).pp 77-83.

[39] J. Suminto, G. Yeh, T. Spear and W. Ko, "Silicon diaphragm capacitive sensor for

pressure, flow, acceleration and altitude measurements", Proc. 4th Int. Conf. Solid State Senors and Actuators (Tansducers '87), Tokyo, Japan, June 2-5, 1987, pp.336-339.

[40] K. Suzuki, K Najafi and K D. Wise, "A 1024 - element high perfcrmance silicon tactile imager", IEEE transactions on electron devices. vol.37. No.8. August 1990.

[41] A. Jornod and F. Rudolf, "High-precision capacitive absolute pressure sensor", Sensors and Actuators, 17 (1989) pp 415-421.

[42] G. Wallis, "Field assisted glass sealing", Electrocomponent Science and Technology, Vol 2, No.1, 1975, pp.45-53.

[43] G.D. Wallis and D.I. Pomerantz, " Field assisted glass-metal sealing", J. of Applied Physics, Vol 40 No.10, Sept 1969, pp 3946-3949.

[44] D I. Pomerantz, US patent No.3 3,397,278 (1968), US Patent No: 3,417,459 (1968)

[45] T.R Antony, "Anodic bonding of imperfect surfaces", J of Applied Physics, 54(5), May 1983, pp 2419-2428.

[46] D L Kendall, C. B. Fleddermann and Kevin J. Malloy, "Critical technologies for the micromachining of silicon", The Mechanical Properties of Semiconductors - Semiconductors and Semimetals, Volume 37, 1992.

[47] W.H. Ko, "Bonding Techniques for Micro Sensors", Micromachining and micropackaging of transducers, Edited by C.D. Fung, P.W. Cheung, W.H. Ko and D.G Fleming, Elesevier Science Publishers, B.V., Amserdam, 1985, pp. 41-61.

[48] M Esashi, A. Nakano, S. Shoji and H. Hebiguchi, "Low-temperature silicon-to-silicon anodic bonding with intermediate low melting point glass", Sensors and Actuators, A21-A23, 1990, pp 931-934.

[49] J. Lagowski, H.C. Gatos and E.S. Sproles Jr , "Surface stress and the normal mode of vibration of thin crystals: GaAs", Applied Physics Letters, Vol 26 No.9 May 1975, pp.493-495.

[50] K. Gustafsson, "Vibration analysis of micromechanical elements", 1985, International Conference on Solid-State Sensors and Actuators, pp. 284-286.

[51] S Wang, S. Crary and K Najafi, " Electronic determination of the modulus of elasticity and intrinsic stress of thin films using capacitive bridges", Materials Research Society, Symposium Proceedings, Vol. 276 pp 203-208

[52] W.H. Ko and M. Mehregany, "Microfabricated sensors and Actuators", 10th sensor symposium Tokyo, Japan, May 1991.

[53] P Pons, G. Blasquez and R. Behocaray, "Feasibility of capacitive pressure sensors without compensation circuits", Sensors and Actuators A37 - 38 (1993) pp 112-115.

[54] M R. Wolffenbuttel and P P.L. Regtien, "Design consideration for a silicon capacitive tactile cell", Sensors and Actuators A, 24 (1990) pp 187-190.

[55] V. Logiudice," Design fabrication and testing of silicon interdigitated back contact (IBC) solar cells", Master dessertation, Elec Eng Dept , Concordia Univsity, August 1993

[56] H. Seidel, L. Csepregi, A. Heuberger, H. Baumgartel, "Anisotropic etching of crystalline silicon in alkaline solution", J. Electrochemical Soc., Vol.137, No.11, November 1990, pp 3612-3626

[57] H. Seidel, L. Csepregi, A Huberger, H. Baumgartel, "Anisotropic etching of crystalline silicon in alkaline solution", J. Electrochemical Soc., Vol 137, No.11, November 1990, pp 3626-3632.

[58] A Zangwill, "Physics at surfaces", Cambridge University Press, Cambridge, MA (1988) pp 91.

[59] E D Palik , V.M Bermudez, O.J. Glembocki, "Ellipsometric study of the etch stop mechanism in heavily doped silicon", Journal of Electrochemical Society, Vol 132, 1985, pp. 135-141.

60] J.B. Price, in "Semiconductor silicon", H.R. Huffand, R.R. Burgess, Editors, pp 339, The Electrochemical Society Softbound Proccedings Series, Princeton, NJ (1973)

[61] H L. Chau and K.D Wise "Scaling limits in batch-fabricated silicon pressure sensor", 1985, IEEE, pp 174-177.

[62] R F Wolffenbuttel and P.P.L Regtien, "Capacitive-to-phase angle conversion for the detection of extremely small capacities", IEEE Trans. Instrum. Meas., IM-36 (1987) 868-872

[63] A Nilakantan, "The design and implementation of an all digital shear sensitive tactile sensor", Masters dissertation, Department of Electrical Engineering, McGill Univ , 1985.

[64] P W. Barth, "Sensor applications in robotics", Robotics engineering Sept 1986 pp 17-20.

[65] S Johaansson, K. Gustafsson and Jan-Ake Schweitz, "Strength Evaluation of Field-Assisted Bond Seal between Silicon and Pyrex Glass", Sensors and Materials, 3(1988) pp 143-151.

[66] J D. Plummer, "Course notes: Section on Lithography", Elec. Eng. Dept., Stanford University, CA, 1991, pp.2.

[67] Product data sheet - Acheson Colloids Company, 1160 Washington Ave., Port Huron, Mich 48060.

[68] R.G. Friesser, "The chromium-glass interface", J. Electrochem Soc.: Solid-State Science and Technology, March 1972, pp. 360-363.

[69] S. K. Gandhi, "VLSI fabrication principles", Ed. 1983, A. Wiley - Interscience Publication, John Wiley & Sons

[70] K.E. Bean., "Anisotropic etching of silicon", IEEE Transaction on Electron Devices, ED-25, 1978, pp. 1185-1192.

[71] Poduct Information - Scotch VHB joining systems, 3M Canada Inc , Post Office Box 5757, London, Ontario, N6A 4T1

[72] L. Tong, J. Hsu, W.H. Ko, X Ding, "The analysis of capacitive pressure sensors with large deflection", IEEE Transducers, International Solid State Senors and Actuators, 1991, pp. 185-187.

[73] S T. Cho, K. Najafi and K.D. Wise, "Internal stress compensation and scaling in ultrasensitive silicon pressure sensors", IEEE transactions on electron devices, Vol 39, No 4, April 1992, pp 836-842